

**GREEN SYNTHESIS OF METALLIC NANOPARTICLES  
AND THEIR EFFECT ON CORROSION OF STEEL  
USED IN BIOMEDICAL DEVICES**

A Thesis

Submitted in partial fulfillment of the requirements for the

Award of the degree of

**DOCTOR OF PHILOSOPHY (Ph.D.)**

In

**BIOTECHNOLOGY**

By

**POOJA SHARMA**

**11720091**

**Supervised By**

**Dr. VINEET KUMAR**

**ASSOCIATE PROFESSOR**



**LOVELY PROFESSIONAL UNIVERSITY**

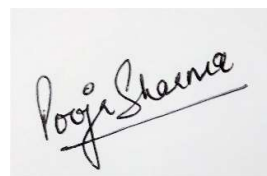
**INDIA (PUNJAB)**

**2022**

## DECLARATION

The research work mentioned in this Ph.D. thesis with the title of “**Green Synthesis of Metallic Nanoparticles and Their Effect on Corrosion of Steel Used in Biomedical Devices**” was carried out by me for the fulfillment of **Doctor of Philosophy in Biotechnology** under the supervision of **Dr. Vineet Kumar, Associate Professor, Department of Biotechnology, Lovely Professional University, Punjab, India.**

I declare that the work mentioned in this thesis is original and has done by me and this thesis has not been submitted in any other degree or other course.

A rectangular box containing a handwritten signature in black ink that reads "Pooja Sharma".

Date:

Pooja Sharma

Place: Jalandhar

Reg. No. 11720091

## **CERTIFICATE**

This is to certify that the thesis entitled “**Green Synthesis of Metallic Nanoparticles and Their Effect on Corrosion of Steel Used in Biomedical Devices**” submitted for the award of the degree of **Doctor of Philosophy in Biotechnology** to Lovely Professional University Punjab, India is a record of bonafide research work carried out by **Ms. Pooja Sharma** under my guidance. To the best of my knowledge, the thesis has not been previously submitted elsewhere for the award of any other degree, diploma or distinction of any kind anywhere before.



**Dr. Vineet Kumar**

**Research supervisor**

**Associate Professor**

**Department of Biotechnology**

**Lovely Professional University**

**Phagwara (INDIA)**

## ABSTRACT

The thesis entitled “**Green Synthesis of Metallic Nanoparticles and Their Effect on Corrosion of Steel Used in Biomedical Devices**” explore the area of environment friendly and cost- effective synthesis of iron oxide nanoparticles (IONPs) for their application as anti-corrosive agent for the prevention of corrosion of biomedical steel, namely stainless steel (SS) 316 L in different biological corrosive environments by applying various analytical techniques. The process of corrosion starts by a chemical reaction which is initiated by the surrounding environment of the metal substrate thus leading to the destruction and dissolution of metallic surface. The chemical reactions occurring on the metal surface renders topographical changes by altering the compositional properties of steel, by permitting diffusion through the disrupted metal layers, by changing pH of the local environment and alteration in electrochemical potential often leading to the destruction of protective barrier of metal surface hence making the metal surface more prone to corrosion. This ultimately leads to the metal damage. The corrosion problem causes huge amount of capital loss to the industries and millions of dollars are spent every year to combat the corrosion process. The process of corrosion cannot be stopped but can be delayed and for this purpose researchers over the world are trying to identify various sources for the corrosion inhibition process and out of all, the use of corrosion inhibitors is found to be most appropriate and effective way to prevent the corrosion of metals.

The area of biomaterials and biomedical research is of great importance for mankind. Since time immemorial, to enhance the proper functioning and longevity of life various biomedical advancement especially in the field of biomaterials has led the way of life. The biomedical steel SS 316 L is mostly used for the manufacture of biomaterials as it is less costly than other titanium-based alloys and are also durable. When these biomedical implants are placed inside the living beings, the surrounding environment of tissues start disrupting the electrochemical equilibrium leading to the start of corrosion process due to exposed anodic and cathodic ends. Due to this process, metal ions start leaching out from the metal causing toxic conditions for the adjacent tissue sometimes leading to the cell injury. Post-surgical operation, the pH of the implant site drops to lower side and become acidic and also the presence of

chloride ions facilitates the corrosion process. It is well known that the chloride ions are one of the main reasons for the occurrence of localized corrosion and subsequent local dissolution of metal ions. In this study, three different corrosive media namely Ringer's solution, Hank's solution and Phosphate Buffer solution were used as the composition of these media mimic the biological fluid composition at the site of implant surgery.

The metallic nanoparticles synthesized in this study were iron oxide nanoparticles (IONPs). For the synthesis of nanoparticles bottom- up approach was used. Different plants were used for the synthesis of IONPs. The prepared nanoparticles were characterized using different techniques like SEM, TEM and AFM for morphological features, X-ray diffraction study was used to identify the chemical formula, nature and type of structure formation, zeta potential was done to analyze the colloidal stability and for the identification of participating functional groups, FTIR analysis was done for IONPs formation and stabilization. Further, the analysis of anti- corrosive property of IONPs, the gravimetric analysis or reduction in weight measurements were performed to identify the rate of corrosion occurrence in the presence and absence of IONPs in corrosive media, electrochemical studies like impedance spectroscopy and potentiodynamic polarization curves were performed to analyze the inhibition efficiency of IONPs against corrosion and to identify the type of inhibition respectively. Further, the surface investigations without and with the addition of IONPs in corrosive media were done by utilizing surface characterization techniques of SEM and AFM.

This thesis contains five chapters namely

### **Chapter 1: Introduction**

This chapter discusses about the general information about corrosion, use of metals and their alloys as biomaterials for biomedical applications, the corrosion of metallic materials in human body and corrosion control methods and nanotechnological applications to prevent the corrosion process.

### **Chapter 2: Literature Review and Problem Formulation**

This chapter discusses about process of corrosion, factors influencing the process of corrosion, interactions of implant materials in human body, types of corrosion which occurs in bio- metals, corrosion inhibitors, advantage of green corrosion inhibitor over chemical inhibitors, metal nanoparticles and their synthesis, plant based green synthesis of nanoparticles, brief introduction of IONPs, application of IONPs in biomedical field, the use of green and plant-based NPs in the field of corrosion prevention and metal protection, use of SS 316 L in biomedical devices, corrosion of SS 316 L, toxicological evaluation of IONPs, research gap, outcomes of this proposed research work, economic importance of the proposed work and objectives of the present study

### **Chapter 3: Materials and Methods**

This chapter contains all the materials which were used to accomplish the deigned work including the chemicals, selected plants, instruments used in completion of the proposed research work. This chapter also contains the methodology and techniques used for the fulfillment of proposed objectives. The synthesis route is discussed along with characterization studies to confirm the IONPs synthesis. After that, the methods to analyze the effects of IONPs in preventing the process of corrosion by inhibition mechanism are discussed.

### **Chapter 4: Results and Discussion**

This chapter containing the results and discussion of the research work that is divided into different parts majorly characterization of synthesized IONPs and their anticorrosive properties in different corrosive media. Selected plants namely *Swertia chirata*, *Terminalia arjuna* and *Ficus benghalensis* were used for the synthesis of IONPs. The synthesized IONPs were then analyzed for their corrosion inhibition property in Ringer's solution, Hank's solution and in Phosphate buffer solution.

### **Chapter 5: Summary and Conclusion**

This chapter summarizes the outcome of the proposed research in terms of synthesized nanoparticles and their potential to inhibit the corrosion of SS 316L. Further, the future scope to enhance the quality of research conducted is also discussed.

## ACKNOWLEDGEMENT

I am utilizing this great opportunity to express my thanks to everyone who supported me directly or indirectly during the time of my research work.

I want to express my gratitude to my supervisor **Dr. Vineet Kumar** for the continuous support in my Ph.D. work and for his patience, motivation, and immense knowledge. His advice towards research played an important role in my research career.

I want to give special thanks to my mother **Mrs. Sheela Sharma** and father **Mr. Jai Bhagwan Sharma** for their love and sacrifices that they have made for me. A special thanks to my sister **Ms. Preeti Sharma** and my brother **Mr. Sonu Sharma** for their support and kind motivation throughout my PhD journey and also for taking care of my responsibilities in my absence.

I want to give a special thanks to my research mate **Mr. Nishant Bhardwaj** for his advices and support during my research work.

Finally, I am thankful to God for giving me good health to accomplish my research work.

Pooja Sharma

**“I dedicate this thesis to my parents**

**(Mrs. Sheela Sharma and Mr. Jai Bhagwan Sharma)**

**For their constant support, motivation and unconditional love”**



## Table of Contents

Title	Page No.
<b>Declaration</b>	ii
<b>Certificate</b>	iii
<b>Abstract</b>	iv-vi
<b>Acknowledgement</b>	vii
<b>List of Tables</b>	xii- xiv
<b>List of Figures</b>	xv- xx
<b>List of Abbreviations</b>	xxi- xxii
<b>Chapter 1: Introduction</b>	
• Metals and their use as biomaterials	2
• Metal corrosion in human body	2-3
• Corrosion control and nanotechnology	3-5
<b>Chapter 2: Review of Literature</b>	
• Factors influencing corrosion process	6-8
• Interaction of implant material in human body	8-11
• Types of corrosion occurring in metallic materials	11-13
• Corrosion inhibitors	13-14
• Advantages of green corrosion inhibitors	14-15
• Metal NPs and their synthesis	15-16
• Plant based green synthesis of NPs	16-17
• Iron oxide nanoparticles (IONPs)	17-19

• Application of IONPs in biomedical field	19-20
• Plant based green synthesized NPs as corrosion inhibitors	20-24
• Use of SS 316L in biomedical devices	24-25
• Corrosion of SS 316L in body fluids	25-26
• Toxicological evaluation of IONPs	26-27
• Research gap	27-28
• Outcomes of the proposed research work	28
• Importance of the proposed research work	28
• Objectives of the present study	28
• <b>Chapter 3: Materials and Methods</b>	
• Chemicals and reagents	29
• Selected plants	29-31
• SS 316L	31
• Corrosive media	31
• Synthesis of IONPs	32
• Preparation of SS 316L working samples	32-33
• Weight loss measurement study	33-34
• Electrochemical studies	34-35
• Instruments used	35-39
<b>Chapter 4: Results and Discussion</b>	
• Characterization of Iron oxide NPs (IONPs) synthesized using <i>S. chirata</i> stem extract	40-48
• Anti- corrosive studies of IONPs synthesized from <i>S. chirata</i> stem extract in Ringer's solution as corrosive media	48-54

• Anti- corrosive studies of IONPs synthesized from <i>S. chirata</i> stem extract in Hank’s solution as corrosive media	54-59
• Anti- corrosive studies of IONPs synthesized from <i>S. chirata</i> stem extract in PBS as corrosive media	59- 64
• Characterization of Iron oxide NPs (IONPs) synthesized using <i>T. arjuna</i> bark extract	64- 71
• Anti- corrosive studies of IONPs synthesized from <i>T. arjuna</i> bark extract in Ringer’s solution as corrosive media	71- 76
• Anti- corrosive studies of IONPs synthesized from <i>T. arjuna</i> bark extract in Hank’s solution as corrosive media	76- 81
• Anti- corrosive studies of IONPs synthesized from <i>T. arjuna</i> bark extract in PBS as corrosive media	81-85
• Characterization of Iron oxide NPs (IONPs) synthesized using <i>F. benghalensis</i> leaves extract	85-92
• Anti- corrosive studies of IONPs synthesized from <i>F. benghalensis</i> leaves extract in Ringer’s solution as corrosive media	92- 96
• Anti- corrosive studies of IONPs synthesized from <i>F. benghalensis</i> leaves extract in Hank’s solution as corrosive media	96-101
• Anti- corrosive studies of IONPs synthesized from <i>F. benghalensis</i> leaves extract in PBS as corrosive media	102-106
• Comparative analysis of the presented study with some already reported work	106-109
<b>Chapter 5: Summary and Conclusion</b>	
• Summary and conclusion	110-112
• Scope of future work	112
• Bibliography	113- 138
• List of publication, conferences and workshop	139- 141

### List of Tables

Table No.	Title	Page number
4.1	Weight loss and adsorption isotherm parameters for <i>S. chirata</i> synthesized IONPs in different concentrations on SS 316L immersed in Ringer's solution	48
4.2	Parameters of electrochemical analysis for SS 316L in Ringer's solution containing different concentration of <i>S. chirata</i> synthesized IONPs	51
4.3	Weight loss and adsorption isotherm parameters for <i>S. chirata</i> synthesized IONPs in different concentrations on SS 316L immersed in Hank's solution	54
4.4	Parameters of electrochemical analysis for SS 316L in Hank's solution containing different concentration of <i>S. chirata</i> synthesized IONPs	57
4.5	Weight loss and adsorption isotherm parameters for <i>S. chirata</i> synthesized IONPs in different concentrations on SS 316L immersed in PBS	59
4.6	Parameters of electrochemical analysis for SS 316L in PBS containing different concentration of <i>S. chirata</i> synthesized IONPs	62
4.7	Weight loss and adsorption isotherm parameters for <i>T. arjuna</i> synthesized IONPs in different concentrations on SS 316L immersed in Ringer's solution	71

4.8	Parameters of electrochemical analysis for SS 316L in Ringer's solution containing different concentration of <i>T. arjuna</i> synthesized IONPs	74
4.9	Weight loss and adsorption isotherm parameters for <i>T. arjuna</i> synthesized IONPs in different concentrations on SS 316L immersed in Hank's solution	76
4.10	Parameters of electrochemical analysis for SS 316L in Hank's solution containing different concentration of <i>T. arjuna</i> synthesized IONPs	78
4.11	Weight loss and adsorption isotherm parameters for <i>T. arjuna</i> synthesized IONPs in different concentrations on SS 316L immersed in PBS	81
4.12	Parameters of electrochemical analysis for SS 316L in PBS containing different concentration of <i>T. arjuna</i> synthesized IONPs	83
4.13	Weight loss and adsorption isotherm parameters for <i>F. benghalensis</i> synthesized IONPs in different concentrations on SS 316L immersed in Ringer's solution	92
4.14	Parameters of electrochemical analysis for SS 316L in Ringer's solution containing different concentration of <i>F. benghalensis</i> synthesized IONPs	94
4.15	Weight loss and adsorption isotherm parameters for <i>F. benghalensis</i> synthesized IONPs in different concentrations on SS 316L immersed in Hank's solution	97
4.16	Parameters of electrochemical analysis for SS 316L in Hank's solution containing different concentration of <i>F. benghalensis</i> synthesized IONPs	99

4.17	Weight loss and adsorption isotherm parameters for <i>F. benghalensis</i> synthesized IONPs in different concentrations on SS 316L immersed in PBS	102
4.18	Parameters of electrochemical analysis for SS 316L in PBS containing different concentration of <i>F. benghalensis</i> synthesized IONPs	104
4.19	Comparative literature studies with the already reported finding	107-109

## List of Figures

Figure No.	Title	Page No.
1.1	Biomedical corrosion and their treatment strategies	5
2.1	Losses faced by industry due to corrosion	8
2.2	Effects of corrosion of bio-implants in human body	11
2.3	Types of corrosion of materials used for biological application at different locations.	12
2.4	Various applications of iron oxide NPs in biomedical field	19
2.5	Proposed mechanism of corrosion inhibition by NPs	21
3.1	Dried and crushed form of selected plants (a) <i>S. chirata</i> (b) <i>T. arjuna</i> (c) <i>F. benghalensis</i>	30
3.2	Working samples of SS 316L used for (a) weight loss measurement (b) electrochemical analysis	32
3.3	(a) UV-vis spectrophotometer (b) zeta potential and particles size analyser (c) X-ray diffractometer	35
3.4	(a) Image showing SEM (b) Image showing TEM	36
3.5	(a) Image showing AFM (source- Anton Paar.com) (b) FTIR spectrophotometer	37
3.6	(a) Electrochemical workstation (b) Electrode cell assembly	38
4.1	UV-vis spectroscopy of IONPs synthesized from <i>S. chirata</i> stem extract at (a) different ferric chloride concentrations (b) different plant extract concentrations (c) different pH (d) different temperatures (e) different incubation time	41
4.2	Image showing (a) zeta potential and (b) size distribution pattern of synthesized IONPs	42

4.3	X-ray diffraction pattern of <i>S. chirata</i> synthesized IONPs	43
4.4	(a) SEM image (b) EDX spectra and (c) TEM image of IONPs	44
4.5	Atomic force microscope images of (a) 2- dimensional image (b) 3-dimensional image and (c) size distribution graph of synthesized IONPs	45
4.6	FTIR spectra of synthesized IONPs along with the FTIR spectra of <i>S. chirata</i> plant extract	46
4.7	Langmuir adsorption isotherm of <i>S. chirata</i> synthesized IONPs on SS 316L surface with the weight loss measurements in Ringer's solution	48
4.8	Electrochemical studies of the effect of different concentrations <i>S. chirata</i> synthesized IONPs on SS 316L surface (a) Nyquist plot (b) Tafel plot (c) Bode plot and (d) phase angle plot in Ringer's solution	50
4.9	Images showing (a) SEM micrograph of SS 316L (b) SEM micrograph of SS 316L immersed only in Ringer's solution (c) SEM micrograph of SS 316L immersed in Ringer's solution with IONPs (d) AFM micrograph of SS 316L (b) AFM micrograph of SS 316L immersed only in Ringer's solution (c) AFM micrograph of SS 316L immersed in Ringer's solution with IONPs	52
4.10	Langmuir adsorption isotherm of <i>S. chirata</i> synthesized IONPs on SS 316L surface with the weight loss measurements in Hank's solution	54
4.11	Electrochemical studies of the effect of different concentrations <i>S. chirata</i> synthesized IONPs on SS 316L surface (a) Nyquist plot (b) Tafel plot (c) Bode plot and (d) phase angle plot in Hank's solution	56
4.12	Images showing (a) SEM micrograph of SS 316L (b) SEM micrograph of SS 316L immersed only in Hank's solution (c) SEM micrograph of SS 316L immersed in Hank's solution with	58



	IONPs (d) AFM micrograph of SS 316L (b) AFM micrograph of SS 316L immersed only in Hank's solution (c) AFM micrograph of SS 316L immersed in Hank's solution with IONPs	
4.13	Langmuir adsorption isotherm of <i>S. chirata</i> synthesized IONPs on SS 316L surface with the weight loss measurements in PBS	59
4.14	Electrochemical studies of the effect of different concentrations <i>S. chirata</i> synthesized IONPs on SS 316L surface (a) Nyquist plot (b) Tafel plot (c) Bode plot and (d) phase angle plot in PBS	61
4.15	Images showing (a) SEM micrograph of SS 316L (b) SEM micrograph of SS 316L immersed only in PBS (c) SEM micrograph of SS 316L immersed in PBS with IONPs (d) AFM micrograph of SS 316L (b) AFM micrograph of SS 316L immersed only in PBS (c) AFM micrograph of SS 316L immersed in PBS with IONPs	63
4.16	UV-vis spectroscopy of IONPs synthesized from <i>T. arjuna</i> bark extract at (a) different ferric chloride concentrations (b) different plant extract concentrations (c) different pH (d) different temperatures (e) different incubation time	65
4.17	Image showing (a) zeta potential and (b) size distribution pattern of synthesized IONPs	66
4.18	X-ray diffraction pattern of <i>T. arjuna</i> synthesized IONPs	67
4.19	(a) SEM image (b) EDX spectra and (c) TEM image of IONPs	68
4.20	Atomic force microscope images of (a) 2- dimensional image (b) 3-dimensional image and (c) size distribution graph of synthesized IONPs	69
4.21	FTIR spectra of synthesized IONPs along with the FTIR spectra of <i>T. arjuna</i> plant extract	70
4.22	Langmuir adsorption isotherm of <i>T. arjuna</i> synthesized IONPs on SS 316L surface with the weight loss measurements in Ringer's solution	71

4.23	Electrochemical studies of the effect of different concentrations <i>T. arjuna</i> synthesized IONPs on SS 316L surface (a) Nyquist plot (b) Tafel plot (c) Bode plot and (d) phase angle plot in Ringer's solution	72
4.24	Images showing (a) SEM micrograph of SS 316L (b) SEM micrograph of SS 316L immersed only in Ringer's solution (c) SEM micrograph of SS 316L immersed in Ringer's solution with IONPs (d) AFM micrograph of SS 316L (b) AFM micrograph of SS 316L immersed only in Ringer's solution (c) AFM micrograph of SS 316L immersed in Ringer's solution with IONPs	75
4.25	Langmuir adsorption isotherm of <i>T. arjuna</i> synthesized IONPs on SS 316L surface with the weight loss measurements in Hank's solution	76
4.26	Electrochemical studies of the effect of different concentrations <i>T. arjuna</i> synthesized IONPs on SS 316L surface (a) Nyquist plot (b) Tafel plot (c) Bode plot and (d) phase angle plot in Hank's solution	77
4.27	Images showing (a) SEM micrograph of SS 316L (b) SEM micrograph of SS 316L immersed only in Hank's solution (c) SEM micrograph of SS 316L immersed in Hank's solution with IONPs (d) AFM micrograph of SS 316L (b) AFM micrograph of SS 316L immersed only in Hank's solution (c) AFM micrograph of SS 316L immersed in Hank's solution with IONPs	79
4.28	Langmuir adsorption isotherm of <i>T. arjuna</i> synthesized IONPs on SS 316L surface with the weight loss measurements in PBS	80
4.29	Electrochemical studies of the effect of different concentrations <i>T. arjuna</i> synthesized IONPs on SS 316L surface (a) Nyquist plot (b) Tafel plot (c) Bode plot and (d) phase angle plot in PBS	83
4.30	Images showing (a) SEM micrograph of SS 316L (b) SEM micrograph of SS 316L immersed only in PBS (c) SEM micrograph of SS 316L immersed in PBS with IONPs (d) AFM micrograph of SS 316L (b) AFM micrograph of SS 316L	84

	immersed only in PBS (c) AFM micrograph of SS 316L immersed in PBS with IONPs	
4.31	UV-vis spectroscopy of IONPs synthesized from <i>F. benghalensis</i> stem extract at (a) different ferric chloride concentrations (b) different plant extract concentrations (c) different pH (d) different temperatures (e) different incubation time	86
4.32	Image showing (a) zeta potential and (b) size distribution pattern of synthesized IONPs	87
4.33	X-ray diffraction pattern of <i>F. benghalensis</i> synthesized IONPs	88
4.34	(a) SEM image (b) EDX spectra and (c) TEM image of IONPs	89
4.35	Atomic force microscope images of (a) 2- dimensional image (b) 3-dimensional image and (c) size distribution graph of synthesized IONPs	90
4.36	FTIR spectra of synthesized IONPs along with the FTIR spectra of <i>F. benghalensis</i> plant extract	91
4.37	Langmuir adsorption isotherm of <i>F. benghalensis</i> synthesized IONPs on SS 316L surface with the weight loss measurements in Ringer's solution	92
4.38	Electrochemical studies of the effect of different concentrations <i>F. benghalensis</i> synthesized IONPs on SS 316L surface (a) Nyquist plot (b) Tafel plot (c) Bode plot and (d) phase angle plot in Ringer's solution	93
4.39	Images showing (a) SEM micrograph of SS 316L (b) SEM micrograph of SS 316L immersed only in Ringer's solution (c) SEM micrograph of SS 316L immersed in Ringer's solution with IONPs (d) AFM micrograph of SS 316L (b) AFM micrograph of SS 316L immersed only in Ringer's solution (c) AFM micrograph of SS 316L immersed in Ringer's solution with IONPs	95
4.40	Langmuir adsorption isotherm of <i>F. benghalensis</i> synthesized	96

	IONPs on SS 316L surface with the weight loss measurements in Hank's solution	
4.41	Electrochemical studies of the effect of different concentrations <i>F. benghalensis</i> synthesized IONPs on SS 316L surface (a) Nyquist plot (b) Tafel plot (c) Bode plot and (d) phase angle plot in Hank's solution	98
4.42	Images showing (a) SEM micrograph of SS 316L (b) SEM micrograph of SS 316L immersed only in Hank's solution (c) SEM micrograph of SS 316L immersed in Hank's solution with IONPs (d) AFM micrograph of SS 316L (b) AFM micrograph of SS 316L immersed only in Hank's solution (c) AFM micrograph of SS 316L immersed in Hank's solution with IONPs	100
4.43	Langmuir adsorption isotherm of <i>F. benghalensis</i> synthesized IONPs on SS 316L surface with the weight loss measurements in PBS	101
4.44	Electrochemical studies of the effect of different concentrations <i>F. benghalensis</i> synthesized IONPs on SS 316L surface (a) Nyquist plot (b) Tafel plot (c) Bode plot and (d) phase angle plot in PBS	103
4.45	Images showing (a) SEM micrograph of SS 316L (b) SEM micrograph of SS 316L immersed only in PBS (c) SEM micrograph of SS 316L immersed in PBS with IONPs (d) AFM micrograph of SS 316L (b) AFM micrograph of SS 316L immersed only in PBS (c) AFM micrograph of SS 316L immersed in PBS with IONPs	105

### List of Abbreviations

SS	Stainless Steel
NPs	Nanoparticles
INPs	Iron Nanoparticles
IONPs	Iron Oxide Nanoparticles
ASTM	American Standards for Testing of Materials
MRI	Magnetic Resonance Imaging
FTIR	Fourier Transform Infrared
DFT	Density Functional Theory
MD	Molecular Dynamics
XRD	X-Ray Diffraction
PBS	Phosphate Buffer Saline
C	Concentration
IE	Inhibition Efficiency
SEM	Scanning Electron Microscopy
EDX	Energy Dispersive X- ray
AFM	Atomic Force Microscopy
TEM	Transmission Electron Microscopy
EIS	Electrochemical Impedance Spectroscopy

PDP	Potentiodynamic polarization
$I_{corr}^0$	Corrosion Current Density
$E_{corr}$	Corrosion Potential
$R_{ct}$	Charge Transfer Resistance
$C_R$	Corrosion Rate
$\theta$	Surface Coverage

## **CHAPTER 1**

### **INTRODUCTION**

Metals have a natural tendency to interact with their surrounding components which make them more vulnerable to corrosion process and finally to its destruction. This interaction initiates the reactions of electrochemical nature on interface of the metal and its environment. Thus, the metallic material is converted into its more stable form by forming oxides or hydroxides and this phenomenon is known as corrosion. It is an unavoidable process and this is the main problem which needs to be addressed. Industries face serious problems due to this process as metal loss occurs and lots of money is spent each year to rectify the losses occurred due to corrosion [1].

For the biomedical purpose, materials of metallic nature are widely employed and comes under the most dominant type of material which has high tension loading capacity as required for the implant and are modified in such a way that they can be helpful in providing support to body organs [2]. The metallic biomaterials are mostly employed for use in replacement of joints like knee and hip joints, as fixation device for spinal injuries, nails, plates and screws for bones, implants for dental use, stents and fixation units for orthopaedic applications. Apart from this, they have also earned great attention for the development of cardiovascular devices and neurovascular implants [3]. Metals' excellent electrical conductivity makes them ideal for devices used for neuromuscular stimulation, the most popular of which are pacemakers which are used for cardiac applications. Metallic biomaterials can be used to replace or repair failed hard tissue and also for the restoration of blood vessels and other soft tissues [4].

The use of implants has increased in the past years due to advancement in the medical and healthcare industry. The biological requirements determine the extent of use of biomedical implants. The biomaterials are used to evaluate and treat, increase the functioning of the damaged part of the body and permanently remove the nonfunctioning organ of the body [5, 6].

## **1.1 Metals and their use as biomaterials**

Metals and their alloys, ceramic materials, polymeric materials, and composite materials are now used to make biomaterials. Stainless steels (SS), alloys of cobalt and chromium, and alloys of titanium are some notable biomaterials applied for biomedical applications [7]. These are also used to make crowns, dentures, inlays, and bridges, among other dental prosthetics. Corrosion is a major consideration when metals and their alloys are selected and specially designed for their use in-vivo. During corrosion processes, allergenic or carcinogenic compounds can be released into the host body [8]. Furthermore, implant loosening and failure can be caused by a variety of corrosion mechanisms. As a result, biomaterials are frequently subjected to corrosion and/or solubility tests before being authorized for use. As a result, for the assurance of quality, analysis of retrieved implants, and their failure mechanisms, the occurrence of corrosion and their corrosion behaviour has been extensively studied [9].

## **1.2 Metal corrosion in human body**

When a metallic material is placed in the harsh body environments then the process of degradation of material starts gradually by electrochemical reactions and this process is termed as corrosion. The body fluid, body constituents containing several ions, water etc. makes hostile environment for implant device which make them more prone to corrosion [10]. Various anions like chloride, bicarbonate, phosphate ions and cations like sodium, calcium, potassium, magnesium and dissolved oxygen are the main components of aqueous medium of the human body [11, 12].

The pH of the human body also determines the rate of corrosion. In normal conditions, the human body maintains a pH of 7 but this pH is varied in cases of accidents, imbalances in the physiological systems and infections. Although, it is considered that the oxide layers formed on the surface of SS (or metal) help in preventing corrosion but clinical evidences suggested that there is release of metal ions in the surrounding tissue due to leaching process and this leaching has been linked to the corrosion process [13].



When an implant is placed in a biological system, it triggers a mutual interaction in which cells present in the close proximity to the implants are first to respond [14]. After that, the cells who are far away from the implant may experience alterations as a result of the corrosion initiation of corrosion process and its products. The occurrence of tissue reaction to implants is time-dependent. The severity of the reactions can be influenced by a number of factors, including the geometry of the implant, any friction or motion, the type of the corrosion products, and their bioactivities.

Due to the corrosion in human body, the ions from the metallic surfaces drain out of the implant site to nearby sites thus affecting the biological activities severely.

When the implant material begins to corrode, the metal dissolution occurs causing erosion, leading to the implant being brittle and fractured. If the metal pieces are not surgically removed, they may disintegrate and fragment further, causing irritation in the surrounding tissues. Corrosion products cause adverse reactions when present in the biological systems and several studies have been reported which discuss about the levels of corrosion products in the body tissues including their presence in organs like liver, kidney and blood [15]. In an in vivo environment, the metals in implant biomaterials can corrode, and the liberated ions trigger the immune system by creating protein complexes [16].

### **1.3 Corrosion control and nanotechnology**

Efforts have been made to establish suitable methods for controlling corrosion, as well as strategies to reduce the rate of corrosion by delaying or entirely preventing the anodic or cathodic reaction, or both. Corrosion damage can be avoided by a variety of approaches, including material upgradation, production fluid blending, process control, and chemical inhibition [17].

Nanotechnology is the modification of matter to the point where one of the dimensions of the matter is in the nanometric range (1–100nm). Since nanoparticles (NPs) have huge specific surface properties, increased surface energy and quantum properties, nanoscale particles have a variety of unique features in terms of their optical, magnetic, and electrical properties [18]. NPs find several applications in medical [19],

cosmetics, electronics, food and chemical industry because to their unique physicochemical features.

The employment of hazardous solvents and chemicals in the chemical process of nanoparticle production is a major drawback, as it affects our fragile ecosystem. Due to extensive use of chemicals for the production of NPs urged the need for development of new technologies for the synthesis process which will employ less chemicals and hence do no effect the environment also. The introduction of green nanotechnology has evolved the ways of NPs synthesis by its cost-effective ways for the production of NPs which are also environment friendly nature. The resulting NPs are free of hazardous substances and environmentally beneficial [20].

Nanotechnology is a rapidly evolving field with numerous research applications. They have found numerous ways of their application in diverse fields such as industrial environmental, biomedical, agriculture, and food [21]. One of the most important area of NPs application in the industrial field is their ability to protect metals from corrosion in a variety of conditions. Nanomaterials and their additives are effective corrosion inhibitors. By blocking active sites on metal surfaces, nano-compounds inhibit surface reactions and limit corrosion rates, as well as providing hardness and stability to the metal surfaces [22]. Metals and their oxide NPs are effective and efficient corrosion inhibitors. These are simple to use on metal surfaces. Many studies have shown that adsorption of metal NPs and their formed oxides on surfaces can reduce corrosion. Metal and their oxide NPs of silver, copper oxide, silicon dioxide, titanium dioxide, zinc oxide etc. have been used as corrosion inhibitors [23].

The current focus of attention is on nanotechnology-enabled metal NPs production. When compared to traditional macro particles, NPs have unique features. Their enormous surface to volume ratio [24] is credited with their unique and remarkable qualities. Corrosion experts have revealed plant extract mediated metal NPs as low-cost, safe, and ecologically friendly products that can be used as metal anticorrosive substances. Metal NPs are thought to have the ability to chemisorb on metal surfaces, preventing corrosion [25]. Nanomaterials, whether nanosized or nanostructured, can be used for corrosion control methods considering the two important factors: first, the understanding of corrosion behaviors of nanostructured materials; and second,

whether a nanostructured material has better corrosion resistance (e.g. corrosion/oxidation/cracking resistance of a steel which is nanostructured) than its micro-structured counterpart and the second factor is where nanotechnology enabled corrosion control benefits are significant. The nanosized materials may be efficiently exploited in corrosion prevention as an automobile or aerospace paint. The corrosion monitoring and inspection industries are likely to benefit from nano technological breakthroughs. Alternatives to chromate conversion coatings, which are harmful due to the presence of poisonous hexavalent chromium, have also been explored [26]. Hence, nanotechnology enabled methods can be developed for better corrosion resistant properties. Fig.1.1 shows the factors influencing biomedical corrosion and different strategies which can be employed to prevent the corrosion process.

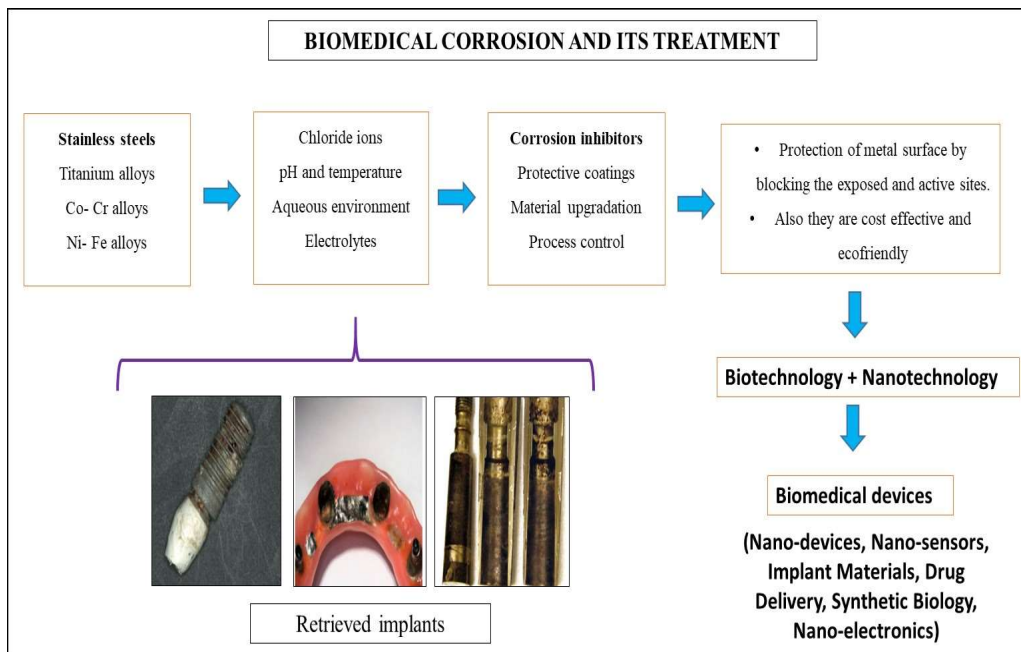


Fig. 1.1 Biomedical corrosion and their treatment strategies

## CHAPTER 2

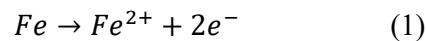
### LITERATURE REVIEW AND PROBLEM FORMULATION

#### 2.1 Factors influencing corrosion process

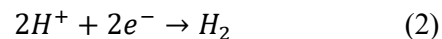
The process of corrosion is natural and like other natural processes, corrosion occurs to reach to the possible lowest energy level. Hence, metals like iron and steel combine with other chemical compounds to stabilize themselves by attaining the lower energy state. To achieve this state, metals combine with water molecules and oxygen from the surroundings to form rust also known as hydrated iron oxides. The iron oxides formed by this process resembles the composition of the original iron ore [27]. The compounds which are formed are known as corrosion products. In the corrosion process, there is movement of ions from the metal to active sites also referred to as anodic site and transfer of electrons to cathodic site which is less active and act as acceptor site, occurrence of ionic current in the solution in which metal is placed and subsequently the flow of electronic current over the metal surface. This process often requires the electron acceptor molecules such as oxygen, oxidizing agents and hydrogen ions [28]. Generally, the metals degrade when there is presence of moisture, salts, acids, bases, gases etc. The corrosive environment can be characterized as physical state which includes solid, liquid or gas, chemical state including chemical constituents and their concentrations, and temperature. Besides these, there are other factors like solution velocity, mechanical load and residual stress on the material [29].

The corrosion process includes an oxidation and reduction reactions at anode and cathode respectively. The general reactions taking place are as following:

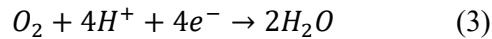
- Oxidation at anode



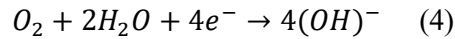
- Reduction at cathode



- Reaction in acidic solution



- Reaction in basic or neutral solution



A variety of internal and external elements influence the corrosion process. Internal factors include factors related to metal, such as metal structure, surface composition, presence of protective layers on the surface, and processing method [30]. Pure metals do not corrode but metals that contain various impurities corrode due to the existence of these impurities in them. External factors are those that go along with corrosion environments, such as the nature of the medium and its chemical makeup, the availability of speeding or inhibiting substances in the medium, the movement of the electrolyte, temperature, pressure, and so on. The concluding factors affecting the rate of corrosion are impurities of the metal which help in the set up voltaic cells, electrolytes present in the corrosive media, presence of carbon dioxide like gases in the corrosive environment etc. [31].

The classification of corrosion is mainly based on three factors

- a) Nature of corroding material: It generally includes dry or wet corrodent. For dry corrosion, there is involvement of gases in corrosive environment while wet corrosion includes the presence of liquid or moisture content
- b) Corrosion mechanism: Depends on the type of reactions occurred like electrochemical or general chemical reactions
- c) Corroded metal appearance: Whether the corrosion occurs at the same rate at whole surface of metal, or corrosion of small areas, cracking on the steel surface

Because industry relies largely on the usage of metallic materials, protecting metals from corrosion has become one of the hardest and difficult tasks. Corrosion is a common problem that affects numerous industrial processes, causing degradation and ultimate failure of equipment materials in the manufacturing and processing industries, as well as a reduction in the service life of key elements (fig. 2.1) [32]. Metal and alloy corrosion control is an expensive process, and companies invest a lot

of money to combat it. In the oil, fertilizer, metallurgical, and other industries, combating metal corrosion in acid media is a severe environmental challenge.

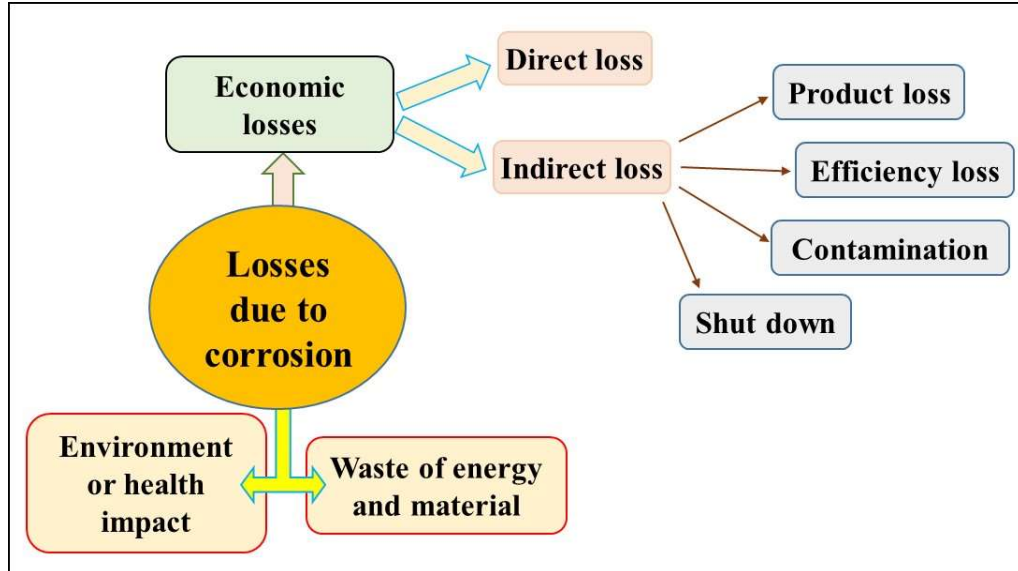


Fig. 2.1 Losses faced by industry due to corrosion

## 2.2 Interactions of implant material in human body

A novel biomaterial's specified anatomic position, pathobiology of activities of tissue, specific mechanical properties, and compatibility with the biological environment, the healing process, and standardization of materials, their regulation and ethical clearance are all taken into account before it is introduced onto the market. International bodies, namely the International Standards Organization (ISO) and the American Society for Testing and Materials (ASTM) [33] which are authorized to issue materials or devices, and their process standards. The countries like United States and Europe have built regulatory procedures to prevent ineffectively analysed devices and other materials from reaching the market, as well as to filter businesses that are plainly ineligible to make biomaterials. In the United States, the assessment is done by a government agency (USFDA), but Notified Bodies (NBs) work for such issues in Europe [34]. A biomaterial's biocompatibility is a must-have feature. In a certain application, a biocompatible substance produces an adequate host reaction (less interruption of normal body function). As a result, in vivo the substance has no thrombogenic, toxic, or allergic inflammatory reaction. The reactions induced into the

host body by implant materials and the material degradation are the two main factors which are essential to determine the biocompatible property of material [35]. Understanding the success of implants requires a thorough examination of the metallic biomaterial. The most often utilized inert metals for prosthetic devices, angioplasty, and bone re-modelling are surgical SS (316L), titanium (Ti) alloys and cobalt-chromium (CoCr) alloys [36]. This is because of their long-term stability in highly reactive in vivo environments. Material deterioration may occur in highly reactive surroundings, resulting in local tissue injury and inflammatory reactions. The principal concerns linked with the injury are metal hypersensitivity and progressive osteolysis of neighbouring tissues [37]. The passive film is formed on the surface of biomaterials which makes them physiological inert and resistant to corrosion. The adverse effects like inflammation, dissolution, stress shielding and restenosis are prevented by formation of these inert oxide layers in implant devices used. Therefore, the metallic material like SS, cobalt- chromium alloy and titanium- based alloys have low corrosion rate and are well protected. Hence the longevity of implant materials is assured by keeping the rate of corrosion under control [38]. The quantity and chemical composition are the major factors which determine the corrosion potential. Apart from this, the microstructural and surface characteristics are also important to analyse the rate of corrosion of metallic material [39]. The properties like chemical nature and their type along with the temperature and pressure determine the corrosion process in the nearby tissue surrounding the implant. Furthermore, the dominance of the corrosion type is determined by the implant's working condition (static and dynamic loads), as well as the implant's construction and thermomechanical properties such as dislocation density, point defects and stress on the material [40]. The equilibrium of the implant surface is disturbed by the presence of these ions from biological media by the initiation of electrochemical reactions at both the sites i.e. anodic and cathodic. The proteins from the surrounding tissues bind themselves to the metal ions and upset the surface equilibrium by transferring the ions at different sites which make the disturbance at the double layer at the surface site by the movement of electrons and transport of extra cations in the solution. Also the absorbed protein molecules decrease the rate of diffusion which cause corrosion at certain sites [41]. The hydrogen ion formed due to reaction at cathodic site can act as corrosion inhibitor but the

microorganism presents at the site of hydrogen release consume the readily formed hydrogen thus making the implant more prone to corrosion.

The total amount of water present in the body is approximately 40 to 60% of the whole body mass. This water in the body is mainly distinguished as two types which are intracellular fluid and other one is extracellular fluid. This division is based on the functionality of the fluid. The extracellular fluid makes up for blood plasma, the fluid surrounding the cells, lymph and also the transcellular fluids. The water inside the cells is referred to as intracellular fluid (ICF). The balance between the distribution of body fluids and other electrolytes is maintained at normal to sustain the body requirements by the process of homeostasis [42]. Electrolytes are essential for proper body function. The electrolytes play an important role in metabolism of the body processes. They also help in determining the potential of cell membrane and maintains the osmolarity of the fluids of body. The main cations which function as electrolytes include hydrogen ion, sodium ion, potassium and calcium ion etc. while the main anions include bicarbonate ion, hydroxide ion, chloride ion etc. these dissolved ions are the major causes of in vivo corrosion process of implant devices. The presence of chloride ions actively disturbs the electrochemical equilibrium at the metal surface and obstruct numerous corrosion-prevention techniques. Temperature and pH are two significant elements that influence material deterioration. The normal body temperature of 37°C is one of the major causes of corrosion as the implant is continuously exposed to this temperature for lifetime [43]. Also, it is continuously exposed to the body fluid and due to this, the implant's exposed metal surface undergoes a finite rate of electrochemical material breakdown. Water, complex chemical molecules, dissolved oxygen, phosphate, potassium, sodium, bicarbonate, chloride, calcium, magnesium, proteins, amino acids, plasma, lymph, saliva and other substances can all be found in the human body's environment [44].

Corrosion can begin as a result of a variety of situations on the implant surface, the localized electrochemical cell is created which leads to pitting corrosion, the occurrence of crevice corrosion can be seen at the plate-locking screw interface. The implantation of the foreign body, of course, damages and changes the interior environment. Hematomas gather at the tissue implant contact and impact the surface



conditions. Additional alterations in the interface conditions may kill some soft tissue and bone. The pH is also crucial, and a variety of disorders might arise as a result of the procedure. After surgery, the pH drops significantly as a result of the damage reaction, CO<sub>2</sub> gathers at the implant site and pH is also lowered to 4 or 5. If the free circulation of blood and diffusion of gases is hindered, the normal conditions in the human body take some time to restore and sometimes the restoration may not occur signifying some problems at the site. The presence of infection can cause the pH to shift to the alkaline side of the scale, which can have negative repercussions for the implant [45]. Fig. 2.2 shows the possible types of effects caused due to bio-implant corrosion.

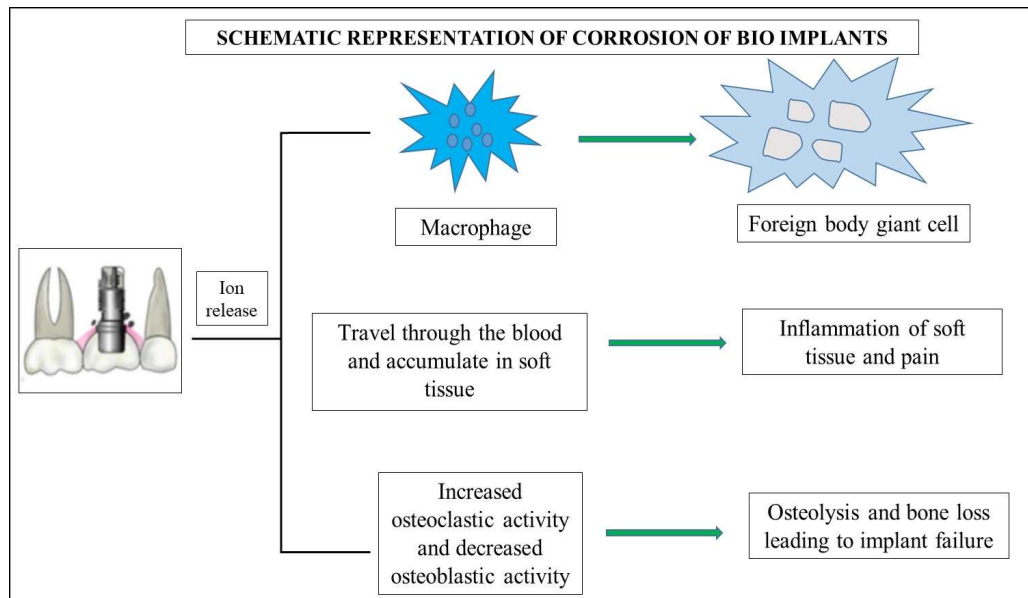


Fig. 2.2 Effect of corrosion of bio-implants in human body [13]

### 2.3 Types of corrosion occurring in metallic materials

Surgical implants are typically constructed of one of three types of materials: austenitic SS, titanium and its alloys or, cobalt-chromium alloy, with 316L austenitic SS being the most widely used implant material due to its low cost. The grades 316 and 316L are the most regularly used steel alloys. The SS 316L type SS is highly recommended by ASTM for its low carbon content which helps in reducing its probability of formation of chromium carbide, which leads to intergranular corrosion. Lower the carbon content, the more corrosion resistant this type of SS becomes

making it resistant to chlorine-containing fluids in the human body, such as physiological saline [46]. However, chloride ions and reduced sulphur compounds can cause localized corrosion in stainless steel [47]. Highly localized changes caused by the presence of microorganisms on the surface of metal frequently by altering the concentration of electrolytic components, as well as pH and oxygen levels [48]. More than 90% of the implant failure of 316L SS happens due to pitting and crevice corrosion attack [49]. These localized corrosion attacks and metallic ion leaching from implants demand bulk alloying or surface modification to improve the corrosion resistance of the currently used 316L SS [50]. Biomedical materials which are deployed for cyclic loading and high stresses, fail owing to fatigue in the presence of a harsh environment [51]. The oxide layer is disrupted during fatigue, and the material's inability to passivate quickly results in corrosion. Fatigue strength is reduced dramatically when re-passivation was suppressed, demonstrating the role of oxide layer formation in evaluating the fatigue life of materials subjected to harsh corrosive environments [52]. Furthermore, fretting between the implant and the bone has been reported to exacerbate fatigue since re-passivation is more difficult in the presence of fretting. Different types of corrosion occurring in materials used for biological application at different locations are given in Fig. 2.3.

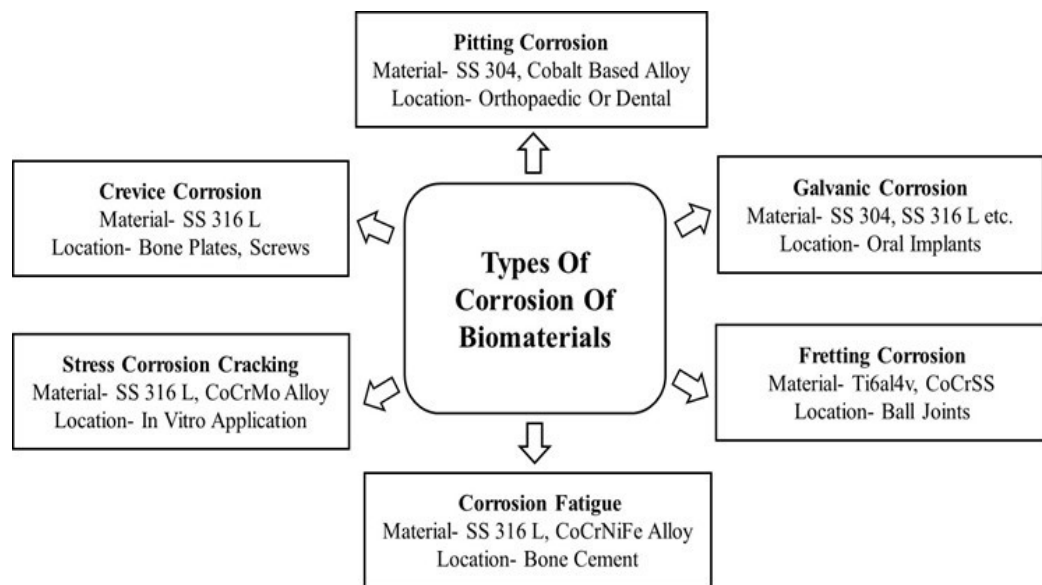


Fig. 2.3 Types of corrosion of materials used for biological application at different locations.

Corrosion failure affects the performance of permanent implants as well as the behaviour of temporary implants manufactured of surgical grade type 316L stainless steel [53]. Magnesium and its alloys, on the other hand, quickly corrode due to the presence of ions in the physiological fluids causing mechanical integrity to be lost before the tissues have had enough time to recover [54]. The type of nature of corrosion products and their distribution into the body by orthopedic implants, on the other hand, remains a major concern [55]. As a result, various researchers are actively working to improve the surface properties of titanium-based alloys [56].

The body's hypersensitive reactions are triggered by these metal protein complexes. Sensitizers include beryllium, nickel, cobalt, and chromium, with tantalum, titanium, and vanadium showing infrequent responses. Nickel, cobalt, and chromium are the most common metal sensitizers in humans [57]. Swelling, itching, and the production of rashes (dermatitis), as well as asthma, are the most common symptoms associated with allergic reactions to metal. Symptoms differ based on the allergen and the individual. Symptoms of dental implantation might appear at the implant site or elsewhere in the mouth [58]. The body's high-water content, which forms a vast "pool" in which corrosion processes must balance, is neglected. The body is 70% water, with a 14-litre extracellular volume and a 28-litre intracellular volume. Water intake and excretion, which can reach 2.5 litres every 24 hours, results in an effective pool of 1000 litres per year [59, 60].

## **2.4 Corrosion Inhibitors**

For better corrosion control, selection of better material, inhibitors, materials for coating and modifications in the design of machinery are highly employed. The use of corrosion inhibitors is the most widely employed approach out of all the corrosion preventive methods. The properties like adsorption of protective ions on the surface of the metal, ability to influence the electrochemical reactions, lowering the reactants diffusion rates at the metal surface etc. gives the advantage to the corrosion inhibitors to be used widely. However, factors like cost effectiveness, easy availability and safety to environment are the main points which are taken into account while selecting a corrosion inhibitor [61]. Heteroatoms like oxygen, sulphur, nitrogen etc. are generally found in organic inhibitors and have the property of higher basicity and

electron density which makes them helpful to be used as inhibitor for corrosion. This type of inhibitors prevents the corrosion by binding themselves in place of water molecules on the surface of the metal and form a strong protective barrier [62]. The transfer of electrons from inhibitor molecules to the surface of metal is done by the non-bonded or lone pair and  $\pi$ -electrons from inhibitor [63]. The chemical structure and physical qualities of an organic inhibitor like presence of functional groups, p-orbital character, are some of the factors that influence its performance. The inhibition could be caused by (i) adsorption of molecules or their ions on the active sites of metal surface, (ii) by increasing the voltage at anodic or cathodic sites and (iii) protective barrier film formation. Chain length, bond strength, molecule bonding, crosslinking ability, molecule size, and solubility are the characteristics that influence inhibitor action. Inhibitors protect molecular layers from acid damage by forming a barrier [64]. This protective effect is linked to chemical and/or physical adsorption, which involves a change in the charge of the adsorbed substance as well as charge transfer from one phase to the next. Corrosion inhibitors that contain sulphur and/or nitrogen and have a variety of substituents and are thought to be effective. For preventing metal corrosion in acid solutions, the use of thiophene and hydrazine derivatives serve a good purpose. Phosphates, chromates, dichromate, molybdate silicates, tungstate, borates and arsenic compounds have been used effectively as corrosion inhibitors for metals in different media [65]. These inhibitors are extensively used for the manufacture of primers and anticorrosive coatings. The major concern posed by such inhibitors is their toxic nature and for this reason their use has been heavily criticized. The alternative form of corrosion inhibitors is identified and the compounds containing nitrogen, oxygen and sulphur like polar functional groups are of good choice in the form of organic inhibitors [66, 67].

## **2.5 Advantage of green corrosion inhibitors**

Green synthesized corrosion inhibitors, often known as "eco-friendly inhibitors," are compounds which are biodegradable in nature and are free of any heavy metals and other harmful substances. They're biocompatible with the environment. Natural compounds as corrosion inhibitors have sparked a lot of interest in the scientific community [68, 69]. There has been a flood of study into corrosion inhibition using

extracts from various parts of the plant. Plant extracts as corrosion inhibitors in various types of corrosive conditions have been reported by some authors. Organic and inorganic inhibitors are the two main categories of green corrosion inhibitors. Alkaloids, quinones, phenol, organic acid, and phenylpropanoid flavonoids along with other natural compounds obtained from natural sources such as plants are examples of organic green inhibitors [70]. Plant extracts, gums, medicines, and oils have all been used as green corrosion inhibitors for corrosion. Another strategy to expand the applicability of usage of plants and hence improve municipal waste management is to use plant wastes as corrosion inhibitors. Alkaloids, flavonoids steroids, tannins, phenolic compounds, and terpenoids are some of the bioactive molecules found in aquatic plants, and the majority of them are known to have corrosion inhibitory properties [71]. Many active components can be found in plant extracts. These comprises of polar or heteroatoms containing sulphur, nitrogen, oxygen, phosphorous, and aromatic rings, which enhance adsorption via a donor-acceptor interaction between donor atom electrons and metal surface atoms' unoccupied d-orbitals [72]. The metal surface is separated from the contact of corrosive solution by the formation of a protective layer due to the adsorption of the molecules from the inhibitors thereby preventing the metal substrate from deterioration. Mild steel [73], different kinds of steel [74], cast iron [75], aluminum and its alloys, zinc and its alloys, and copper [76] have been treated with large amounts of organic extracts of plant materials. Most studies to test the anticorrosive nature of plant extracts is done in acidic medium rather than in basic medium [77]. To decrease corrosion, various plant elements such as roots, leaves, bark, flowers, and fruits (shell, juice, and seed) has been employed. Since then, green inhibitors have demonstrated much improved environmental qualities as compared to current inhibitors with hazardous levels exceeding 50%. Inorganic green inhibitors work by increasing the passivity of metals and alloys [78]. Many studies have reported that naturally occurring chemicals can effectively prevent metal corrosion in both acidic and alkaline environments [79].

## **2.6 Metal NPs and their synthesis**

Metallic NPs synthesis can be done in various ways including physical, chemical, and biological methods [80]. The mechanisms for NPs synthesis includes numerous

physicochemical and biological methods and can be divided into two categories: top-down approach and the bottom-up approach [81]. The physical methods of NPs synthesis require lots of time and also consume huge amount of energy which raise the temperature of the surroundings [82]. As a result, the physical synthesis process is ineffective for producing NPs. While the chemical synthesis methods employ use of chemicals which act as strong reducing agents [83]. For these reasons, biological synthesis pathways are favored for the production of NPs over physical and chemical synthesis approaches. Bacteria [84], fungus, algae, and plants are used in the biological synthesis process for the creation of NPs. The use of microbes for the generation of NPs is in practice but their pathogenicity problem along with the problem of maintenance of large number of cultures are some of the difficulties which arise while using microorganisms. Also, the synthesis process is slow with the use of microbes. When the plant parts are used for the reduction of metal ions then this process is known as green NPs synthesis [85]. The mechanism of green synthesis by plant based reducing agents is highly preferred due to the use of nontoxic and cost-effective materials. Further, the synthesis by this method can be scaled up easily. Since there is no use of microbes, so this method also does not possess any biohazard. Green synthesis has been used to make a variety of NPs, including silver, gold, palladium, iron, and zinc oxide [86]. The phytochemicals found in plant extracts, such as polyphenols, terpenoids, and polyols are responsible for the bio-reduction of metallic ions. Because of the phytochemicals that reduce them to NPs, the NPs have outstanding antibacterial, antioxidant, and catalytic characteristics [87].

## **2.7 Plant based green synthesis of NPs**

NPs can be made in a variety of methods, but the production of NPs via physical and chemical pathways causes toxicity and environmental concerns [88]. Plant extracts have several advantages over microbes in terms of silver NPs synthesis: they are readily available, harmless, and nontoxic in most situations. These have a wide range of metabolites that can aid in the reduction of metal ions, and are faster to synthesize. Plant-assisted reduction is the key mechanism postulated for this process due to phytochemicals. Steroids, saponins, carbohydrates, and flavonoids are present relatively in high amounts, operate as reducing agents while phytoconstituents act as

capping agents, providing stability to silver NPs [89]. Plant-mediated nanomaterial synthesis has significantly greater kinetics than other biosynthetic approaches that are comparable to chemical NPs formation. The production and stabilization of NPs generated by biological entities are controlled by a variety of parameters as following:

- pH of the reaction medium is one of the parameters that influences biogenic NPs formation. The pH of the reaction media is critical in determining the morphological features of the NPs [90].
- Temperature of the reaction has an important influence in the synthesis of metallic NPs, influencing structural features of the final NPs.
- The NPs synthesized from this route are considered better and superior in quality as compared to other synthetic routes [91].
- The length of time spent incubating NPs has a significant impact on their quality and form. Long periods of NPs incubation may cause aggregation or shrinkage, lowering the NPs' potential [92].

As a result, it can be argued that green biotechnology has emerged as a key instrument for producing environmentally safe, nontoxic, and cost-effective NPs. Nano biotechnology has huge promise and a wide range of undiscovered applications. Green synthesis is used to create several types of NPs that can then be used in a variety of applications [93].

## **2.8 Iron Oxide Nanoparticles (IONPs)**

IONPs are among the most fascinating novel materials due to their extraordinary properties and biomedical applications [94]. IONPs (magnetite;  $\text{Fe}_3\text{O}_4$ , hematite:  $\text{Fe}_2\text{O}_3$ , maghemite;  $-\text{Fe}_2\text{O}_3$ ), iron oxide hydroxide NPs, and zero-valent iron NPs are the three main categories of IONPs. Drug delivery, hyperthermia, stem cell sorting, magnetic targeting, negative MRI contrast enhancement, thermal-ablation, gene therapy, bio-separation, antimicrobial agents, environmental remediation, food preservation, ferro-fluids, bioprocess intensification, lithium-ion batteries, and pigments are just a few of the applications for these particles [95]. For the generation of IONPs, various physical and chemical techniques have been established to date.

Biological systems, such as plants, algae, and various microorganisms, have been used by several researchers to synthesize IONPs (yeast, fungi, diatoms, and bacteria). Plant-mediated synthesis has inspired researchers' to developed biological systems [96, 97]. However, using living organisms to make IONPs has several disadvantages like size variation, differently shaped NPs can be produced by the biogenic synthesis process in different locations but the isolation of produced NPs using this method is quite difficult, tedious and time-consuming. The yielded NPs by these methods are of low purity and the synthesis process is also very slow. The synthesis of IONPs using plant extracts is a quick, easy to perform and scale-up for production at industrial level [98]. The extracts of various dried parts of plant like leaves, seed, peels, bark, stem are extensively used. Phytochemicals in plant extracts play a critical role in the biosynthesis of IONPs, according to research [99]. FTIR spectroscopy was commonly used to look into the biomolecules that were responsible for the formation of metallic NPs. These organic molecules act as a capping agent on the surface of NPs, improving their physicochemical properties [100], as well as capping of NPs during the process of NPs formation by phytochemicals, according to FTIR study [101]. Plants with high phenolic component have been found to be the better alternative for producing INPs, according to studies. The spectroscopic studies were conducted for INPs produced by green tea, *Melaleuca nesophila*, *Mansoa alliacea*, *Rosmarinus officinalis*, *Salvia officinalis*, *Shirazi thyme*, and pistachio green hulls, *Eucalyptus tereticornis* for example, revealed that functional groups of phenolic compounds were the most important factor in the production of NPs [102]. The factors which play an important role in the synthesis of NPs include the concentration of metal precursor used, the amount of extract of plant used, temperature and incubation time of the reaction, plant extract pH and their antioxidant activity [103]. Because of their magnetic characteristics, INPs have a significant tendency to agglomerate and settle. INP aggregation is linked to a low surface charge and less reactivity. It has been suggested that NPs synthesized from plant extract based route are protected by biological compounds derived from plant extracts, resulting in increased colloidal stability in aqueous matrixes [104-106]. Magnetic NPs have been extensively studied in recent decades due to their vast range of uses in biology and medicine. Below a particular size (usually 10–20 nm), NPs consisting of ferro- or ferromagnetic materials can



exhibit a unique sort of magnetism known as super paramagnetic. This is a significant occurrence that can only be found in iron NPs [107].

## **2.9 Application of IONPs in biomedical field**

Because of their non-toxic nature, IONPs have a lot of significance in biomedical applications. Because IONPs contain both magnetic and semiconductor properties, they can be used in a variety of biomedical applications. Because of its biocompatibility, biodegradability, ease of manufacturing, and various magnetic properties, iron oxide plays an important role in biological activity. Particle size, shape, surface, aggregation, and electrical characteristics of IONPs all have a unique impact on biological applications [108]. IONPs serve an important role in the biomedical system and in everyday demands. A large number of NPs are available to support advanced development in biological applications. IONPs are used in a variety of applications, including magnetics, electrochemistry, gas sensors, energy storage, cancer therapy, magnetic storage, and medicinal treatments [109]. Hematite is one of the most frequent types of NPs, as well as one of the most natural and environment friendly. It plays an important role in iron biogeochemical cycles in the environment. Hematite, maghemite, goethite, and magnetite are the distinct phases of iron oxide crystallites [110]. Hematite is thought to have a more stable n-type semiconductor behavior. Researchers are now focusing their efforts on stable hematite iron oxide for biomedical applications. The choice of  $\text{Fe}_2\text{O}_3$  (hematite) iron oxide as unique NPs came solely based on its inexpensive cost and lack of toxicity.

Although superparamagnetic characteristics and high magnetic susceptibility are known in nanostructures of iron, cobalt, and nickel, the magnetite ( $\text{Fe}_3\text{O}_4$ ) form of IONPs, their hematite and maghemite form are the most widely explored forms [111]. IONPs are also an attractive candidate for biomedical applications due to their improved colloidal stability, biocompatibility, and persistent magnetic characteristics [112, 113]. IONPs were also identified as viable candidates in both physiological and metabolic activities due to their possible polymorphism and electron hopping nature. To improve the utilization of IONPs in advanced applications/technologies, bioactive additive compounds have been added to NPs in recent years. Surface engineering of

IONPs can be accomplished in a number of ways like surface coating or NPs dispersion in suitable matrix [114].

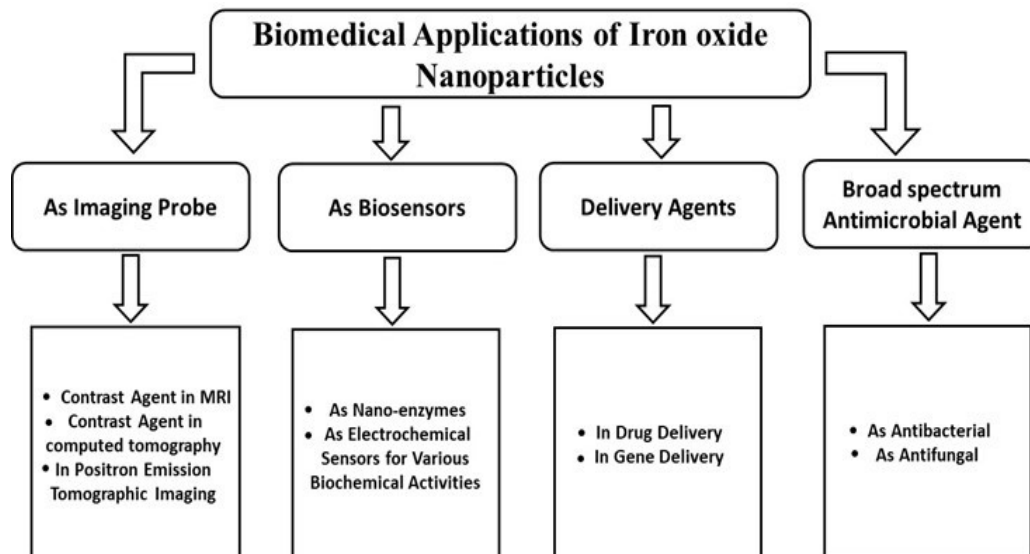


Fig. 2.4 Various applications of IONPs in biomedical field.

Low toxicity of IONPs, their biocompatible and biodegradable nature, long retention period, and magnetic properties to localise the IONPs at the target are all important for biomedical applications. IONPs are used in diagnostic imaging, positron emission tomography, near-infrared fluorescence imaging, and biosensors to detect biomolecules such as glucose, proteins, and urea [115]. IONPs have acquired popularity in therapeutic nano-medicine, with applications ranging from cancer treatment to antibacterial activities. IONPs are used in theranostic as nano-carriers, to enhance medication action and also as hyperthermia agents [116].

### 2.10 Plant based green synthesized NPs as corrosion inhibitors

Use of plant extract in the synthesis of NPs is very promising as it offers ecofriendly and cost-effective type of NPs free from adverse effects of chemically synthesized NPs. The presence of phytochemicals in the plants helps in the effective synthesis of NPs and provide functional surface groups to the NPs [117]. The adsorption property of NPs is attributed to these functional groups also. When the NPs are used as anticorrosive

agents, their adsorption property is highly beneficial in providing protection to the metals [118]. Many researchers have used plant extracts for the synthesis of NPs and their utilization as anticorrosive agents and fig. 2.5 shows the proposed mechanism of inhibition of corrosion by nanoparticles.

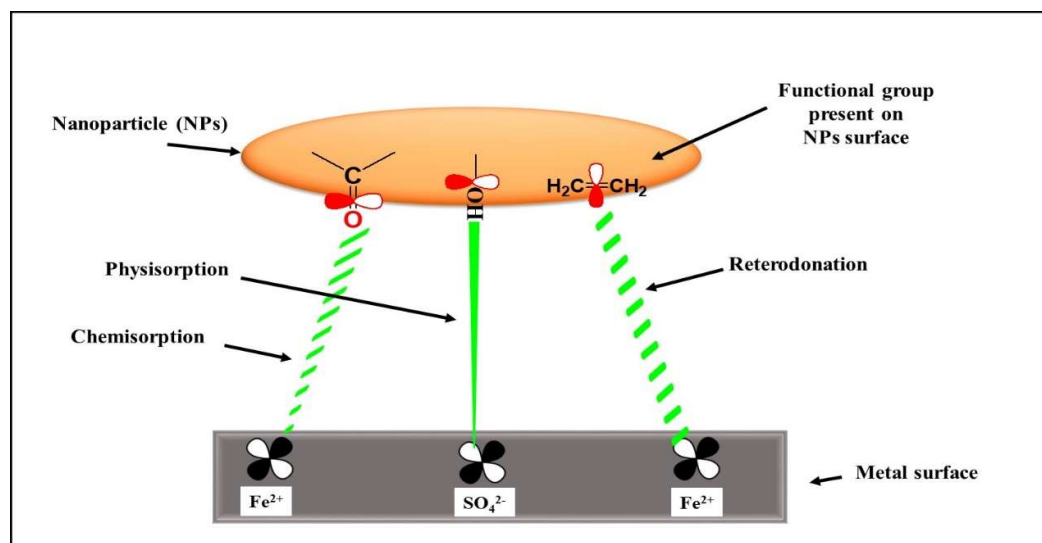


Fig. 2.5 Proposed mechanism of corrosion inhibition by NPs

Some of the green NPs of plant origin which were used as corrosion inhibitor are Titania NPs synthesized from *Aganonerion polymorphum* leaf extract, extracted with the help of ethyl acetate as solvent was used as corrosion inhibitor for carbon steel in simulated ethanol fuel blend. The electrochemical studies suggested around 97% inhibition efficiency. This work suggested the self-healing ability of titania NPs. They act as potent corrosion inhibitor by blocking the defects by protective film formed on the steel surface. The DFT and MD simulation studies indicated the formation of heat stable protective film on the steel surface. The presence of inhibitor molecules in the corrosive media significantly reduced the corrosion current densities thus by enhancing the surface resistance of carbon steel from corrosion [119].

Johnson et al. (2014) worked on the anticorrosive properties of silver NPs synthesized from the leaf extracts of *Sida acuta* and *Artemisia annua* in aqueous solution. The test sample was mild steel and corrosive media used was hydrochloric acid. The finding from this study proposed that the green synthesized silver NPs behaved as good corrosion inhibitors. A maximum of approximate 87% efficiency against corrosion.

Further, the NPs acted as mixed type of inhibitor, protecting the steel surface at both-anodic and cathodic site [120].

Leaf extract of *Tectona grandis* in methanol was used to synthesize silver NPs for application in microbial induced corrosion for the specially designed metallic material for condition prevalent for corrosion induced from microbes. The susceptibility testing against both gram positive and negative bacteria in microbiologically induced corrosion conditions was done. It was found that the *Tectona grandis* capped silver NPs effectively prevented the significant occurrence of corrosion. The silver NPs were found suitable for application of metal protection in the areas where the chances of microbial induced corrosion are present [121].

Silver NPs synthesized from aqueous extract of *Azadirachta indica* leaves were also used by Narenkumar et al. 2018. The substrate used was mild steel and hydrochloric acid was used as corrosive media in their study. Various techniques like electrochemical studies, weight loss analysis, antimicrobial activity etc. were used to estimate the corrosion inhibitive property of synthesized silver NPs. The results of this study revealed that the silver NPs showed an inhibition efficiency of 77%. The adsorption of NPs on the steel surface was confirmed by XRD and FTIR analysis. A protective layer was formed due to the adsorption of NPs on the surface of mild steel thus inhibiting the corrosion process [122].

The analysis of anticorrosive property of copper oxide NPs for SS 316L in simulated body fluid has been documented earlier. The copper oxide NPs were synthesized using *Aloe vera* leaves extract as reducing agents. For the estimation of corrosion inhibitory action of copper oxide NPs, potentiodynamic polarization curve was studied. The analysis revealed that the addition of copper oxide NPs in coatings of PDMS- SiO<sub>2</sub> enhanced the hydrophobicity of the coating and also significantly improved roughness of surface. This led to an increase in the anticorrosion activity of copper oxide NPs [123].

The ethanolic extract of *Musa sapientum* peel was used for the biogenic synthesis of iron oxide NPs. The iron oxide NPs were investigated for their corrosion inhibition property for mild steel and hydrochloric acid was used as simulated descaling solution.

From the electrochemical analysis, maximum inhibition efficiency of 94.4% was observed. As the amount of NPs in solution was increased, there is also subsequent increase in charge transfer resistance. From the potentiodynamic polarization curves, it was observed that the IONPs acted as mixed type inhibitor but the more prominent protection was on anodic site. From the scanning electron microscopy, it was revealed that the surface of steel was smooth in case of IONPs application while the surface was rough without the application of NPs. From the density functional theory, it was suggested that the bananadine acted as main phytochemical which helped in the adsorption of IONPs on the steel surface. Also, Fukui analysis and Forcite neutron scattering were done which revealed that the nitrogen (N8) site was the main site for adsorption process [124].

Titanium NPs synthesized from the ethanolic extract of *Olea europae* leaves were used to test their corrosion inhibition property on mild steel. The corrosive media used in this study was hydrochloric acid. The anticorrosive behavior was analyzed at different temperatures from 30°C to 60°C with the help of gravimetric analysis. The corrosion inhibition efficiency was around 94.3% with titanium NPs. The increase in efficiency was seen with increasing amount of titanium NPs at 30°C but the efficiency decreased to 85.4% at 60°C and hence it was concluded that the inhibition of corrosion with titanium NPs was temperature dependent. Also, the potentiodynamic studies suggested the mixed type of inhibition mechanism. The surface analysis of the samples in the presence and absence of NPs was also investigated by SEM and AFM. From the surface studies, it was seen that there is significant decrease in the roughness of surface in the presence of titanium NPs while the rough and damaged surface was seen in case of steel samples exposed to hydrochloric acid solution. It was predicted that the mode of adsorption was physical adsorption [125].

*Elaeis guineensis* leaf extract synthesized novel and ecofriendly silver NPs were utilized for protection of metal against corrosion by hydrochloric acid attack. Different concentrations of silver NPs were used to analyze their corrosion inhibitory action on mild steel. For the investigation of anti-corrosive properties, gravimetric tests, electrochemical studies were conducted. The further investigation of effects of acid solution and silver NPs were done with the help of FESEM, AFM and XRD. The

gravimetric analysis revealed that with the addition of 10% v/v of the inhibitor concentration the maximum inhibition efficiency reached approximately up to 93.1%. The electrochemical studies revealed the 94.1% corrosion inhibition efficiency at 10% v/v. The mechanism of inhibition was found to be by physical adsorption of inhibitor molecules on the steel surface. The mixed type of inhibition was revealed by the potentiodynamic polarization analysis. Further, the studies indicated that the formation of protective barrier prevented the dissolution of mild steel with the acid attack [126].

### **2.11 Use of SS 316L in biomedical devices**

The biomedical devices also known as implants are used to repair or replace any damaged biological structure. Apart from injury rectifications or tissue repair, such implantable devices are also used as cosmetic products. These implantable devices are made of metals and SS is one of the metal alloys which is used extensively for biomedical purpose [127]. The addition of chromium of around 11% makes the steel more resistant to corrosion. By addition of 30% nitric acid, passivation is done which helps in providing more resistance to corrosion. Also, by adding carbon and nickel in the steels make them more stabilized than the parent steels and hence make them stainless steels [128]. The main elements used for the alloying of SS 316L are chromium, nickel and molybdenum. The application of these three elements is based on their significant property to resist the corrosion process [129]. The chromium added to the SS helps in reducing the effect of corrosive agents from environment while the molybdenum and nickel addition helps in reducing the corrosion caused by the presence of chloride ions in the physiological body fluids.

The SS 316L type of SS is generally selected as the metal for surgical implants due to the addition of chromium, low carbon and 14% of nickel in their metal composition. It is a prerequisite condition for SS used for biomedical applications that they do not corrode in biological media so to overcome this problem; molybdenum is added which helps in forming a protective layer [130]. This layer helps in preventing the dissolution of metal ions in the presence of acid containing environment. Also, the addition of molybdenum makes them more resistant to pitting corrosion. They are more responsive to cold working to improve the hardness property rather than heat treatment. Due to the non-magnetic property of SS 316L, they show more corrosion resistant than their other

steel groups. The toughness property of SS 316L is attributed to the presence of its face centered cubic (FCC) structure [131].

The SS 316L is used for application in cranial plates, fracture plates for orthopaedic implantations. Major group of dental implants is made of SS 316L due to their diverse properties like good mechanical strength, tensile strength and toughness. For the fabrication of dental crowns, prostheses, dentures, bridges etc., this type of steel is mostly applied [132]. Apart from this, the prostheses for joint replacements are also mostly made up of SS of 316L grade. Stents and catheters are also manufactured from this type of steel. Due to their property of electrical conductivity, these metals are employed for the manufacture of neuromuscular stimulation devices [133]. SS 316L finds its application in the fabrication of various types of bio-implants e.g. dental implants, knee joint prosthesis, as bone fixation material, in prosthetic arthroplasty, cardiovascular implants, cochlear implants, for lumbar disc replacements [134].

### **2.12 Corrosion of SS 316L in body fluids**

Since, the implant is placed in the body of a living beings, many issues arise with respect to implant material and working. One of the basic concerns is the interaction of the implant surface with the surrounding physiological tissue environment. Sometimes these interactions are so strong that it may lead to the internal injury or the failure of the implant device. This generally happens post-surgery as it is considered that the human body does not provide best protective condition for the implant alloy [135]. The studies which have been conducted on the SS 316L as an implant material. These studies reveal that the human body contains elements which make the internal environment of human body very harsh. The presence of oxygenated solutions, salts containing hydrogen and chloride ions, pH of 7.4 and normal body temperature of 37°C makes the physiological environment very aggressive against the implant material. SS are considered to be corrosion resistant and SS 316L is regarded as one of the most corrosion resistant materials but still when placed in human body environments, these metals also undergo degradation due to chemical or electrochemical reactions and start dissolution at a very slow rate [136]. The fluids in the body contains water, dissolved oxygen, complex chemical compounds, large amount of sodium and chloride ions, bicarbonates and other electrolytes in small amounts like phosphate, magnesium,

calcium, potassium, sulphate, proteins, plasma constituents [137]. When the implant is placed, the disturbance in body environment leads to the setup of electrochemical cells. These electrochemical cells make the dissolution of metal faster leading to the formation of localized spots and lead to the corrosion of the implant material.

Studies by several researchers on retrieved implants from the body suggested that due to the pitting and crevice type corrosion process, approximately 90% SS 316L implant failure occurs [138]. This process of leaching out of metal ions in the nearby tissues have raised concerns to improve the resistance against corrosion for the currently used SS 316L either by modifying the surface with more corrosion resistant materials or by alloying it with more elements which can help in protection the implants from dissolution [139].

### **2.13 Toxicological evaluation of IONPs**

Since the use of IONPs in biomedical sector is very attractive due to the non-toxic and biocompatible behavior in biological systems [140]. The magnetic susceptibility and semiconductor like activity makes them more prominent to their counterparts in terms of use in multifunctional applications in biomedical field. Several reports have been given for the potential of IONPs in their biological activities for their biodegradability and easy synthesis [141]. However, the chemical synthesis of IONPs require the use of toxic chemicals like hydrazine, sodium borohydride or potassium bi-tartrate which can be present in very trace amounts in the formulations of NPs. But the use of green synthesis or biological synthesis mechanism for IONPs, it is somewhat possible to prepare non-toxic NPs. The most important factor which prevent the possible toxicity of IONPs is the formation of biocompatible coating which can be made by the presence of phytochemicals from the biological systems. These phytochemicals surround the IONPs surface naturally and prevent their possible toxic effects [142-145]. The biocompatibility of biologically synthesized IONPs have been studied extensively like no or minimal cytotoxicity against diverse healthy cells such as 3T3 fibroblast cells was shown when up to 15  $\mu\text{g/mL}$  of IONPs dosage was used and it was found that the cytotoxicity associated with cellular inhibition of IONPs was lower 30% [146], no toxicity or minimum cytotoxic effects in Neuro2A cells and HUVEC cells of brain with the usage of 150  $\mu\text{g/mL}$  of IONPs [147], in red blood cells and macrophage cells of



humans with the usage of 15 µg/mL of IONPs [148], in HEK- 293 cells OF embryonic kidney with the usage of 500 µg/mL of IONPs [149], For an IONPs concentration of less than 5 mg/L, there was no cytotoxicity to zebrafish embryos [150], a number of aquatic animals, including cyanobacteria, algae, and invertebrates, have shown no substantial toxicity [151]. When IONPs were administered orally up to a maximum dosage of 2000 mg per kg of the body weight of mouse, no acute toxicity was found to occur [152]. Most excitingly, bio-synthesized IONP were found to be less harmful to biological systems than amorphous compounds of free iron ions [153], implying that the nanosized formulation can avoid or minimize iron toxicity when compared to free iron ions. Some studies have also shown that the reduction of metal ion using biological precursors resulted in less toxic NPs than the conventional chemical methods which employ toxic chemicals for the reduction process for example the synthesis of IONPs using extract of sorghum bran resulted in water soluble and biodegradable IONPs which were coated with phenolic compounds and were less toxic than the IONPs synthesized by using NaBH<sub>4</sub> for reduction process [154]. Apart from these, there are lots of reported results in the literature which suggest that the toxicity of IONPs was dosage dependent. Although some researchers have reported the cytotoxicity associated with the administration of IONPs in biological systems [155- 160]. Hence, the studies on the use of IONPs in biological systems should be done extensively in order to eliminate any chances of possible ill effects associated with the usage of IONPs in various biological applications.

#### **2.14 Research gap**

The use of NPs for corrosion inhibition is an emerging field. NPs are good adsorbents due to their large surface area, Further, they can act as potent and suitable alternative to the existing inhibitors. The use of inhibitors as corrosion control methods is applied for various types of materials of metallic origin and for such protection from corrosion, nanotechnology enabled methods can be developed in the form of NPs as novel approach materials. The NPs as an inhibitor in the form of additives or coatings can also help in developing novel diagnostic techniques. Hence, the use of NPs finds their application in major theranostic applications.

### **2.15 Outcomes of the proposed research work**

The proposed project will help in designing a new and an innovative, alternate solution to the identified problem and also help in assessing impacts in areas of environmental pollution and health related to the defined problem of this work and also help in improving the existing policies and also give some alternative ideas to frame new policies in future.

### **2.16 Importance of the proposed work**

Despite the tremendous increment in the applications of science of technology in developing the methods to control corrosion, the process of corrosion occurrence and its effects is the major concern shown by the industries around the globe. The costs borne by the industries in combating the corrosion problem is very huge (estimated to be US\$2.2 trillion annually in direct costs worldwide) [161]. Lots of money can be saved by applying proper methods to control and monitor the corrosion process. Since, nanomaterials are considered very superior in their mechanical and electronic properties so the enhancement in the resistance of metallic materials by the application of nanotechnology can be very helpful and will also save huge capital. Nanotechnology enabled materials are expected to be tougher, stronger, harder and can also be applied efficiently in combating the corrosion attack and can be useful in defence, armour, aerospace components, construction equipment, medical devices and sports equipment, etc.

### **2.17 Objectives of the present study**

The objectives of this research work are:

- Green synthesis and characterization of iron oxide nanoparticles
- To evaluate iron oxide nanoparticles as anticorrosive agents
- To study the mechanism of adsorption of iron oxide nanoparticles on the steel surface

## CHAPTER 3

### MATERIALS AND METHODS

Various experiments were conducted to synthesize, characterize and analyse the corrosion inhibition property of IONPs. Green plant extract-based method was used for the synthesis of IONPs. After the successful synthesis of IONPs, characterization studies were conducted. The analysis of anticorrosive properties was done using various techniques. These include weight loss gravimetric analysis also known as weight loss or weight reduction measurements, electrochemical studies like impedance spectroscopy and potentiodynamic polarization. Surface analysis was done by using SEM and AFM. The materials required to complete the design work and the methodology used for this purpose are discussed in the following sections.

#### 3.1 Chemicals and Reagents

Chemicals and reagents used in this work were of analytical grade. The ferric chloride salt used as metal precursor for the synthesis of IONPs was purchased from Loba Chemical, Hank's solution was obtained from Hi-media, the Ringer's solution was prepared in the laboratory with the help of high-grade analytical chemicals and the phosphate buffer salt was supplied by Himedia.

#### 3.2 Selected Plants

Plants used for the synthesis of IONPs were as following:

##### *Swertia chirata*

It is a plant of Gentianaceae family. The common name of this plant is "Chiretta". It is a plant of sub temperate region and is generally found at very high altitudes. This plant has been used as medicinal herb for many centuries. There are large number of phytochemicals which are found in this plant like swerchirin, amarogentin, amaroswin, and swertiamarin etc. The compound amarogentin found in this plant is known to be the bitterest tested compound [162]. The part of the plant which was used for the study

was stem and was purchased from Jalandhar, Punjab, India. Fig. 3.1 (a) shows the powder form of the *S. chirata* stem part.

### ***Terminalia Arjuna***

This plant belongs to the Combretaceae family. It is perennial plant which is indigenous to India and is found in main plain areas of the Indian land. The common name of *T. arjuna* is arjun or arjuna. The main chemical constituents of this plant include arjunetosides- I, II, III, IV, arjunertein, arjunolic acid, arjunolone, arjunine, casuarinin, Epicatechin,  $\beta$ -sitosterol, ellagic acid, arjunic acid, etc. [163]. The plant was taken from the Herbal Garden, Lovely Professional University, Phagwara, Punjab. The bark of the plant was used for the synthesis of IONPs. Fig. 3.1 (b) shows the dried and crushed form of *T. arjuna* bark.

### ***Ficus benghalensis***

It belongs to the Moraceae family and is commonly known as Indian banyan. The banyan tree is native to India and is a perennial, subtropical tree. The major phytochemicals which are found in the plant are lupeol, 3-galactoside, beta-amylin, rutin, beta-sisterol, bergapten, from leaves, caoytchoue, cerin, malic acid etc. from latex and 5, 7 dimetheyl ether of leucopelargonidin-3-0-alpha-D galctosyl cellobside, meso-inositol etc. from bark [164]. The leaves of the *F. benghalensis* plant were used for the synthesis of IONPs. The leaves were taken from the Herbal Garden, Lovely Professional University, Phagwara, Punjab. Fig. 3.1 (c) shows the dried and grounded form of leaves which was used for the synthesis process.

All the three plants were identified from Botanical Survey of India, Dehradun, Uttarakhand. The identification was done to confirm the selected plants for their authenticity.

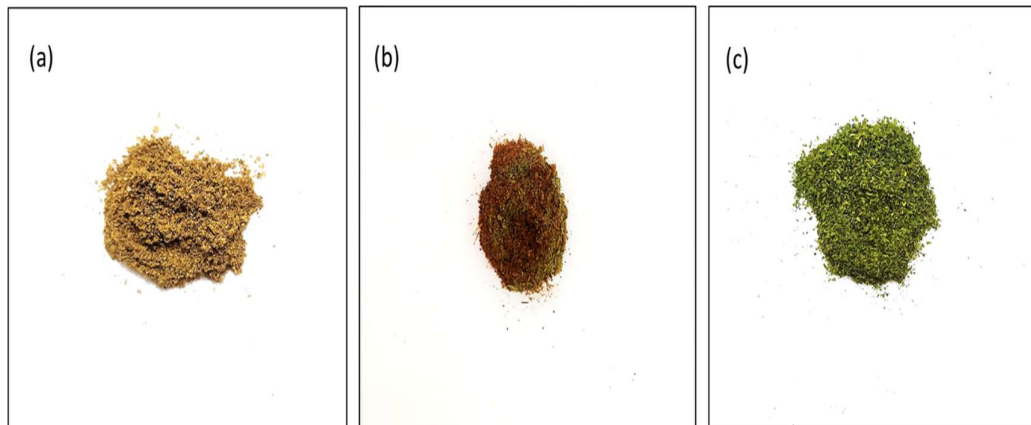


Fig 3.1 Dried and crushed form of selected plants (a) *S. chirata* (b) *T. arjuna* (c) *F. benghalensis*

### 3.3 SS 316L

The SS 316L was purchased from Saharanpur, Uttar Pradesh, India. After the selection of steel, the identification and elemental analysis of steel was done to confirm the type of steel from Central Institute of Hand tools Technology, Jalandhar, Punjab. The composition of the steel was found to be Fe (65.73%), Ni (12.36%), Cr (17.54%), Mo (2.43%), Mn (1.26%), C (0.6%), P (0.018%), S (0.017%) and Si (0.58%).

### 3.4 Corrosive Media

Three different media namely Ringer' solution, Hank's solution and phosphate buffer saline were used as corrosive media for this work. The corrosive media were chosen on the basis of chemical composition as all these media contains large amounts of chloride ions, bicarbonate, sodium, calcium and potassium [165]. Also, the chosen media represent the simulated body fluid composition which is present over whole-body tissues. The pH of the corrosive media was kept at 7.4 which is normal pH of the human body and the temperature was also kept at 37°C which is normal human body temperature. The normal human body environment facilitates the conditions for the initiation of corrosion process inside the human body. The electrochemical cell formed due to the interaction of implant material surface and the fluid in the nearby tissues makes the body environment as a very harsh corrosive environment [166, 167].

### **3.5 Synthesis of IONPs**

The selected plants were dried and then crushed to powder form. The 2 g crushed plant powder was added to 50 ml double distilled water. The mixture is then boiled for 10 min. The boiled mixture was then allowed to cool and after that it was centrifuged at 10,000 rpm for 10 min. The clear supernatant was taken out after centrifugation and further used as plant extract for the synthesis process. The IONPs were synthesized by adding 1ml of plant extract with 1 ml of 10mM ferric chloride solution (1:1). The NPs were formed readily within seconds just after the mixing of plant extract and ferric chloride. The reaction mixture was then allowed to stand for 10 min. after 10 min, the reaction mixture was centrifuged for 10 min at 10,000 rpm. The NPs were obtained after the centrifugation. The NPs were then thrice washed with ethanol and kept for drying at 35°C [168- 170]. After the proper drying, the NPs were finely crushed and further characterization and their effect on corrosion of SS 316L was done.

### **3.6 Preparation of SS 316L working samples**

The SS 316L working samples were utilized for weight loss measurements and electrochemical studies. For the surface characterization study, the SS 316L working samples were also used. For the weight loss measurement, circular coupons of SS 316L with an area of 1 cm<sup>2</sup> were used and for the electrochemical studies, the working electrode were prepared by immersing the SS 316L specimen in epoxy resin. The cylindrical rod-shaped steel specimen with a diameter of 10mm and the exposed area of 1 cm<sup>2</sup>. The working samples of SS 316L were abraded with emery papers of different grades to remove the previous dust or impurities from the SS 316L surface before the immersion of steel specimen in the test solution for all the studies [171]. The concentration of IONPs used for the anti-corrosive studies were 10 ppm, 25 ppm, 50 ppm, 75 ppm and 100 ppm. The IONPs with these concentrations were dispersed in corrosive solution and then the SS 316L samples were immersed. Fig 3.2 (a) and (b) shows the working SS 316L sample used for weight loss analysis and electrochemical analysis, respectively.

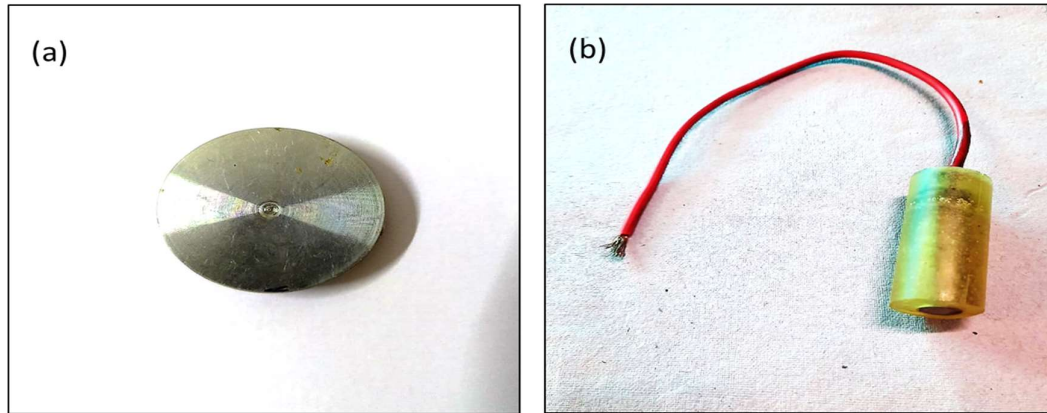


Fig. 3.2 Working samples of SS 316L used for (a) weight loss measurement (b) electrochemical analysis.

### 3.7 Weight loss measurement study

For the analysis of corrosion rate and to find out the corrosion inhibition efficiency of IONPs, weight loss studies were conducted. For this study, the SS 316L samples were weighed before and after immersion of SS 316L samples in corrosive media and also in the corrosive solution containing IONPs in different concentrations for 120 hours at 37°C. After immersion for 120 hours, the SS 316L samples were taken out and cleaned with acetone, dried under nitrogen flow and again weighed [172]. The difference in the weight of the SS 316L samples was measured and was used to calculate the rate of corrosion and corrosion inhibition efficiency with the help of the following equation [173].

$$C_R = \frac{K \times W}{A \times t \times \rho} \quad [1]$$

In the formula,  $C_R$  signifies corrosion rate which is given as mm/year,  $W$  is loss of weight of SS 316L,  $A$  is the area of the steel sample,  $t$  is the immersion time,  $\rho$  is the density ( $7.86 \text{ g cm}^{-3}$ ) and  $k$  denotes the constant for corrosion which is  $8.76 \times 10^4$ .

The inhibition efficiency (I.E) and surface coverage ( $\theta$ ) of IONPs was calculated as per the following equations [174, 175]

$$IE = \frac{C_R^0 - C_R^i}{C_R^0} \times 100 \quad [2]$$

$$\theta = \frac{IE}{100} \quad [3]$$

In the above formulae,  $C_R^0$  signifies the rate of corrosion of SS 316L immersed only in the corrosive solution and  $C_R^i$  stands for the SS 316L sample immersed in corrosive solution containing IONPs.

The adsorption isotherm study was also conducted with the help of weight loss measurements. The surface coverage ( $\theta$ ) value and the concentration of IONPs ( $C$ ) were used as main components. The graph was plotted between  $C$  and  $C/\theta$  by using following equation [176]

$$\frac{C}{\theta} = \frac{1}{K_{ads}} + C \quad [4]$$

### 3.8 Electrochemical Studies

#### (i) Electrochemical Impedance Spectroscopy

To conduct the electrochemical impedance spectroscopy study, the working electrode was immersed in the corrosive media and also in the corrosive media containing the different concentrations of IONPs. The results are taken at open circuit potential value. The charge transfer resistance value and corrosion inhibition efficiency (I.E.) were obtained from this study and calculated with the help of the following equation [177]

$$IE = \frac{R_{ct} - R_{ct}^0}{R_{ct}} \times 100 \quad [5]$$

Where  $R_{ct}$  stands for the charge transfer resistance values at different concentration of IONPs and  $R_{ct}^0$  signifies the charge transfer resistance value for the corrosive media only.

#### (ii) Potentiodynamic Polarization Study

To conduct this study, the working electrode was immersed in the corrosive media and also in the corrosive media containing the different concentrations of IONPs. The results are taken at open circuit potential value. The corrosion current density value and



IE were obtained from this study which were calculated with the help of the following equation [178]

$$IE = \frac{I_{corr}^0 - I_{corr}^i}{I_{corr}^0} \times 100 \quad [6]$$

Where  $I_{corr}^0$  stands for the corrosion current density value for the corrosive media only and  $I_{corr}^i$  signifies the corrosion current density values at different concentration of IONPs.

### **3.9 Instruments Used**

The instruments used in this work for the characterization of synthesized IONPs and to check their effects on the corrosion of SS 316 are

#### **(a) UV- Vis Spectrophotometer**

The UV- Vis spectrophotometer–UV 800 from Shimadzu was used for the initial confirmation of synthesis of IONPs. The UV spectra were taken at different parameters. After the mixing of ferric chloride salt with the plant extract, the reaction mixture was observed for change in color that indicated synthesis of NPs visibly [179]. The UV-vis spectra were taken by varying the concentration of ferric chloride, plant extract, at different pH, at different temperatures and at different incubation times. Fig 3.3 (a) shows the image of UV- Vis spectrophotometer used for this study.

#### **(b) Zeta Potential and Particle Size Analyser**

To understand the stability and size distribution pattern of synthesized NPs in solutions, zeta potential analysis was done. For the analysis of zeta potential, the suspension of synthesized NPs was prepared by using double distilled water. The instrument used was Malvern Zetasizer Nano ZS90 and is shown in fig 3.3 (b) this is an ideal study to identify the surface charge of dispersed particles. This technique is mostly used to study the characterization of colloidal systems, NPs dispersion and particulate materials.

### **(c) X- ray Diffractometer**

The Bruker D8 Advance multipurpose X-ray Diffractometer was used to analyse the nature of the synthesized NPs. This is a non-destructing technique instrument which do not harm the test samples. The detector used in this instrument was SSD-XE which provide ultrafast speed to the analyser. The instrument also contains the ICDD PDF2, PDF4+, PDF4/ORGANICS, PDF4/minerals data base. This database helps in identifying the elemental composition of the new and unknown synthesized materials. The NPs were ground to fine powder for the analysis. The instrument is shown in Fig. 3.3 (c).



Fig. 3.3 (a) UV-vis spectrophotometer (b) zeta potential and particles size analyser (c) X-ray Diffractometer

### **(d) Scanning electron microscopy**

The JEOL JSM-7610F plus was used for the morphological analysis of the synthesized NPs. The microscope is also equipped with EDS: OXFORD EDS LN2 detector which helps in identifying the chemical makeup of the synthesized NPs. Fig 3.4 (a) shows the SEM used for the study. For the characterization of NPs, very fine powder of NPs was prepared. The instrument was also used for the surface characterization of the samples of SS 316L for the anticorrosive action of IONPs. The analysis was done when the

samples of SS 316L are immersed in corrosive solution and also in the corrosive solution containing the optimum amount of NPs. The images for polished SS 316L sample surface were also taken to do the comparative study between the polished, corroded and NPs inhibited steel surface.

#### **(e) Transmission electron microscopy**

The instrument used for this study was FEI Technai TF20 and is equipped with field emission gun (FEG) source (fig. 3.4 (b)). The synthesized IONPs were prepared in the powder form and placed on the TEM grid and subjected to transmission electron microscope (TEM) to analyse the internal structure of the IONPs.

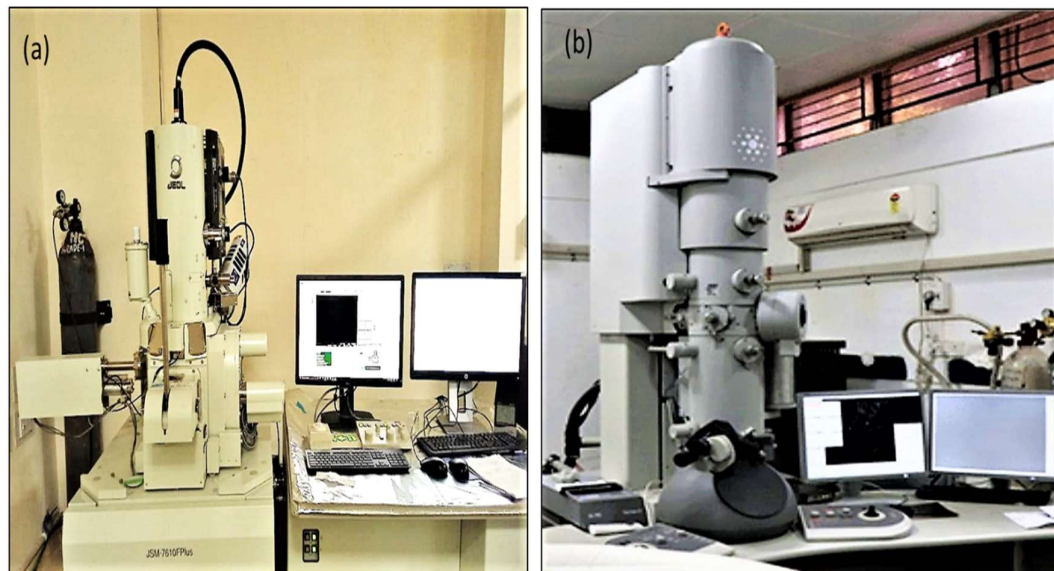


Fig. 3.4 (a) Image showing SEM (b) Image showing TEM

#### **(f) Atomic force microscope**

The AFM was used to understand the three-dimensional structural properties of the synthesized IONPs. For the analysis, 5  $\mu$ l of NPs suspension was pipetted onto a glass slide and kept for some time to let the NPs adsorb on the glass slide. The glass slide was then placed in the AFM instrument. The Anton Paar Tosca<sup>TM</sup> 400 AFM was used for the analysis and is shown in Fig. 3.5 (a). The AFM was also used to study the surface morphology of SS 316L samples. The surface analysis for SS 316L samples exposed to corrosive solution and exposed to corrosive solution containing optimum

concentrations of synthesized IONPs was done by placing the treated SS 316L specimens in the sample analyser of instrument. The surface roughness values obtained from the AFM analysis were used to conclude the protective layer formation on the SS 316L sample surface.

#### **(g) FTIR Spectrophotometer**

The FTIR spectroscopy was used to identify the functional groups present in plant extract. This was done using Shimadzu FTIR 8400S. This technique is very useful to understand the role of chemical components of plants in capping and stabilizing the NPs surface. Fig. 3.5 (b) shows the FTIR spectrophotometer used for this study.

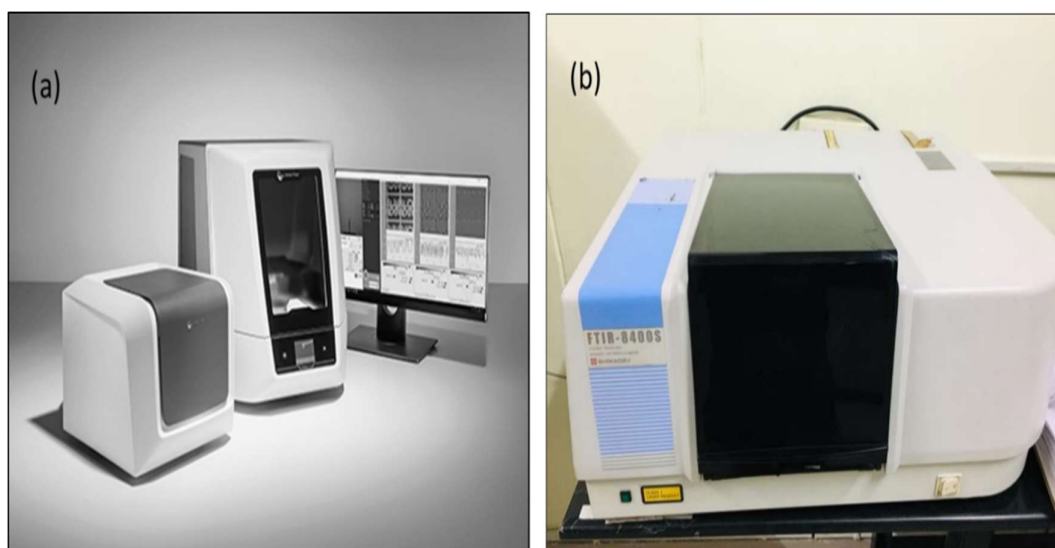


Fig. 3.5 (a) Image showing AFM (source- Anton Paar.com) (b) FTIR spectrophotometer

#### **(h) Electrochemical workstation**

The electrochemical studies were conducted to check the effect of synthesized IONPs on the corrosion behaviour of different corrosive media for SS 316L. The electrochemical studies were done with the help of Auto Lab Electrochemical Workstation by Metrohm. The workstation consists of three chambered electrode cell.

The three electrodes comprised of one counter electrode which is made up of platinum, one reference electrode which is also known as saturated calomel electrode and is made up of silver and filled with potassium chloride. For the corrosion studies, electrochemical impedance spectroscopy and potentiodynamic polarization analysis was done [180]. The data for electrochemical impedance spectroscopy was obtained in the form of Nyquist plot and the data for potentiodynamic polarization study was obtained in the form of Tafel plot or Tafel curves. The tests for electrochemical measurements were obtained at an amplitude of 10mV and at frequency in the range of 100 kHz to 0.01 Hz frequency [181]. The data for potentiodynamic polarization was observed between -200 to +200 mV versus SCE (saturated calomel electrode) which is Ag/AgCl (3 M KCl) with scanning rate of 0.1 mV/s. The results obtained from the electrochemical studies were analysed and calculated with the help of CHI 760C software for electrochemical work station [182]. The electrochemical workstation and electrode cell assembly are shown in fig. 3.6 (a) and (b) respectively.

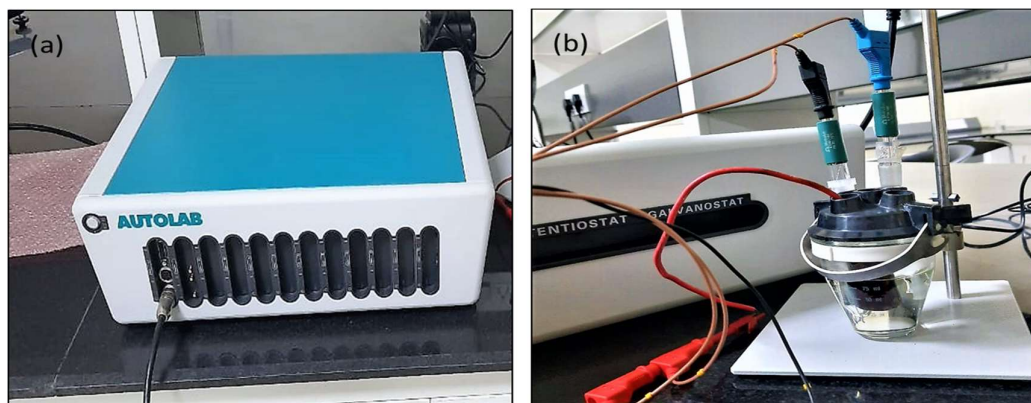


Fig. 3.6 (a) electrochemical workstation (b) Electrode cell assembly

## CHAPTER 4

### RESULTS AND DISCUSSION

#### 1. Iron oxide NPs (IONPs) synthesized using *S. chirata* stem extract

##### 1.1 Characterization studies for synthesized NPs

After the synthesis process, the nanoparticles were first characterized to analyse their physical and chemical properties. Techniques like UV- vis spectroscopy was used for the initial identification of synthesis of NPs, zeta potential was done to analyze the surface charge and associated properties, dynamic light scattering or size distribution pattern was also analyzed to identify the distribution pattern of NPs in colloidal solution, X- ray diffraction study was done to study the nature of NPs whether they are crystalline or amorphous, SEM and TEM were used to analyze the morphological features, AFM was used to analyze the topographical features of the NPs, FTIR spectroscopic characterization was done to analyze the type of functional groups present in the plant extract which helped in the formation of stable NPs.

##### 1.1.1 UV-Vis Spectroscopy

After the initiation of reaction for IONPs synthesis, UV-vis spectroscopy was the first study which was done for the confirmation of NPs synthesis. The yellow color of the ferric chloride solution readily changed to dark brown after the addition of *S. chirata* stem extract that indicated the formation of NPs [183]. The occurrence of surface plasmon resonance and formation of colloidal solution indicated the formation of IONPs. The adsorption maxima were recorded in the 250- 300 nm range [184]. According to earlier reports, IONPs shows adsorption peaks in the recorded wavelength region. This study was done at various parameters for the determination of optimum conditions for the effective synthesis of stabilized NPs. Factors like concentration of ferric chloride solution, volume of plant extract, effect of pH and incubation temperature were taken into consideration. By increasing the concentration of

ferric chloride salt in the reaction mixture, there was increment in the intensity of absorption peak. The high peak intensity indicated the formation of more NPs [185]. However, formation of precipitate like material occurred and it was observed visually that the NPs synthesized with more than 10mM ferric chloride concentration, aggregated and settled down. Hence, 10 mM was chosen as optimum ferric chloride concentration for the synthesis of stable NPs which were uniformly dispersed thus making a stable colloidal solution. Volume of plant extract was also varied from 0.5 ml to 4 ml and it was found that the colloidal solution of NPs without the formation of any precipitates or aggregated mass was attained at 4 ml of plant extract volume. Also, pH from 3 to 9 was varied to get the idea of the pH of synthesized NPs [186]. It was found that pH at 6 was optimal for synthesizing the stable NPs. Reaction mixture incubation at different temperatures was also tested to find the optimum temperature for the effective synthesis of NPs [187, 188]. The optimum temperature was found out to be 25°C as even after 2 hour of incubation time for the reaction mixture, there was increase in the peak intensity but the peak intensity decreased after 2-hour incubation in all the higher incubation temperatures. Also, an increase in aggregation was also observed at higher temperatures. The aggregation of NPs indicated by higher peak intensities was also reported in the literature [189]. The optimum reaction parameters are necessary to enable the effective synthesis of NPs with high stability. Hence, for the synthesis of IONPs, 10 mM ferric chloride concentration, 4 ml volume of plant extract, pH at 6 and 25°C temperature were taken as optimum parameters. Also, the NPs synthesized with the identified optimum parameters were also subjected to UV –Vis spectroscopy at different incubation time to check the rate of NPs synthesis and maximum reduction of ferric chloride [190]. It was found that, after 10 min of incubation time, there was no significant change in the rate of synthesis of IONPs synthesis, as there was decrease in the peak intensity with increasing incubation time indicating the maximum reduction time for ferric chloride salt solution at 10 minutes [191]. Hence, for the other characterization studies, NPs were synthesized after giving an

incubation time of 10 minutes to the reaction mixture for maximum reduction process.

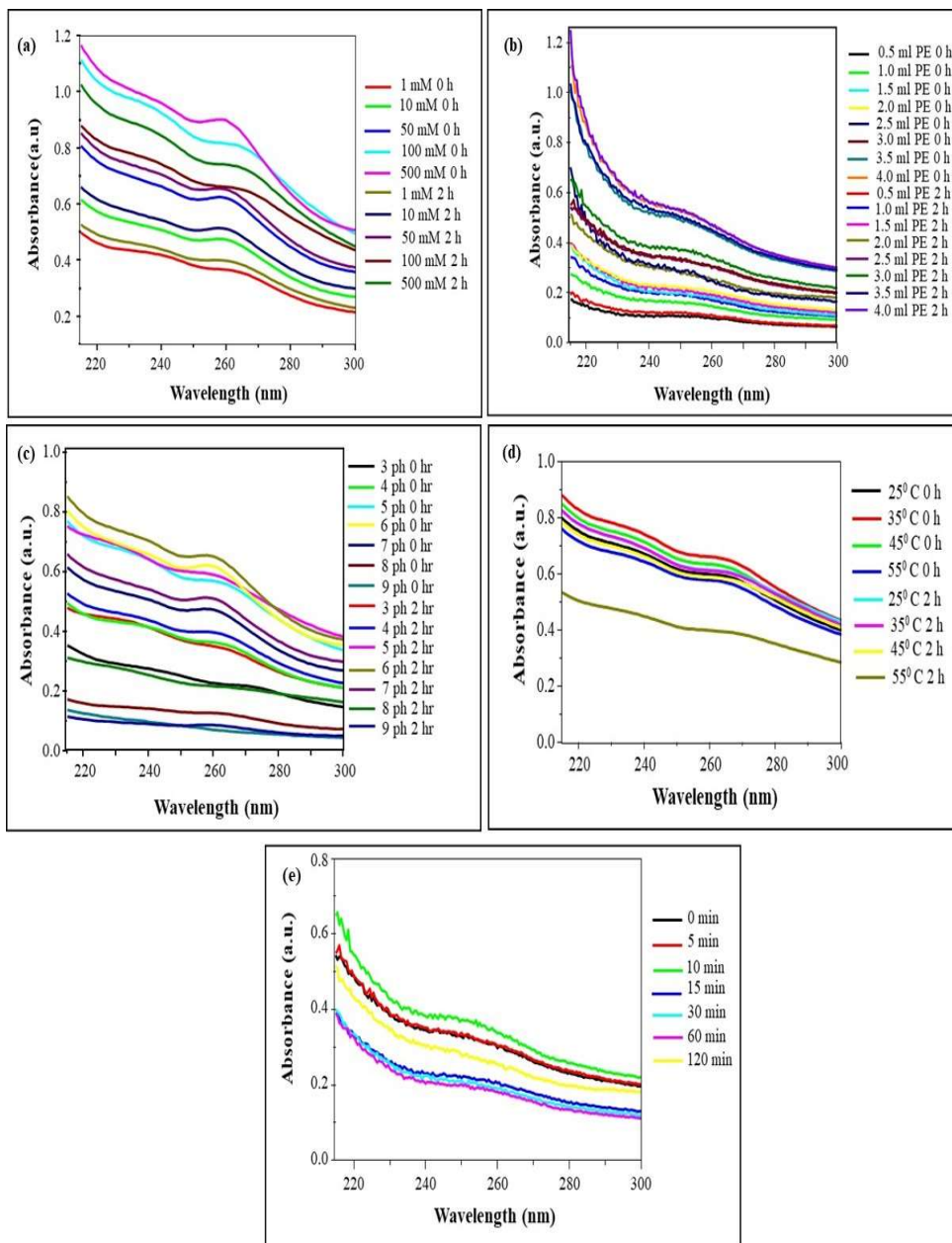


Fig. 4.1 UV-vis spectroscopy of IONPs synthesized from *S. chirata* stem extract at (a) different ferric chloride concentrations (b) different plant extract concentrations (c) different pH (d) different temperatures (e) different incubation time.



### 1.1.2 Zeta potential and size distribution

Since NPs form colloidal solutions when added to a solvent and it is necessary to check their stability in such solutions in order to facilitate their proper application. Hence, to determine the stability of NPs in colloidal solutions, zeta potential analysis was done. Fig. 4.2 (a) shows the zeta potential of synthesized IONPs. From the results, it was found that the NPs possess a zeta potential of -10 mV. From the literature, it can be concluded that the NPs with zeta potential value comes in the range of -10 to +10 mV are generally considered as neutral particles having no charge on their surface. If the zeta potential value comes above +30 mV then the NPs are considered to be cationic in nature while if the value comes out to be lower than -30 mV then the NPs are considered to be anionic in nature. If the NPs are cationic in nature, then they can readily enter the cell wall as the charge on the cell wall is negative. If such NPs are introduced in the biological systems, they can disrupt the membrane of cell and leads to toxicity. Sometimes by the introduction of positively charged NPs leads to serum protein aggregation [192, 193].

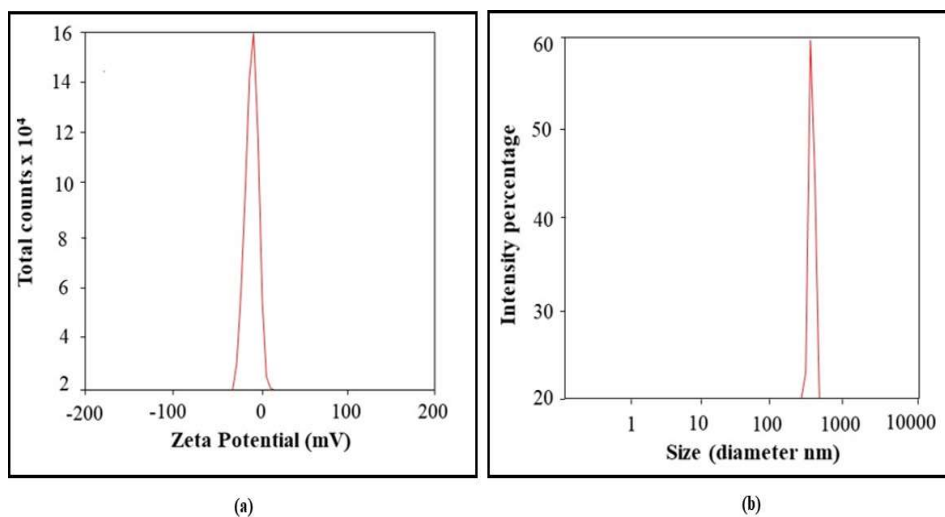


Fig. 4.2 Image showing (a) zeta potential and (b) size distribution pattern of synthesized IONPs.

In case of negatively charged NPs, the reticuloendothelial system readily takes them up and a toxic response is generated. While the NPs having neutral charge,

possess low toxicity due to less interaction with plasma membrane. Hence, neutral NPs are good choice for the applications in biological systems [194, 195]. The size distribution analysis done by dynamic light scattering which is shown in fig. 4.2 (b) suggested the hydrodynamic diameter of synthesized NPs to be around 500 nm and this also suggest that the particles are of nanometric size with broad range of size distribution in the colloidal solution.

### 1.1.3 X- ray diffraction study

For the analysis of the physical nature of the prepared NPs, x-ray diffraction study was conducted. Fig 4.3 shows the obtained XRD pattern of prepared IONPs. There is a presence of broad peak in the graph which indicated small size of IONPs and amorphous like surface topography which may be attributed due to the presence of phytochemicals from plant extract giving amorphous nature to the NPs [196]. The Bragg's angles or  $2\theta$  are shown by XRD graph at 27.9, 35.5, 38.3, 46.9, 49.1, 55.4, 65.0 corresponding to 002, 110, 111, 130, 131, 132, 133 lattice planes respectively. Also, the chemical formula of synthesized NPs as given by XRD is  $\text{Fe}_2\text{O}_3$  known as hematite and the structural lattice of iron oxide NPs was found to be orthorhombic.

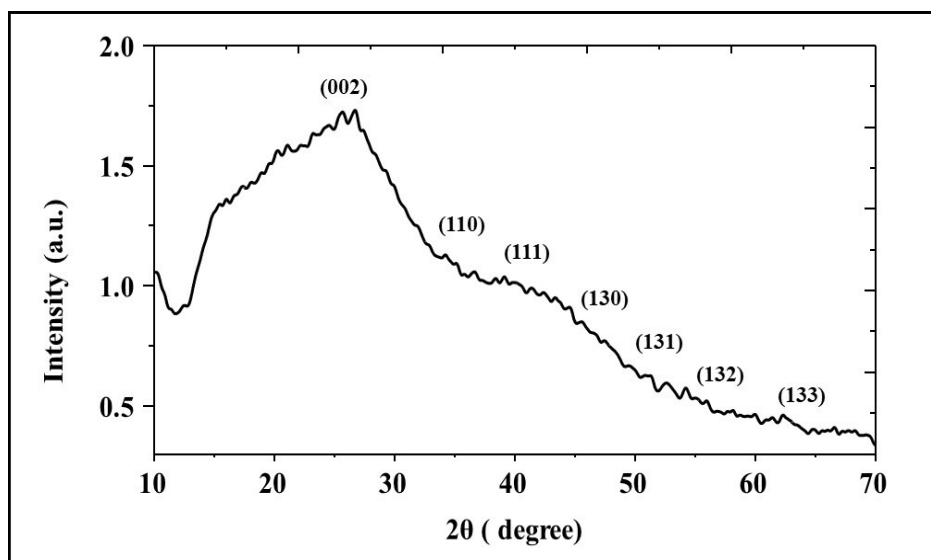


Fig. 4.3 X-ray diffraction pattern of *S. chirata* synthesized IONPs.

#### 1.1.4 SEM and TEM studies

The spherical shape of 10- 20 nm in size was clearly visible from the SEM images shown in fig 4.4 (a) from the SEM images it can be seen that there is clustering of NPs due to very low charge on the surface of NPs as analyzed from the zeta potential study. The agglomeration of synthesized NPs may be due to the presence of strong H- bonding between the adjacent NPs [197]. The EDX spectra revealed iron and oxygen peaks present in the analyzed samples which confirm that the synthesized NPs were of iron oxide as shown in fig. 4.4 (b). To confirm the exact morphological features and size characteristics of synthesized IONPs, TEM analysis was done and it was found that the IONPs were of approximately 10 nm in size as given in fig. 4.4 (c). Hence, the spherical shaped, 10- 20 nm in diameter synthesized IONPs were obtained from the stem extract of *S. chirata*. Some clustering of IONPs was noticed with agglomeration properties which are helpful in their effective applicability [198].

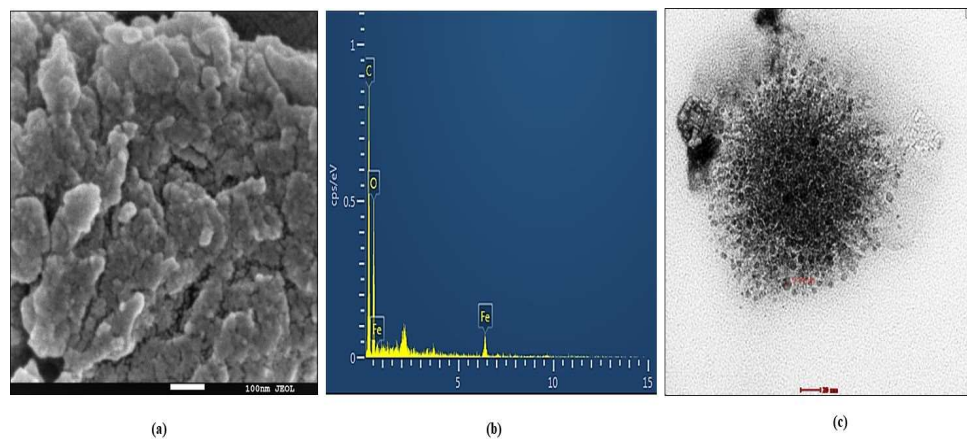


Fig. 4.4 (a) SEM image (b) EDX spectra and (c) TEM image of IONPs

#### 1.1.5 Atomic force microscopy (AFM)

Three dimensional topographical features of synthesized IONPs was determined by AFM (Fig. 4.5). It can be seen that there is presence of spherical IONPs with few aggregated IONPs. Spherical shape of IONPs is clearly visible from the 2-D AFM image (fig. 4.5 (a) and (b)). The agglomerated or clustered NPs can be suggested with the help of size distribution maxima shown in fig.

4.5 (c) which suggest the presence of strong bonding between the molecules present on the surface and the phytochemical constituents on the IONPs surface thus providing it a characteristic property which can be useful for corrosion and other applications [199, 200].

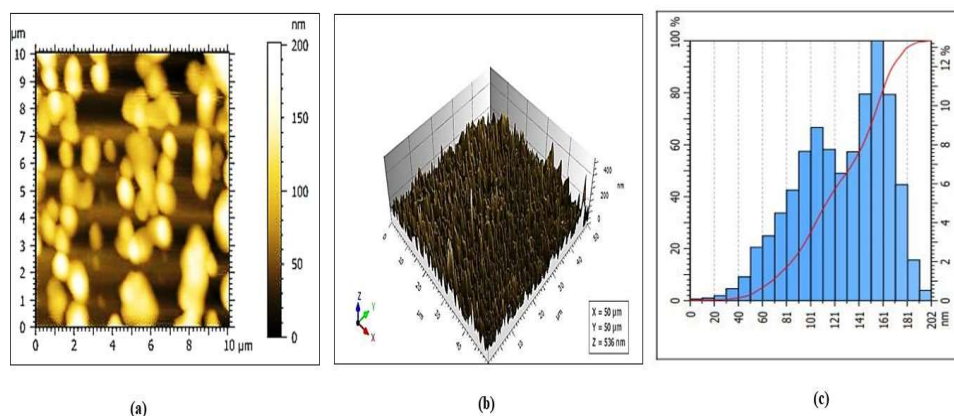


Fig. 4.5 Atomic force microscope images of (a) 2- D image (b) 3-D image and (c) size distribution graph of synthesized IONPs.

### 1.1.6 Fourier Transform Infrared Spectroscopy

The components present in plant extract contains diverse chemical compounds which help in reducing the metal precursors and also capping the formed NPs for stabilization. The FTIR study was used to identify the phytochemicals from plant extract which were involved in the green synthesis mechanism. The shift in the wavelength and occurrence of characteristic peaks in the FTIR spectroscopy is generally used to analyze the bonding of phytochemicals on the NPs surface. In general, the peaks which comes in the region of 4000 to 3000  $\text{cm}^{-1}$  suggests the presence of stretching of O-H, N-H groups from aliphatic amines which contains alcoholic or phenolic compounds with strong intensities [201]. The region of 2000 to 1540  $\text{cm}^{-1}$  suggests the presence of the strong and medium C-H or weak S-H bonds and also attribute to the presence of weak S-H bonding of alkyne, aldehyde or thiol [202]. The peaks which come in the region from 2000 to 1540  $\text{cm}^{-1}$  indicated the presence of strong C=O and C=N

bonding corresponding to the aromatic compounds, esters, acid halide or carboxylic acid. The peaks present in the range of 1400 to 1000  $\text{cm}^{-1}$  corresponds to the presence of O-H, S=O and C-F functional groups [203]. The presence of C-H bond is represented by the peaks which are observed from 1000- 400  $\text{cm}^{-1}$ . The peaks which come near to the region of 400  $\text{cm}^{-1}$  are attributed to the liberation of water from the compounds of plant extract [204]. The different FTIR peaks observed for the *S. chirata* stem extract and for the IONPs are shown in fig. 4.6.

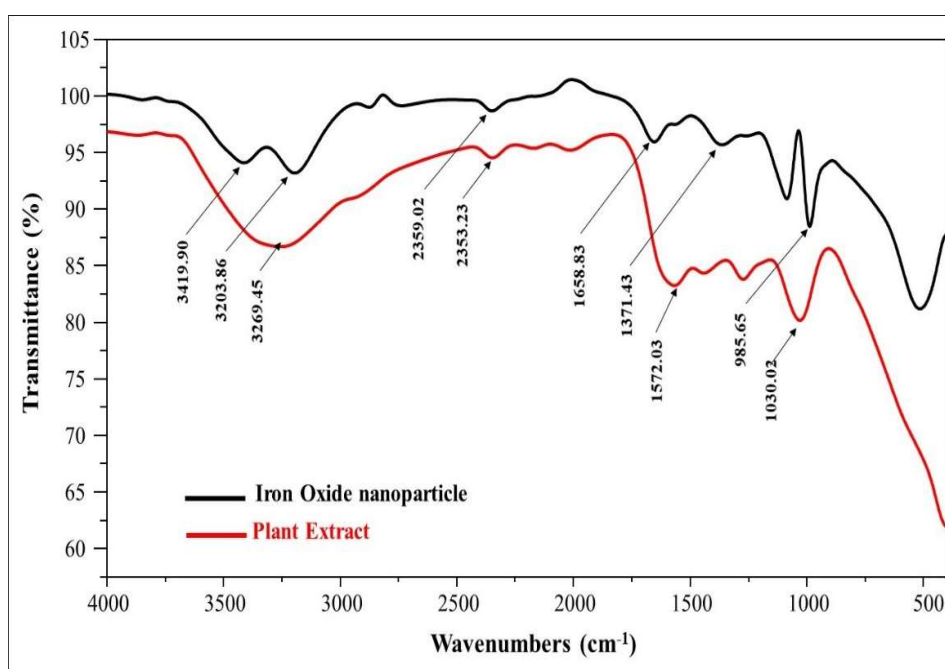


Fig. 4.6 FTIR spectra of synthesized IONPs along with the FTIR spectra of *S. chirata* plant extract.

From the FTIR spectra, it can be seen that there are peaks present at 3269.45  $\text{cm}^{-1}$  corresponds to the presence of stretching of C-H bonds, 2353.23 and 1572.03  $\text{cm}^{-1}$  which corresponds to the carbonyl group stretching from ketones suggesting the presence of compounds like amaroswin and amarogentin [205]. The occurrence of C-N stretching indicated the presence of amines and the presence of C-H or O-H deforming vibrations attributed to the alkaloids as indicated by the peaks observed at 1246.06 and 1030.02  $\text{cm}^{-1}$ , respectively. Also, the observed spectra for IONPs showed various peaks corresponding to

the FTIR spectra of *S. chirata* stem extract. The peaks for IONPs were observed at 3419.90, 3203.86, 2359.02, 1658.83, 1371.43, and 985.65  $\text{cm}^{-1}$  which suggested the action of various phyto functional groups which collectively acted as reducing agent as well as stabilising agents for the effective IONPs formation. The interaction of compounds from the stem extract of *S. chirata* with the IONPs causes a shift in the wavelength corresponding to the functional group movement from plant extract to the surface of IONPs in order to facilitate the capping and stabilizing process [206, 207].

## **1.2 Anti- corrosive studies of IONPs synthesized from *S. chirata* stem extract in Ringer's solution as corrosive media**

### **1.2.1 Weight loss measurements**

The I.E of IONPs against the corrosion of SS 316 L in the presence of Ringer's solution as corrosive media was analysed with the help of weight loss measurement studies. The values obtained are shown in table 4.1. From the obtained data, it was concluded that by increasing the concentration of IONPs in the corrosive media, the subsequent decrease in corrosion rate was seen and it was also observed that the increment in the I.E was depended on concentration of IONPs and maximum I.E against corrosion was 78.61 % ( $\pm 2.638$ ) at 100 ppm IONPs concentration. It was assumed that the IONPs get adsorbed on the surface of the SS 316L leading to an increased efficiency against corrosion thus by decreasing the rate of corrosion [208]. The linear coefficient value obtained was 0.9992 which is near to 1 suggesting the adsorption of IONPs on SS 316L surface follows the pattern of Langmuir adsorption isotherm (fig. 4.7).

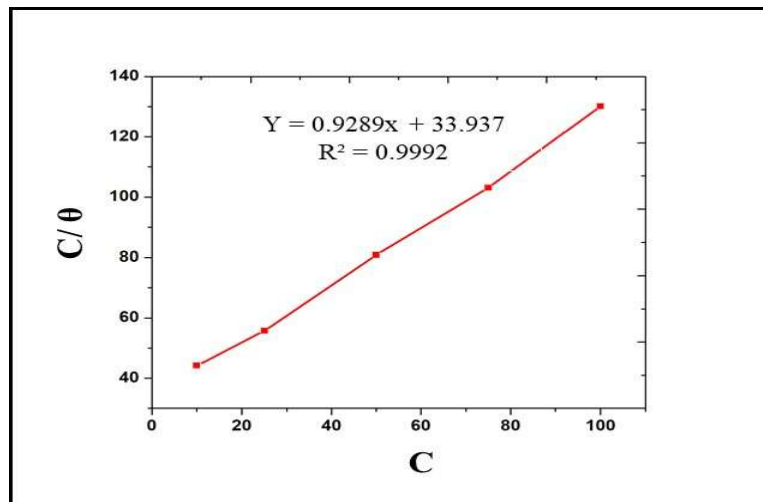


Fig. 4.7 Langmuir adsorption isotherm of *S. chirata* synthesized IONPs on SS 316L surface with the weight loss measurements in Ringer's solution

Table 4.1 Weight loss and adsorption isotherm parameters for *S. chirata* synthesized IONPs in different concentrations on SS 316L immersed in Ringer's solution

Concentration (C)	$C_R$ (mm $y^{-1}$ )	I.E (%) $\pm$ St. Dev.	$\theta$	$C/\theta$
Ringer's solution	0.0073	-	-	-
Ringer's solution + 10 ppm IONPs	0.0056	22.59 $\pm$ 1.499	0.2259	44.26
Ringer's solution + 25 ppm IONPs	0.0040	44.86 $\pm$ 0.585	0.4486	55.72
Ringer's solution + 50 ppm IONPs	0.0027	61.79 $\pm$ 0.516	0.6179	80.91
Ringer's solution + 75 ppm IONPs	0.0019	72.77 $\pm$ 2.654	0.7277	103.06
Ringer's solution + 100 ppm IONPs	0.0015	78.61 $\pm$ 2.638	0.7861	127.21

### 1.2.2 Electrochemical studies

Electrochemical studies were done by obtaining the data from electrochemical impedance spectroscopy obtained from Nyquist plot, potentiodynamic polarization data given as Tafel plot, Bode plot and phase angle values. It was seen that the charge transfer resistance increased with the increase in the amount of concentration of IONPs and the obtained Nyquist plot is shown in fig. 4.8 (a). The calculated corrosion I.E reached up to a maximum of 75.12 % at 100 ppm of IONPs concentration. The IONPs get adsorbed on the surface of SS 316 L sample and formed a layer and hence reduces the flow of electrons [209]. The polarization curves or Tafel plots were also obtained for analysing the corrosion inhibitory effect of IONPs. From this study, the extrapolation of the curves at anodic or cathodic site at their intersection point gave the values for corrosion current density. The data obtained from polarization studies is given in fig. 4.8 (b). The decrease in corrosion current density was observed with increase in the concentration of IONPs in corrosive media which corresponds to the increment in the corrosion I.E of IONPs [210]. It can be concluded that a protective layer of IONPs was formed on the SS 316L surface thus protecting it from dissolution in the presence of corrosive media, Ringer's solution [211]. The value obtained for  $E_{corr}$  was in between the range of 30- 35 mV. From the reported literature it is concluded that the IONPs behaved as inhibitor of mixed type. The protection from corrosion at both anode and cathode because it is considered that less than 85mV shift in the corrosion potential leads to mixed type of inhibition [212]. Also, the maximum inhibition efficiency obtained was 78.37% with 100 ppm of IONPs concentration. The electrochemical reactions which takes place at the interface of steel surface and the corrosive media causes dissolution of the metal. In setting up these electrochemical reactions, the anodic and cathodic sites participate significantly [213]. Hence, to protect the metal surface from dissolution, inhibitors are used. The inhibitors target the anodic and cathodic sites actively by inhibiting the mechanism of charge transfer in the electrochemical set up. IONPs contains functional groups contributed by phytochemicals on their surface which possesses heteroatoms. These



heteroatoms help in the adsorption of IONPs at the SS 316L surface by making strong coordination bonds. The adsorption can be of chemical nature or physical nature or both. From the potentiodynamic study, it can be concluded that the IONPs get adsorbed on the SS 16L surface and decreased the corrosion current density hence protecting the surface of SS 316L from corrosion [214]. The obtained data from the electrochemical analysis are shown in table 4.2.

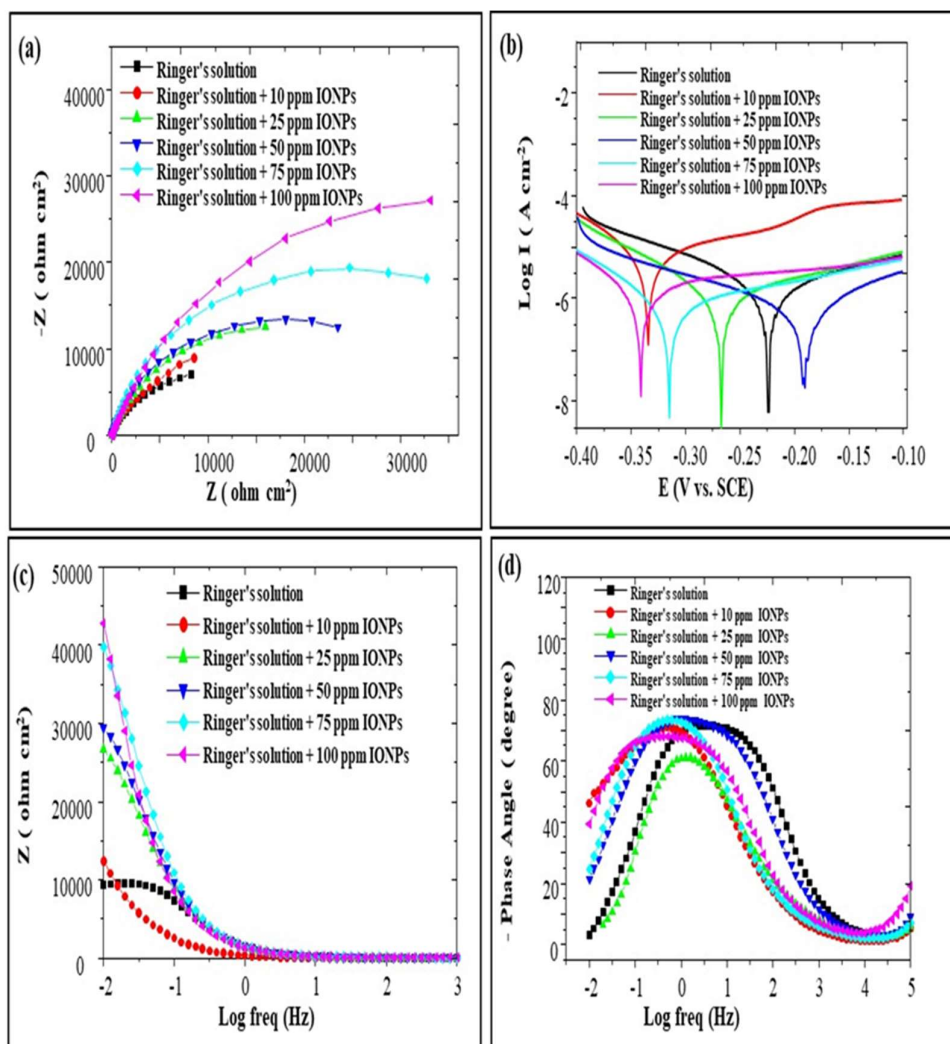


Fig. 4.8 Electrochemical studies of the effect of different concentrations *S. chirata* synthesized IONPs on SS 316L surface (a) Nyquist plot (b) Tafel plot (c) Bode plot and (d) phase angle plot in Ringer's solution

Table 4.2 Parameters of electrochemical analysis for SS 316L in Ringer's solution containing different concentration of *S. chirata* synthesized IONPs

Concentration (C)	Electrochemical parameters		Potentiodynamic parameters	
	R <sub>ct</sub> (Ω cm <sup>-2</sup> )	I. E (%)	I <sup>0</sup> <sub>corr</sub> (A cm <sup>-2</sup> ) * 10 <sup>-7</sup>	I. E (%)
Ringer's solution	8231.75	-	9.94	-
Ringer's solution + 10 ppm IONPs	8578.52	4.04	8.96	9.85
Ringer's solution + 25 ppm IONPs	15925	48.30	6.09	38.73
Ringer's solution + 50 ppm IONPs	23528.09	65.01	3.54	64.38
Ringer's solution + 75 ppm IONPs	32696.88	74.82	2.56	74.24
Ringer's solution + 100 ppm IONPs	33097.41	75.12	2.15	78.37

The adsorption of IONPs on the surface of SS 316L substrate is also well supported by the data obtained from bode plot and phase angle graph given in fig. 4.8 (c) and (d) respectively and it has been reported that if the phase angles are equal to 90°, then the electrochemical behaviour is capacitive at the steel and corrosive solution interface and if the phase angle values are equal to 0° then the electrochemical behaviour is resistive in nature at the steel and corrosive solution interface [215]. The phase angle values obtained suggest the resistive nature against corrosion due to the presence of different concentration of IONPs. From the obtained data from these graphs, it is suggested that the anticorrosive property of IONPs increased with the increment in the concentration of IONPs. Also, the formation of protective barrier leads to lower capacitance values, hence making the SS 316L steel less prone to dissolution thus by preventing the corrosion process in the harmful corrosive environments

[216]. The results given by electrochemical analysis collectively suggest the anti-corrosive property of IONPs and their use as potent corrosion inhibitor in aggressive body environments.

### 1.2.3 Surface investigation studies by SEM and AFM

The SEM and AFM images of polished SS 316L sample, SS 316L sample immersed only in Ringer's solution as corrosive media and SS 316L sample immersed in Ringer's solution containing 100 ppm of IONPs are shown in fig. 4.9 (a, b, c) and fig. 4.9 (d, e, f) respectively.

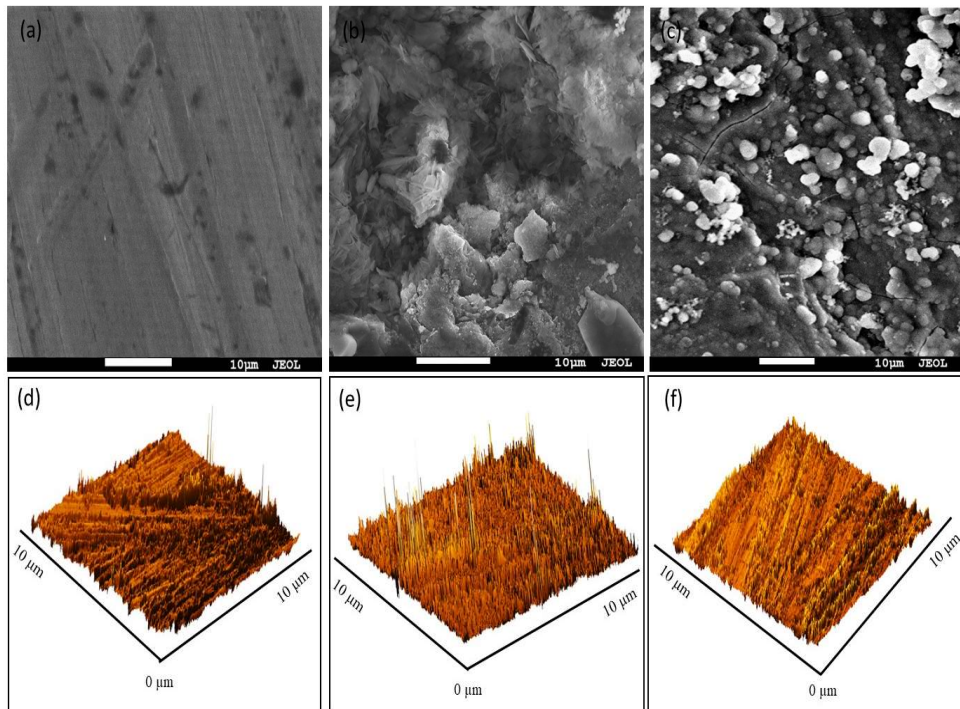


Fig. 4.9 Images showing (a) SEM micrograph of SS 316L (b) SEM micrograph of SS 316L immersed only in Ringer's solution (c) SEM micrograph of SS 316L immersed in Ringer's solution with IONPs (d) AFM micrograph of SS 316L (e) AFM micrograph of SS 316L immersed only in Ringer's solution (f) AFM micrograph of SS 316L immersed in Ringer's solution with IONPs

From the SEM analysis, it was revealed that SS 316L sample which was immersed in only Ringer's solution showed very rough and damaged surface in

comparison to the SS 316 L sample containing 100 ppm IONPs in Ringer's solution [217]. This difference in the surface images of the SS 316L samples is attributed to protective barrier presence on the surface of steel formed by the presence of IONPs. From the AFM analysis, the roughness values of the surface of the steel samples were obtained and it was found that the polished SS 316 L surface and the SS 316 L placed in Ringer's solution only, has a surface roughness value of around 39.8 nm and 999.0 nm respectively. However, the surface roughness value obtained for SS 316L immersed in Ringer's solution containing 100 ppm of IONPs was around 523.0 nm. This decrease in roughness of surface is thought to be due to the presence of protective layer which helped in blocking the transfer of electrons and hence protecting the surface from corrosion attack [218].

### **1.3 Anti- corrosive studies of IONPs synthesized from *S. chirata* stem extract in Hank's solution as corrosive media**

#### **1.3.1 Weight loss measurements**

The I.E of IONPs against the corrosion of SS 316 L in the presence of corrosive media (Hank's solution) was analysed with the help of weight loss measurement study. The values obtained are shown in table 4.3. From the obtained data, it was concluded that by increasing the concentration of IONPs in the corrosive media, the subsequent decrease in corrosion rate was seen and it was also observed that the increment in the I.E was depended on concentration of IONPs and maximum I.E against corrosion was 80.30 % ( $\pm 1.746$ ) at 100 ppm IONPs concentration. It was assumed that the IONPs get adsorbed on the surface of the SS 316L leading to an increased efficiency against corrosion thus by decreasing the rate of corrosion [208]. The linear coefficient value obtained was 0.9969 which is near to 1 suggesting the adsorption of IONPs on SS 316L surface follows the pattern of Langmuir adsorption isotherm (fig. 4.10)

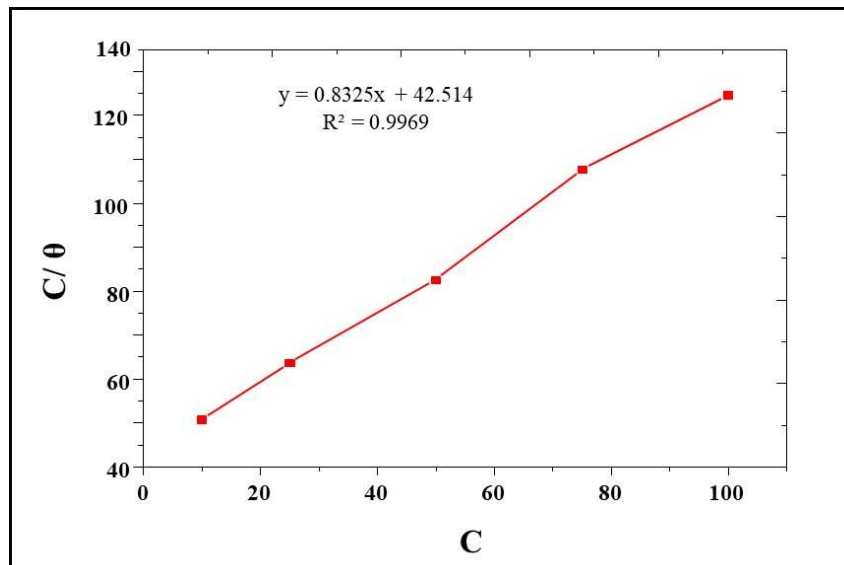


Fig. 4. 10 Langmuir adsorption isotherm of *S. chirata* synthesized IONPs on SS 316L surface with the weight loss measurements in Hank’s solution

Table 4.3 Weight loss and adsorption isotherm parameters for *S. chirata* synthesized IONPs in different concentrations on SS 316L immersed in Hank’s solution

Concentration (C)	$C_R$ (mm $y^{-1}$ )	I.E (%) $\pm$ St. Dev.	$\theta$	C/ $\theta$
Hank’s solution	0.00066	-	-	-
Hank’s solution + 10 ppm IONPs	0.00053	19.69 $\pm$ 0.636	0.1969	50.78
Hank’s solution + 25 ppm IONPs	0.00040	39.30 $\pm$ 5.930	0.3930	63.61
Hank’s solution + 50 ppm IONPs	0.00026	60.61 $\pm$ 2.155	0.6061	82.49
Hank’s solution + 75 ppm IONPs	0.00020	69.69 $\pm$ 1.039	0.6969	107.61
Hank’s solution + 100 ppm IONPs	0.00013	80.30 $\pm$ 1.746	0.8030	124.53

### 1.3.2 Electrochemical studies

Electrochemical studies were done by obtaining the data from electrochemical impedance spectroscopy obtained from Nyquist plot, potentiodynamic polarization data given as Tafel plot, Bode plot and phase angle values. The obtained Nyquist plot is shown in fig. 4.11 (a). Around 76.83 % of I.E at 100 ppm of IONPs concentration was observed. The IONPs get adsorbed on the surface of SS 316 L sample and formed a layer and hence reduces the flow of electrons thus by increasing the charge transfer resistance of the reaction process [220]. The polarization curves or Tafel plots were also obtained for analysing the corrosion inhibitory effect of IONPs. The extrapolation of the curves at anodic or cathodic site at their intersection point gave the values for corrosion current density. The data obtained from polarization tests are shown in fig. 4.11 (b). [221]. This can be attributed to the adsorption of IONPs on the SS 316L surface thus protecting it from dissolution in the presence of Hank's solution [222]. The value obtained for  $E_{corr}$  was in between the range of 30- 35 mV. From the reported literature it is concluded that the IONPs behaved as inhibitor of mixed type thus protecting it from corrosion at both anode and cathode because it is considered that less than 85mV shift in the corrosion potential leads to mixed type of inhibition [223]. The maximum inhibition efficiency obtained was 78.98% with 100 ppm of IONPs concentration. The electrochemical reactions which takes place at the interface of steel surface and the corrosive media causes dissolution of the metal. In setting up this electrochemical reactions, the anodic and cathodic sites participate significantly [224]. Hence, to protect the metal surface from dissolution, inhibitors were used. The inhibitors target the anodic and cathodic sites actively by inhibiting the mechanism of charge transfer in the electrochemical set up [225]. The obtained data for the electrochemical studies are shown in table 4.4. The adsorption of IONPs on the steel substrate is also well supported by the data obtained from bode plot and phase angle graph are given in fig. 4.11 (c) and (d). It has been reported that if the phase angles are equal to  $90^{\circ}$ , then the electrochemical behaviour is capacitive at the steel and corrosive solution interface and if the

phase angle values are equal to  $0^\circ$  then the electrochemical behaviour is resistive in nature at the steel and corrosive solution interface [215]. The phase angle values obtained suggest the resistive nature against corrosion due to the presence of different concentration of IONPs. From the obtained data from these graphs it is suggested that the anticorrosive property of IONPs increased with the increment in the concentration of IONPs. Also, the formation of protective barrier makes the steel less prone to dissolution thus by preventing the corrosion process in the harmful corrosive environments [226]. The results given by electrochemical analysis collectively suggest the anti- corrosive property of IONPs and their use as potent corrosion inhibitor in aggressive body environments.

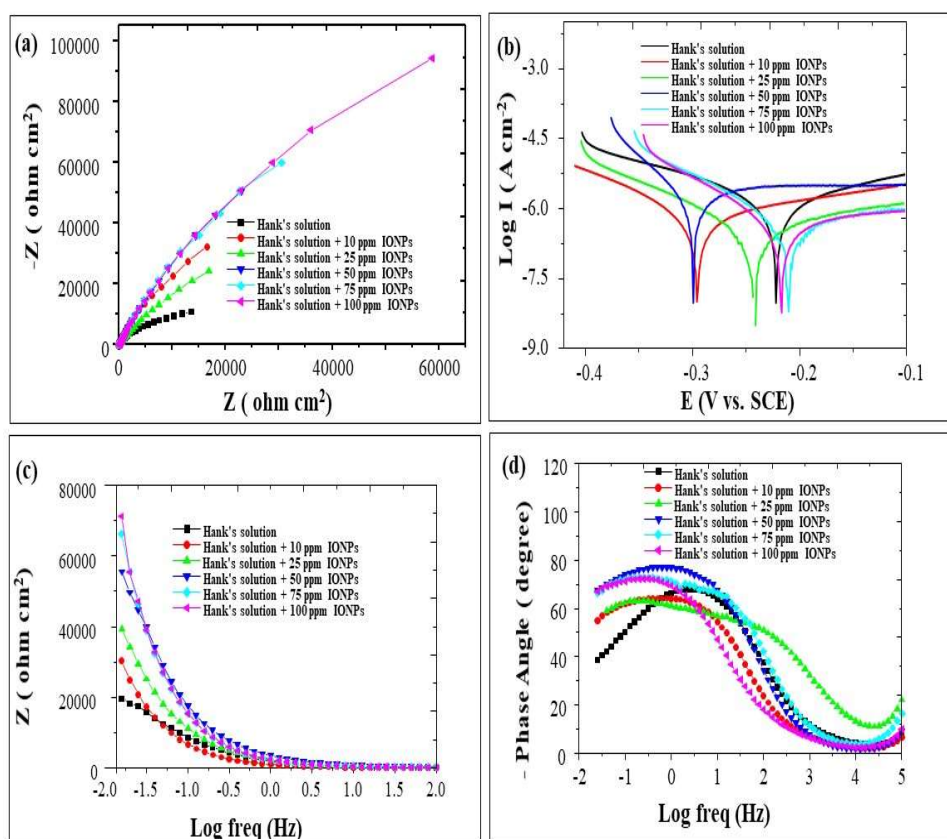


Fig. 4.11 Electrochemical studies showing the effect of different concentrations *S. chirata* synthesized IONPs on SS 316L surface (a) Nyquist plot (b) Tafel plot (c) Bode plot and (d) phase angle plot in Hank's solution

Table 4.4 Parameters of electrochemical analysis for SS 316L in Hank's solution containing different concentration of *S. chirata* synthesized IONPs

Concentration (C)	Electrochemical parameters		Potentiodynamic parameters	
	$R_{ct}$ ( $\Omega \text{ cm}^{-2}$ )	I. E (%)	$I_{corr}^0$ ( $\text{A cm}^{-2}$ ) * $10^{-7}$	I. E (%)
Hank's solution	13588.78	-	8.71	-
Hank's solution + 10 ppm IONPs	16567.93	17.98	7.10	18.48
Hank's solution + 25 ppm IONPs	16884.19	19.51	6.85	21.35
Hank's solution + 50 ppm IONPs	22880.33	40.60	5.11	41.33
Hank's solution + 75 ppm IONPs	30479.31	55.41	3.84	55.91
Hank's solution + 100 ppm IONPs	58668.96	76.83	1.83	78.98

### 1.3.3 Surface investigation studies by SEM and AFM

The SEM and AFM images of polished SS 316 L sample, SS 316 L sample immersed in Hank's solution and SS 316 L sample immersed in Hank's solution containing 100 ppm of IONPs are shown in fig. 4.12 (a, b, c) and fig. 4.9 (d, e, f) respectively. It can be seen from SEM images that the SS 316 L sample which was immersed in Hank's solution showed very rough and damaged surface in comparison to the SS 316 L sample containing 100 ppm IONPs in Hank's solution [227]. This difference in the surface images of the steel samples is attributed to the presence of protective barrier on the surface of steel formed by the presence of IONPs. From the AFM analysis, the roughness values of the surface of the steel samples were obtained and it was found that the polished SS 316 L surface and the SS 316 L placed in Hank's solution only, has a surface roughness value of around 39.8 nm and 880.0 nm, respectively while the surface roughness value of SS 316L subjected to Hank's solution with 100 ppm of IONPs was around 423.0 nm. This decrease in roughness of surface was assigned to the protective layer formation which helped in blocking the transfer



of electrons and hence protecting the SS 316L surface from the attack of corrosive solution [228].

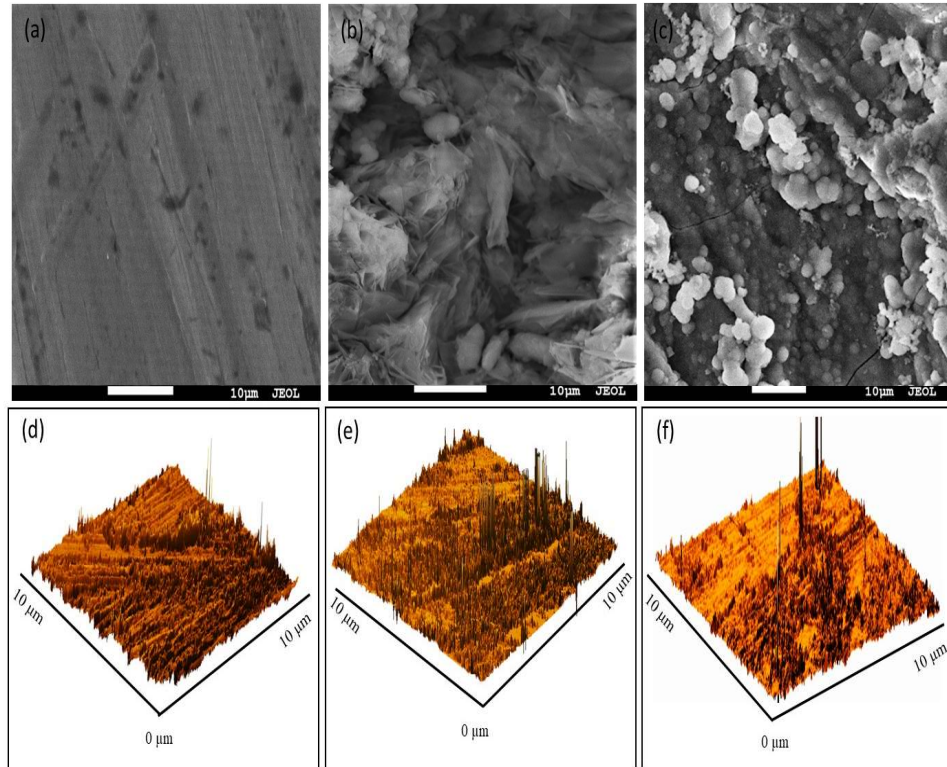


Fig. 4.12 Images showing (a) SEM micrograph of SS 316L (b) SEM micrograph of SS 316L immersed only in Hank's solution (c) SEM micrograph of SS 316L immersed in Hank's solution with IONPs (d) AFM micrograph of SS 316L (e) AFM micrograph of SS 316L immersed only in Hank's solution (f) AFM micrograph of SS 316L immersed in Hank's solution with IONPs

#### 1.4 Anti- corrosive studies of IONPs synthesized from *S. chirata* stem extract in PBS as corrosive media

##### 1.4.1 Weight loss measurements

The I.E of IONPs against the corrosion of SS 316 L in the presence of PBS as corrosive media was analysed with the help of weight loss measurement study as shown in table 4.5. The reduction in corrosion rate with increasing IONPs content was seen and it was also observed that the increment in the I.E was depended on concentration of IONPs and maximum I.E against corrosion was

76.74 % ( $\pm 0.377$ ) at 100 ppm IONPs concentration. It was assumed that the IONPs get adsorbed on the surface of the SS 316L leading to an increased efficiency against corrosion thus by decreasing the rate of corrosion [208]. The linear coefficient value obtained was 0.9950 which is near to 1 suggesting the adsorption of IONPs on SS 316L surface follows the pattern of Langmuir adsorption isotherm (fig. 4.7)

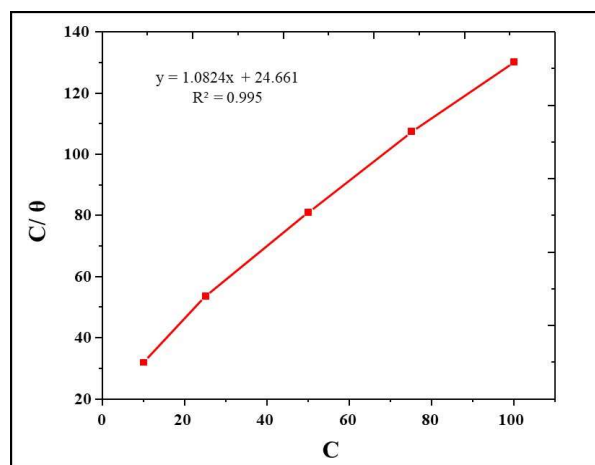


Fig. 4.13 Langmuir adsorption isotherm of *S. chirata* synthesized IONPs on SS 316L surface with the weight loss measurements in PBS

Table 4.5 Weight loss and adsorption isotherm parameters for *S. chirata* synthesized IONPs in different concentrations on SS 316L immersed in PBS

Concentration (C)	$C_R$ (mmy <sup>-1</sup> )	I.E (%) $\pm$ St. Dev.	$\theta$	C/θ
PBS	0.00086	-	-	-
PBS + 10 ppm IONPs	0.00066	31.23 $\pm$ 2.334	0.3123	32.02
PBS + 25 ppm IONPs	0.00046	46.51 $\pm$ 0.883	0.4651	53.75
PBS + 50 ppm IONPs	0.00033	61.62 $\pm$ 0.284	0.6162	81.14
PBS + 75 ppm IONPs	0.00026	69.76 $\pm$ 1.065	0.6976	107.51
PBS + 100 ppm IONPs	0.00020	76.74 $\pm$ 0.377	0.7674	130.31

### 1.4.2 Electrochemical study

The impedance study revealed the increase in charge transfer resistance values suggesting the increasing efficiency against corrosion and the obtained Nyquist plot is shown in fig. 4.14 (a). The resultant efficiency against corrosion was seen around 75.98 % at 100 ppm of IONPs concentration. The IONPs get adsorbed on the surface of SS 316 L sample and formed a layer and hence reduces the flow of electrons thus by increasing the charge transfer resistance of the reaction process [230]. The polarization curves or Tafel plots were also obtained for analysing the corrosion inhibitory effect of IONPs. From this study, the extrapolation of the curves at anodic or cathodic site at their intersection point gave the values for corrosion current density. Fig. 4.14 (b) shows the obtained Tafel plots. As the content of IONPs in the PBS increases, the current density decreased [231]. The formation of protective layer on the SS 316L surface can be the reason for decrease in the corrosion current density. This can be attributed to the adsorption of IONPs on the SS 316L surface thus protecting it from dissolution in the presence of corrosive medium PBS [232]. The value obtained for  $E_{corr}$  was in between the range of 30- 35 mV and less than 85mV shift in the corrosion potential is considered as mixed type of inhibition [233]. Also the maximum inhibition efficiency obtained was 76.16 % with 100 ppm of IONPs concentration [234]. From the potentiodynamic study, it can be concluded that the adsorption of IONPs leads to a protecting action on the surface of SS 316L from corrosion [235]. The obtained data for the electrochemical impedance spectroscopy and potentiodynamic polarization are shown in table 4.6. The adsorption of IONPs on the steel substrate is also well supported by the data obtained from bode plot and phase angle graph shown in fig. 4.14 (c) and (d). The phase angle values obtained suggest the resistive nature against corrosion due to the presence of different concentration of IONPs. From the obtained data from these graphs it is suggested that the anticorrosive property of IONPs increased with the increment in the concentration of IONPs. Also the formation of protective barrier leads to decrement in the value of capacitance hence making the surface of the steel less prone to dissolution thus by preventing the

corrosion process in the harmful corrosive environments [236]. The results given by electrochemical analysis collectively suggest the anti-corrosive property of IONPs and their use as potent corrosion inhibitor in aggressive body environments.

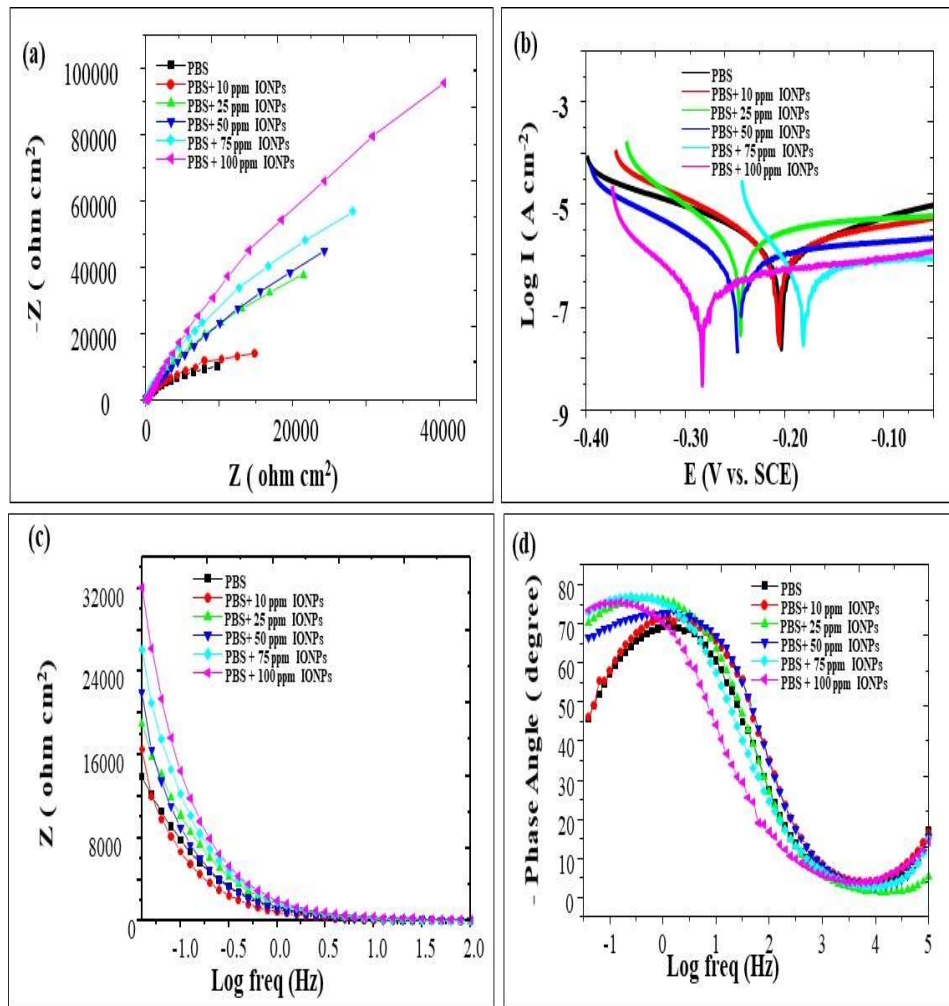


Fig. 4.14 Electrochemical studies of the effect of different concentrations *S. chirata* synthesized IONPs on SS 316L surface (a) Nyquist plot (b) Tafel plot (c) Bode plot and (d) phase angle plot in PBS

Table 4.6 Parameters of electrochemical analysis for SS 316L in PBS containing different concentration of *S. chirata* synthesized IONPs

Concentration (C)	Electrochemical parameters		Potentiodynamic parameters	
	R <sub>ct</sub> (Ω cm <sup>-2</sup> )	I. E (%)	I <sub>corr</sub> <sup>0</sup> (A cm <sup>-2</sup> ) * 10 <sup>-7</sup>	I. E (%)
PBS	9751.60	-	6.21	-
PBS + 10 ppm IONPs	14817.39	34.18	3.88	37.52
PBS + 25 ppm IONPs	21457.97	54.55	2.57	58.61
PBS + 50 ppm IONPs	24313.21	59.89	2.40	61.35
PBS + 75 ppm IONPs	28172.66	65.38	1.95	68.48
PBS + 100 ppm IONPs	40610.32	75.98	1.48	76.16

### 1.4.3 Surface investigation studies by SEM and AFM

The SEM and AFM images of polished SS 316 L sample, SS 316 L sample immersed in PBS and SS 316 L sample immersed in PBS containing 100 ppm of IONPs are shown in fig. 4.15 (a, b, c) and fig. 4.15 (d, e, f) respectively. From the analysis of images by SEM, it can be seen that the SS 316 L sample which was immersed in PBS showed very rough and damaged surface in comparison to the SS 316 L sample containing 100 ppm IONPs in PBS [237]. This difference in the surface images of the steel samples is attributed to the presence of protective barrier on the surface of steel formed by the presence of IONPs. From the AFM analysis, the roughness values of the surface of the steel samples were obtained and it was found that the polished SS 316 L surface and the SS 316 L placed in PBS only, has a surface roughness value of around 39.8 nm and 949.0 nm respectively while the surface roughness value of SS 316L immersed in PBS with 100 ppm of IONPs was around 585.0 nm. This decrease in roughness of surface can be attributed to the formation of a protective coating

which helped in blocking the transfer of electrons and hence protecting the SS 316L surface from the attack of corrosive solution [238].

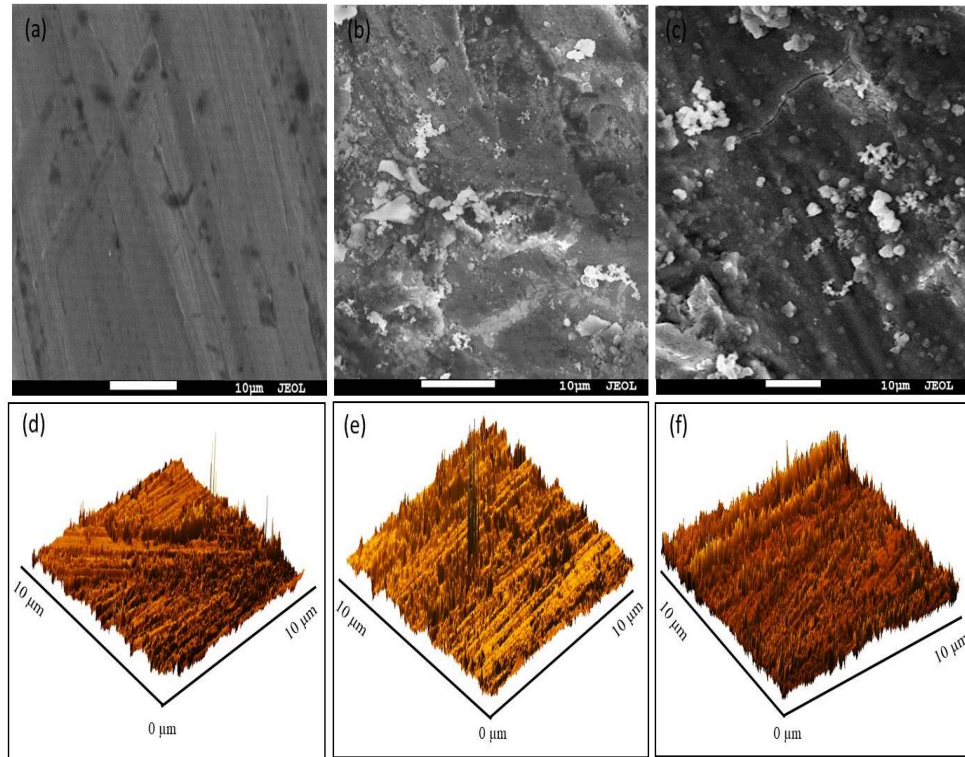


Fig. 4.15 Images showing (a) SEM micrograph of SS 316L (b) SEM micrograph of SS 316L immersed only in PBS (c) SEM micrograph of SS 316L immersed in PBS with IONPs (d) AFM micrograph of SS 316L (e) AFM micrograph of SS 316L immersed only in PBS (f) AFM micrograph of SS 316L immersed in PBS with IONPs

## 2. Iron oxide NPs (IONPs) synthesized from *T. arjuna* bark extract

### 2.1 Characterization studies for synthesized NPs

#### 2.1.1 UV-vis spectroscopy

After the initiation of reaction for the synthesis of IONPs, UV –vis spectroscopy was the first study which was done for the initial identification of NPs. The yellow color of the ferric chloride solution readily changed to dark brown after the addition of *Terminalia arjuna* bark extract as recorded from visual

observation which indicated the formation of NPs [183]. The occurrence of surface plasmon resonance and formation of colloidal solution indicated the formation of IONPs. The formation of metal NPs was confirmed by taking the adsorption spectra of the colloidal solution containing the synthesized NPs. The adsorption maxima were recorded in between the range of 250- 300 nm [184]. Factors like concentration of ferric chloride salt solution, volume of plant extract, effect of pH and various incubation temperature were taken into concentration.

With the increase in the concentration of ferric chloride salt in the solution, there is also increment in the intensity of absorption peak. The high peak intensity generally states that there is formation of more NPs at that concentration but it also shows their tendency to aggregate [185] and formation of precipitate like material and it was observed visually that the NPs synthesized with more than 50mM ferric chloride concentration, aggregated and settled down. Hence, 50 mM was chosen as optimum ferric chloride concentration for the synthesis of stable NPs which were uniformly dispersed thus making a stable colloidal solution. Volume of plant extract was also varied from 0.5 ml to 4 ml and it was found that the colloidal solution of NPs without the formation of any precipitates or aggregated mass was attained at 4 ml of plant extract volume. Also pH from 3 to 9 was varied to get the idea of the pH of synthesized NPs [186]. It was found that pH at 6 was optimal for synthesizing the stable NPs. Nanoparticle's incubation at different temperatures was also tested to find the optimum temperature for the effective synthesis of NPs [187, 188]. The optimum temperature was found out to be 25°C as even after 2 hour of incubation time for the reaction mixture, there is increase in the peak intensity but the peak intensity decreased after 2-hour incubation in all the other temperatures. Also, an increase in aggregation was also observed at higher temperatures. The aggregation of NPs indicated by higher peak intensities was also reported in the literature [189]. The optimum reaction parameters are necessary to enable the effective synthesis of NPs with high stability. Hence, for the synthesis of iron oxide NPs, 50 mM ferric chloride concentration, 4 ml volume of plant extract, pH at 6 and 25°C temperature were taken as optimum

parameters. Also, the NPs synthesized with the identified optimum parameters were also subjected to UV-Vis spectroscopy at different incubation time to check the rate of nanoparticle synthesis and maximum reduction of ferric chloride [190]. It was found that, after 15 min of incubation time, there is no or very minimum change in the synthesis mechanism as there is decrease in the peak intensity with increasing incubation time indicating the maximum reduction time for ferric chloride salt solution at 15 minute [191]. Fig. 4.16 shows the UV-vis spectra of synthesized IONPS at different parameters.

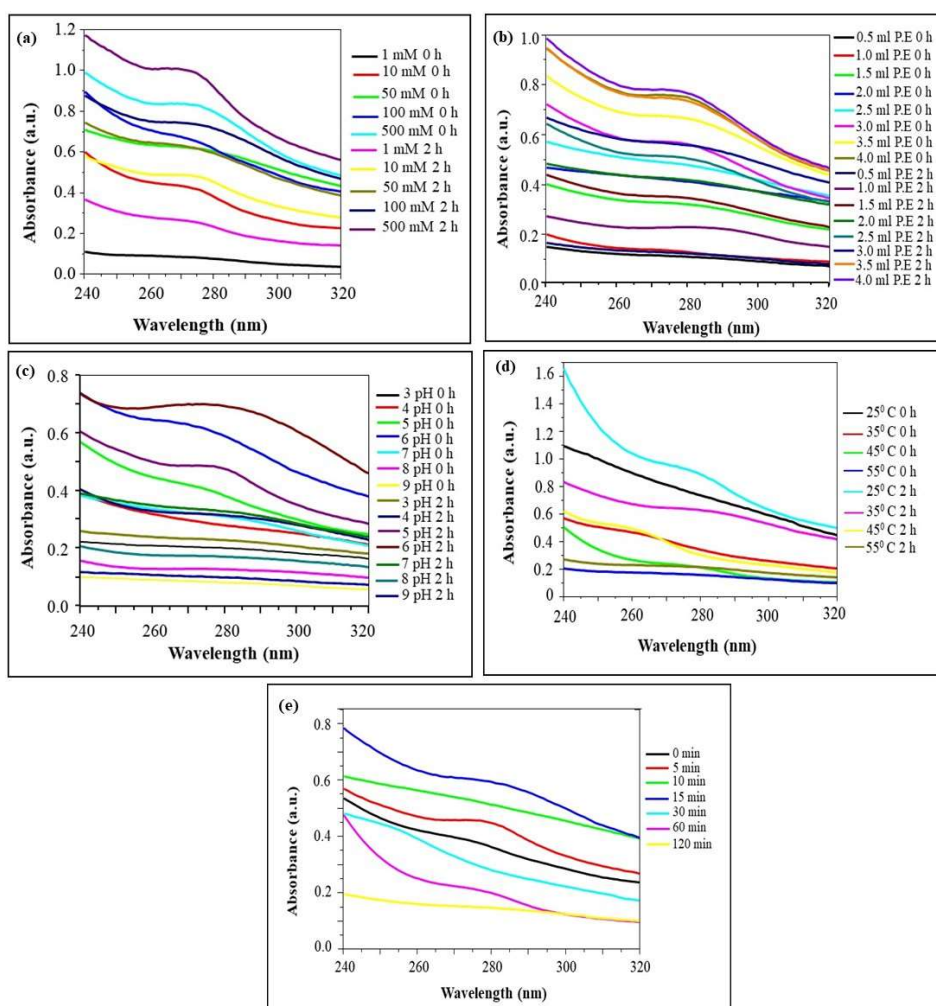


Fig. 4.16 UV-vis spectroscopy of IONPs synthesized from *T. arjuna* bark extract at (a) different Ferric chloride concentrations (b) different plant extract concentrations (c) different pH (d) different temperatures (e) different incubation time



Hence for the characterization studies, the IONPs were synthesized using optimal reaction condition to ensure stable synthesis.

### 2.1.2 Zeta potential and size distribution

Fig. 4.17 (a) shows the zeta potential graph of synthesized NPs. From the results, it was found that the synthesized NPs possess a zeta potential of -11.8 mV. The size distribution analysis done by dynamic light scattering and is shown in fig. 4.17 (b) suggested the hydrodynamic diameter of synthesized NPs to be around of 150 nm and this also suggest that the particles are of nanometric size with broad range of size distribution in the colloidal solution.

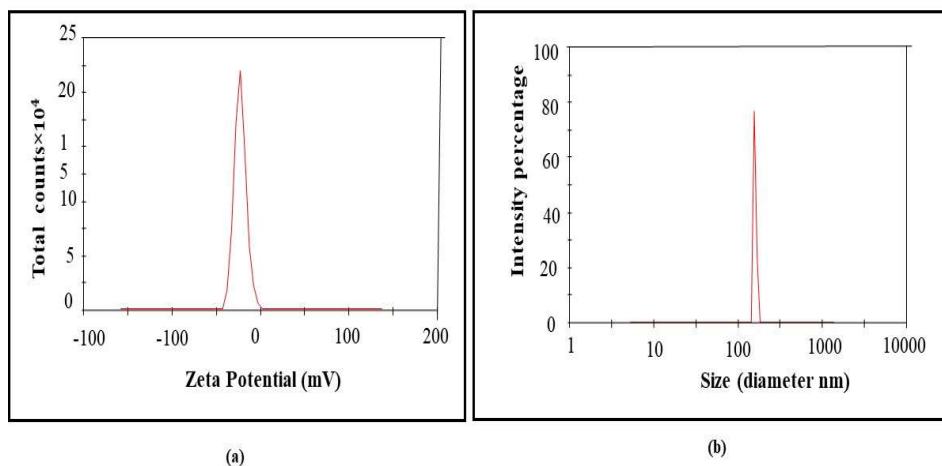


Fig. 4.17 (a) zeta potential and (b) size distribution pattern of synthesized IONPs

### 2.1.3 X- ray diffraction study

For the analysis of the physical nature of the prepared NPs, x-ray diffraction study was conducted. Fig 4.18 shows the obtained XRD pattern of prepared IONPs. There is a presence of broad peak in the graph which suggested the small size of synthesized NPs and crystalline in nature which can be attributed to the phytochemicals present in the plant extract giving crystalline nature to the NPs [196]. The Bragg's angles or  $2\theta$  are shown by XRD graph at 14.9, 18.3, 23.8, 26.1, 30.2, 33.9, 37.2, 38.8, 44.7, 47.4, 53.7 corresponding to 110, 111, 210, 211, 220, 310, 222, 320, 410, 331, 422 lattice planes, respectively. Also

the chemical formula of synthesized NPs as given by XRD is  $Fe_2O_3$  with the mineral form maghemite and the structural lattice of IONPs was found to be cubic. The cubic lattice structure contains oxygen which causes loosely packed cubic structure and ferric ions are present at tetrahedral and octahedral sites. These IONPs when given ambient conditions, are considered as most stable and find wide use in catalysts, gas sensors, pigments and for biomedical applications [239, 240].

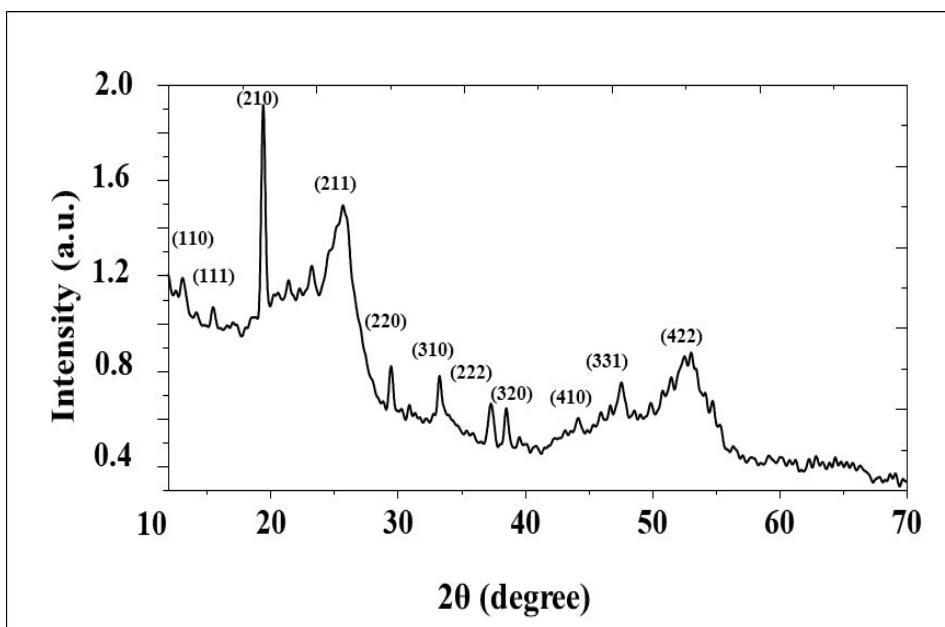


Fig. 4.18 X-ray diffraction pattern of *T. arjuna* synthesized IONPs

#### 2.1.4 Scanning electron microscopy (SEM) and Transmission electron microscopy (TEM)

The spherical shape of 50- 60 nm in size was clearly visible from the SEM images shown in fig. 4.19 (a) from the SEM images it can be seen that there is clustering of NPs due to very low surface charge as analyzed from the zeta potential study. The EDX spectra revealed iron and oxygen peaks present in the analyzed samples which confirm that the synthesized NPs were of iron oxide as shown in fig. 4.19 (b). For the confirmation of exact size and morphological features of NPs, TEM analysis was done and it was found that the IONPs were

of approximately 50 nm in size as given in fig. 4.19 (b). Hence, the spherical shaped, 50- 60 nm in diameter synthesized IONPs were obtained from the bark extract of *T. arjuna* with agglomeration properties which are helpful in their effective applicability [198].

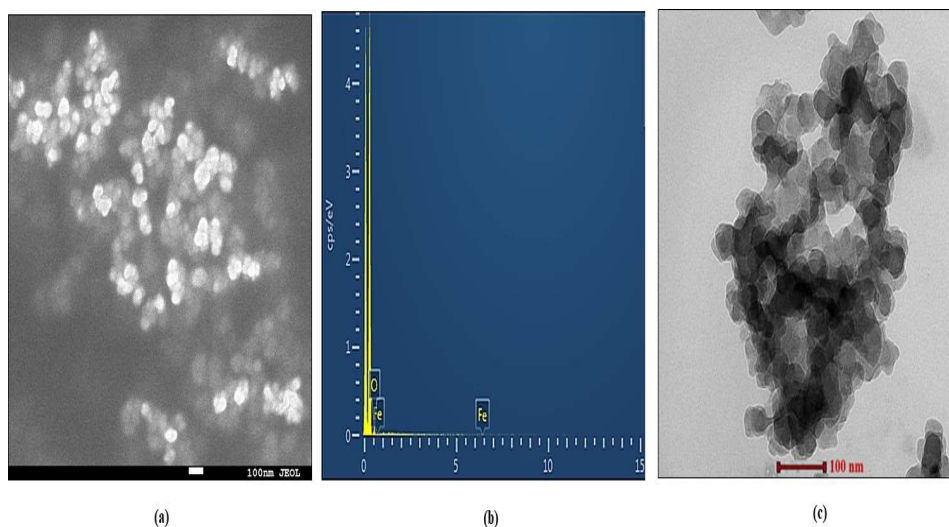


Fig. 4.19 (a) SEM image (b) EDX spectra and (c) TEM image of IONPs

### 2.1.5 Atomic force microscopy (AFM)

Three dimensional topographical features of synthesized IONPs was determined by AFM and the results are given in fig. 4.20 (a, b, c). It can be seen that there is presence of spherical IONPs with few aggregated IONPs. Spherical shape of IONPs is clearly visible from the 2-D AFM image. The agglomerated or clustered NPs can be seen which can be attributed to the presence of strong intermolecular bonding which takes place between the phytochemical constituents on the IONPs surface thus providing it a characteristic property which can be explored for various applications [199, 200].

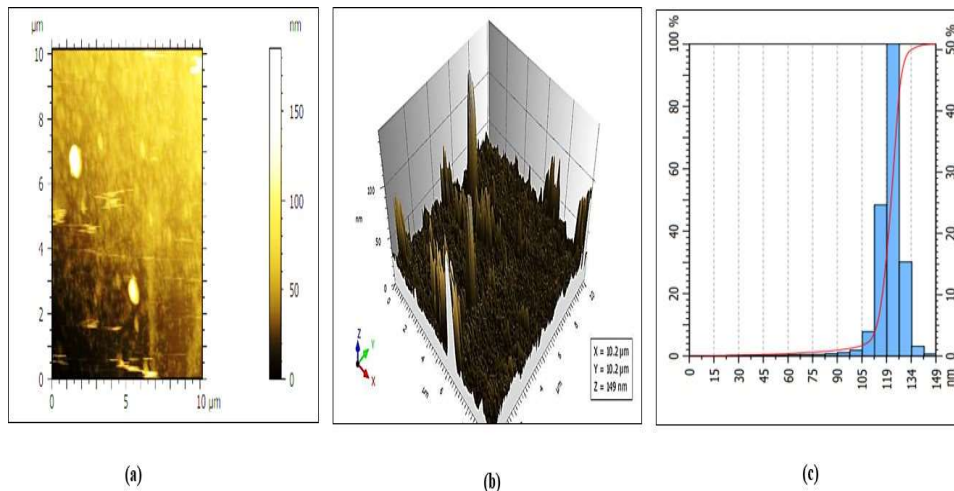


Fig. 4.20 Atomic force microscope images of (a) 2- D image (b) 3-D image and (c) size distribution maxima of synthesized IONPs

### 2.1.6 Fourier Transform Infrared Spectroscopy

The different FTIR peaks observed for the *T. arjuna* bark extract and for the IONPs are shown in fig. 4.21. From the FTIR spectra of bark extract, it can be seen that there are peaks present at 3323 which corresponds to the presence of stretching of O-H bonds from hydroxyl aliphatic or aromatic group, 2368.66 peak is also present which corresponds to the carbonyl group stretching from ketones [205]. The occurrence of N-O stretching due to the presence of amines and the presence of C-O band from molecules containing  $-\text{OCH}_3$  deforming vibrations attributed to the alkaloids as indicated by the peaks observed at 1310.23 and 1026.16.02 respectively. Further, the observed spectra for IONPs showed various peaks corresponding to the FTIR spectra of *T. arjuna* bark extract. The peaks for IONPs were observed at 3365.89, 2347.44, 1566.25 and 1057.02  $\text{cm}^{-1}$  which indicated the action of various phyto functional groups. The interaction of compounds from the leaves extract of *T. arjuna* with the IONPs causes a shift in the wavelength corresponding to the functional group movement from plant extract to the surface of IONPs in order to facilitate the capping and stabilizing process [206, 207].

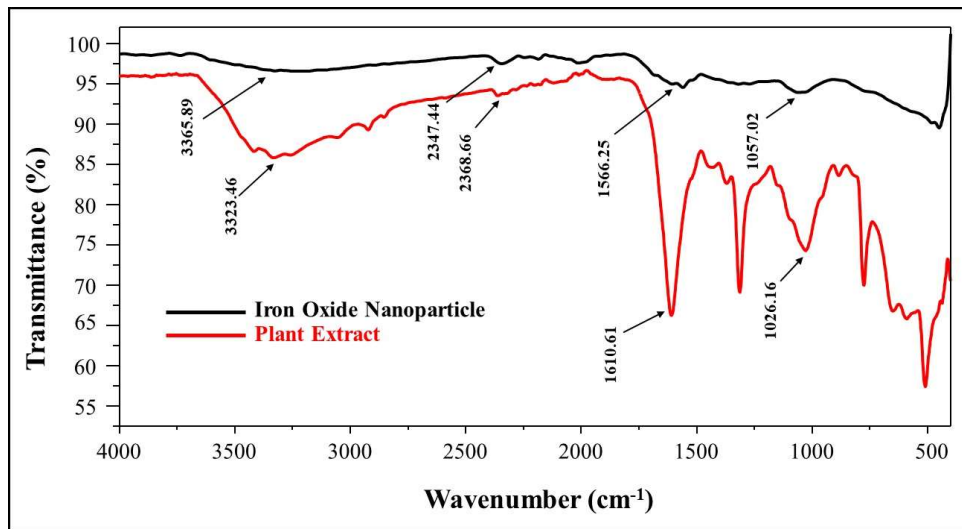


Fig. 4. 21 FTIR spectra of synthesized IONPs along with the FTIR spectra of *T. arjuna* plant extract

## 2.2 Anti- corrosive studies of IONPs synthesized from *T. arjuna* bark extract in Ringer’s solution as corrosive media

### 2.2.1 Weight loss measurements

The I.E of IONPs against the corrosion of SS 316 L in the presence of Ringer’s solution as corrosive media was analysed with the help of weight loss measurement study. The values obtained are shown in table 4.7. From the obtained data, it was concluded that by increasing the concentration of IONPs, the subsequent decrease in corrosion rate was seen and it was also observed that the increment in the I.E depends on the concentration of IONPs. Maximum  $89.05 \pm 0.949$  % I.E was obtained using 100 ppm IONPs. It was assumed that the IONPs get adsorbed on the surface of the SS 316L leading to an increased efficiency against corrosion thus by decreasing the rate of corrosion [208]. The linear coefficient value obtained was 0.9959 which is near to 1 suggesting the adsorption of IONPs on SS 316L surface follows the pattern of Langmuir adsorption isotherm (fig. 4.22).

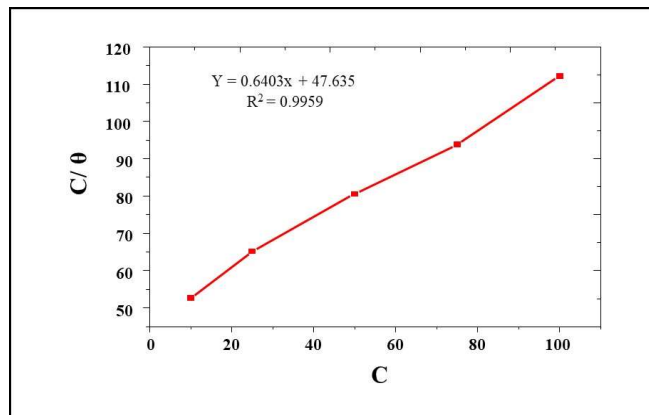


Fig. 4. 22 Langmuir adsorption isotherm of *T. arjuna* synthesized IONPs on SS 316L surface with the weight loss measurements in Ringer’s solution.

Table 4.7 Weight loss and adsorption isotherm parameters for *T. arjuna* synthesized IONPs in different concentrations on SS 316L immersed in Ringer’s solution

Concentration (C)	$C_R$ (mmy <sup>-1</sup> )	I.E (%) ± St. Dev.	$\theta$	C/θ
Ringer’s solution	0.0182	-	-	-
Ringer’s solution + 10 ppm IONPs	0.0148	18.97 ±0.605	0.1897	52.69
Ringer’s solution + 25 ppm IONPs	0.0112	38.32 ±0.181	0.3832	65.23
Ringer’s solution + 50 ppm IONPs	0.0069	62.04 ±0.261	0.6204	80.58
Ringer’s solution + 75 ppm IONPs	0.0036	79.92 ±0.412	0.7992	93.83
Ringer’s solution + 100 ppm IONPs	0.0020	89.05 ±0.949	0.8905	112.29

### 2.2.2 Electrochemical studies

The value of charge transfer resistance increased with an increase in the amount of concentration of IONPs and the obtained Nyquist plot is shown in fig. 4.23 (a), the calculated corrosion inhibition efficiency reached up to a maximum of 77.37 % at 100 ppm of IONPs concentration. The IONPs get adsorbed on the

surface of SS 316 L sample and formed a layer and hence reduces the flow of electrons thus by increasing the charge transfer resistance of the reaction process [209]. The polarization curves or Tafel plots were also obtained for analysing the corrosion inhibitory effect of IONPs. The extrapolation of the curves at anodic or cathodic site at their intersection point gave the values for corrosion current density. The data obtained from polarization analysis is shown in fig. 4.23 (b). The corrosion current density values decreased with an increase in the concentration of IONPs in corrosive media which corresponds to the increase in the corrosion inhibition efficiency of IONPs [210].

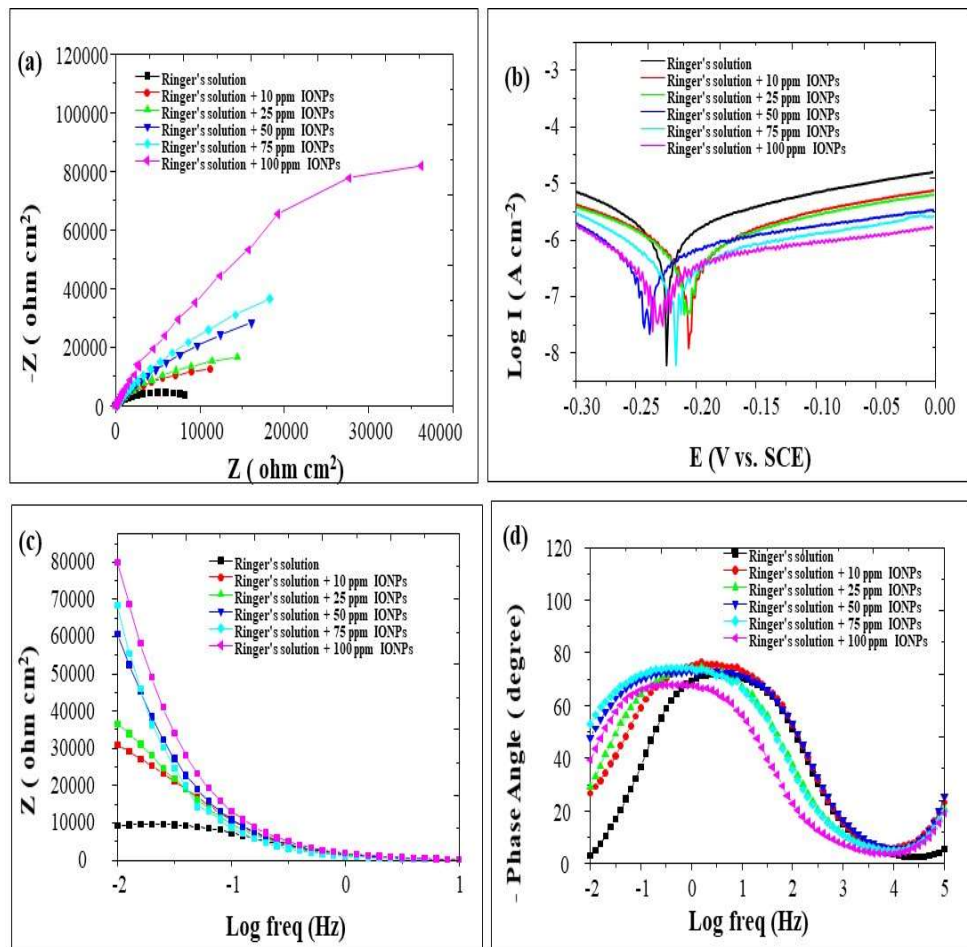


Fig. 4. 23 Electrochemical studies of the effect of different concentrations of *T. arjuna* synthesized IONPs on SS 316L surface in Ringer's solution. (a) Nyquist plot (b) Tafel plot (c) Bode plot and (d) phase angle plot

The formation of protective layer on the SS 316L surface can be the reason for decrease in the corrosion current density. This can be attributed to the adsorption of IONPs on the SS 316L surface thus protecting it from dissolution in the presence of Ringer's solution [211]. The value obtained for  $E_{corr}$  was in between the range of 30- 35 mV. As per reported literature it is concluded that the IONPs behaved as mixed type inhibitor as the NPs protected against corrosion at both anode and cathode with less than 85mV shift in the corrosion potential [212]. The maximum inhibition efficiency obtained was 79.15 % at 100 ppm of IONPs concentration. The electrochemical reactions which takes place at the interface of steel surface and the corrosive media causes dissolution of the metal. In setting up this electrochemical reactions, the anodic and cathodic sites participate significantly [213]. Hence, to protect the metal surface from dissolution, inhibitors are used. The inhibitors target the anodic and cathodic sites actively by inhibiting the mechanism of charge transfer in the electrochemical set up. IONPs contains functional groups on their surface which have heteroatoms present in them. These heteroatoms help in the adsorption of IONPs at the SS 316L surface by making strong coordination bonds. The adsorption can be of chemical nature or physical nature or both. From the potentiodynamic study, it can be concluded that the IONPs get adsorbed on the SS 16L surface and decreased the corrosion current density hence protecting the surface of SS 316L from corrosion [214]. The adsorption of IONPs on the steel substrate is also well supported by the data obtained from bode plot and phase angle graph shown in fig. 4.23 (c) and (d). The results given by electrochemical analysis collectively suggest the anti- corrosive property of IONPs and their use as potent corrosion inhibitor in aggressive body environments. The obtained data for the electrochemical impedance spectroscopy and potentiodynamic polarization are shown in table 4.8.



Table 4.8 Parameters of electrochemical analysis for SS 316L in Ringer's solution containing different concentration of *T. arjuna* synthesized IONPs.

Concentration (C)	Electrochemical parameters		Potentiodynamic parameters	
	R <sub>ct</sub> (Ω cm <sup>-2</sup> )	I. E (%)	I <sup>0</sup> <sub>corr</sub> (A cm <sup>-2</sup> ) * 10 <sup>-7</sup>	I. E (%)
Ringer's solution	8200.286	-	9.98	-
Ringer's solution + 10 ppm IONPs	11169.86	26.58	7.11	28.75
Ringer's solution + 25 ppm IONPs	14373.32	42.94	5.62	43.68
Ringer's solution + 50 ppm IONPs	16114.95	49.11	4.91	50.80
Ringer's solution + 75 ppm IONPs	18259.20	55.08	4.32	56.71
Ringer's solution + 100 ppm IONPs	36240.73	77.37	2.08	79.15

### 2.2.3 Surface investigation studies by SEM and AFM

The SEM and AFM images of polished SS 316 L sample, SS 316 L sample immersed in Ringer's solution and SS 316 L sample immersed in Ringer's solution containing 100 ppm of IONPs were taken as shown in fig. 4.24 (a, b, c) and (d, e, f) respectively. From the SEM study, it was observed that the SS 316 L sample which was immersed in Ringer's solution showed very rough and damaged surface in comparison to the SS 316 L sample containing 100 ppm IONPs in Ringer's solution [217]. From the AFM analysis, the roughness values of the surface of the steel samples were obtained and it was found that the polished SS 316 L surface and the SS 316 L placed in Ringer's solution only, has a surface roughness value of around 39.8 nm and 999.0 nm, respectively. The surface roughness for IONPs containing SS 316L was 605.0 nm. This decrease in roughness of surface suggested less damaged surface due to the

blocking of transfer of electrons and hence protecting the SS 316L surface from the attack of corrosive solution [218].

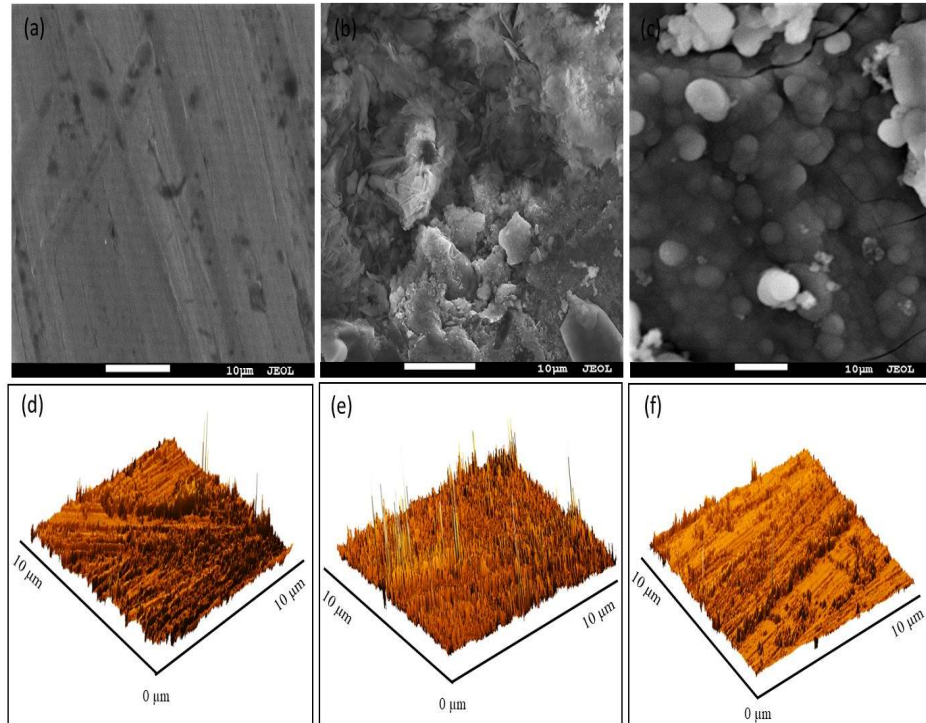


Fig. 4.24 Images showing (a) SEM micrograph of SS 316L (b) SEM micrograph of SS 316L immersed in Ringer's solution (c) SEM micrograph of SS 316L immersed in Ringer's solution with IONPs (d) AFM micrograph of SS 316L (e) AFM micrograph of SS 316L immersed in Ringer's solution (f) AFM micrograph of SS 316L immersed in Ringer's solution with IONPs.

### 2.3 Anti-corrosive studies of IONPs synthesized from *T. arjuna* bark extract in Hank's solution as corrosive media

#### 2.3.1 Weight loss measurements

The I.E of IONPs against the corrosion of SS 316 L in the presence of Hank's solution as corrosive media was analysed with the help of weight loss measurement study. The values obtained are shown in table 4.9. From the obtained data, it was concluded that by increasing the concentration of IONPs,

the subsequent decrease in corrosion rate was noticed and it was also observed that the increment in the I.E was depended on concentration of IONPs and maximum I.E against corrosion was 89.80 % ( $\pm 0.216$ ) at 100 ppm IONPs concentration. It was assumed that the IONPs get adsorbed on the surface of the SS 316L leading to an increased efficiency against corrosion thus by decreasing the rate of corrosion [208]. The linear coefficient value obtained was 0.9926 which is near to 1 suggesting the adsorption of IONPs on SS 316L surface follows the pattern of Langmuir adsorption isotherm (fig. 4.25)

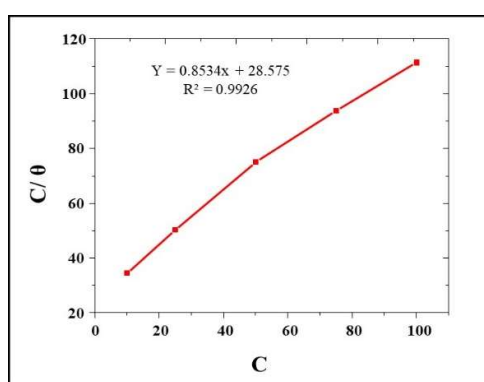


Fig. 4.25 Langmuir adsorption isotherm of *T. arjuna* synthesized IONPs on SS 316L surface with the weight loss measurements in Hank's solution

Table 4.9 Weight loss and adsorption isotherm parameters for *T. arjuna* synthesized IONPs in different concentrations on SS 316L immersed in Hank's solution

Concentration (C)	$C_R$ (mm $y^{-1}$ )	I.E (%) $\pm$ St. Dev.	$\theta$	C/ $\theta$
Hank's solution	0.017	-	-	-
Hank's solution + 10 ppm IONPs	0.0120	29.01 $\pm$ 0.847	0.2901	34.4594
Hank's solution + 25 ppm IONPs	0.0085	49.80 $\pm$ 0.200	0.4980	50.1968
Hank's solution + 50 ppm IONPs	0.0056	66.66 $\pm$ 1.378	0.6666	75.0000
Hank's solution + 75 ppm IONPs	0.0034	80.00 $\pm$ 0.135	0.8000	93.7500
Hank's solution + 100 ppm IONPs	0.0017	89.80 $\pm$ 0.216	0.8980	111.3537

### 2.3.2 Electrochemical studies

Electrochemical studies were done by obtaining the data from electrochemical impedance spectroscopy obtained from Nyquist plot, potentiodynamic polarization data given as Tafel plot, bode plot and phase angle values. The obtained Nyquist plot is shown in fig. 4.26 (a). A maximum of 79.53 % at 100 ppm of IONPs concentration was observed. The IONPs get adsorbed on the surface of SS 316 L sample and formed a layer and hence reduces the flow of electrons thus by increasing the charge transfer resistance of the reaction process [220]. The data obtained from polarization analysis is shown in fig. 4.26 (b). IONPs presence in corrosive media leads to decrease in current density corresponding to the increase in the corrosion inhibition efficiency of IONPs [221].

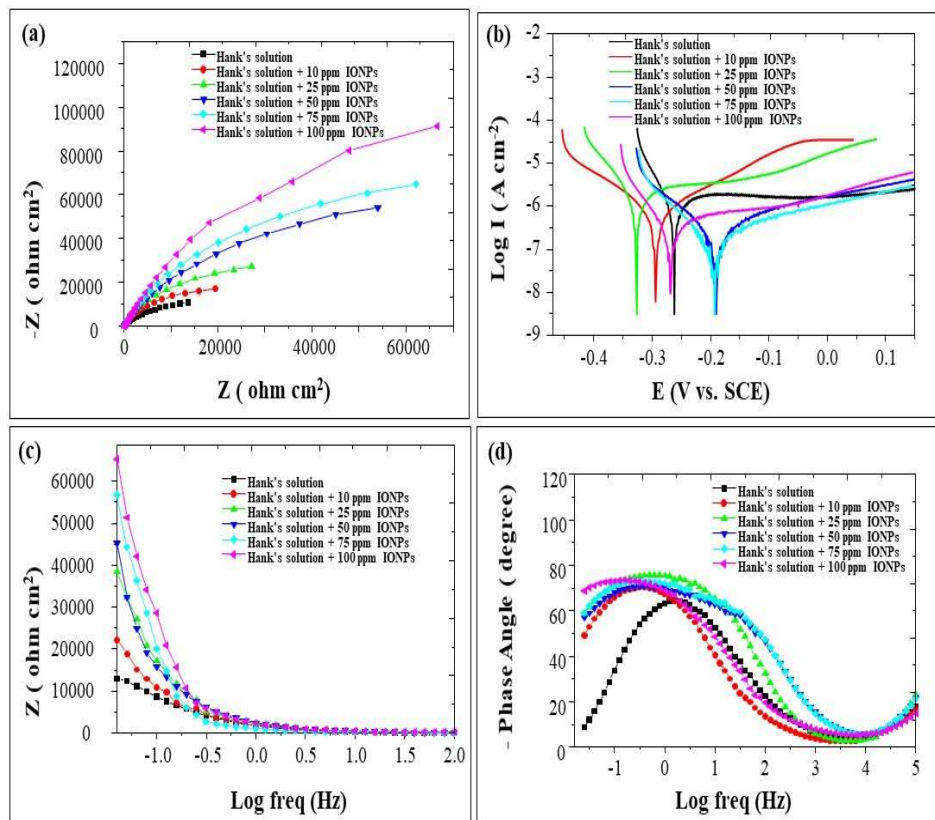


Fig. 4.26 Electrochemical studies of the effect of different concentrations *T. arjuna* synthesized IONPs on SS 316L surface (a) Nyquist plot (b) Tafel plot (c) Bode plot and (d) phase angle plot in Hank's solution

The value obtained for  $E_{corr}$  was in between the range of 30- 35 mV which leads to mixed type of inhibition [223]. Also the maximum inhibition efficiency obtained was 80.06 % with 100 ppm of IONPs concentration. From the potentiodynamic study, it can be concluded that the IONPs helps in protecting the surface of SS 316L from corrosion [225]. The obtained data for are shown in table 4.10. The adsorption of IONPs on the steel substrate is also well supported by the data obtained from bode plot and phase angle graph is given in fig. 4.26 (c) and (d). The phase angle values obtained suggest the resistive nature against corrosion due to the presence of different concentration of IONPs. From the obtained data, it is suggested that the anticorrosive property of IONPs increased with an increase in the IONPs concentration.

Table 4.10 Parameters of electrochemical analysis for SS 316L in Hank's solution containing different concentration of *T. arjuna* synthesized IONPs.

Concentration (C)	Electrochemical parameters		Potentiodynamic parameters	
	$R_{ct}$ ( $\Omega \text{ cm}^{-2}$ )	I. E (%)	$I_{corr}^0$ ( $\text{A cm}^{-2}$ ) * $10^{-7}$	I. E (%)
Hank's solution	13621.78	-	8.93	-
Hank's solution + 10 ppm IONPs	19445.56	29.94	7.23	19.03
Hank's solution + 25 ppm IONPs	27159.23	49.84	6.24	30.12
Hank's solution + 50 ppm IONPs	53978.83	74.76	5.04	43.56
Hank's solution + 75 ppm IONPs	62139.99	78.07	2.99	66.51
Hank's solution + 100 ppm IONPs	66575.63	79.53	1.78	80.06

### 2.3.3 Surface investigation studies by SEM and AFM

The SEM and AFM images of polished SS 316L sample, SS 316L sample exposed to Hank's solution and SS 316L sample exposed to Hank's solution in the presence of 100 ppm of IONPs are shown in fig. 4.27 (a, b, c) and (d, e, f) respectively. The SEM images showed very rough and damaged surface of Hank's solution exposed to SS 316L as compared to the SS 316 L sample exposed to Hank's solution containing 100 ppm IONPs [227].

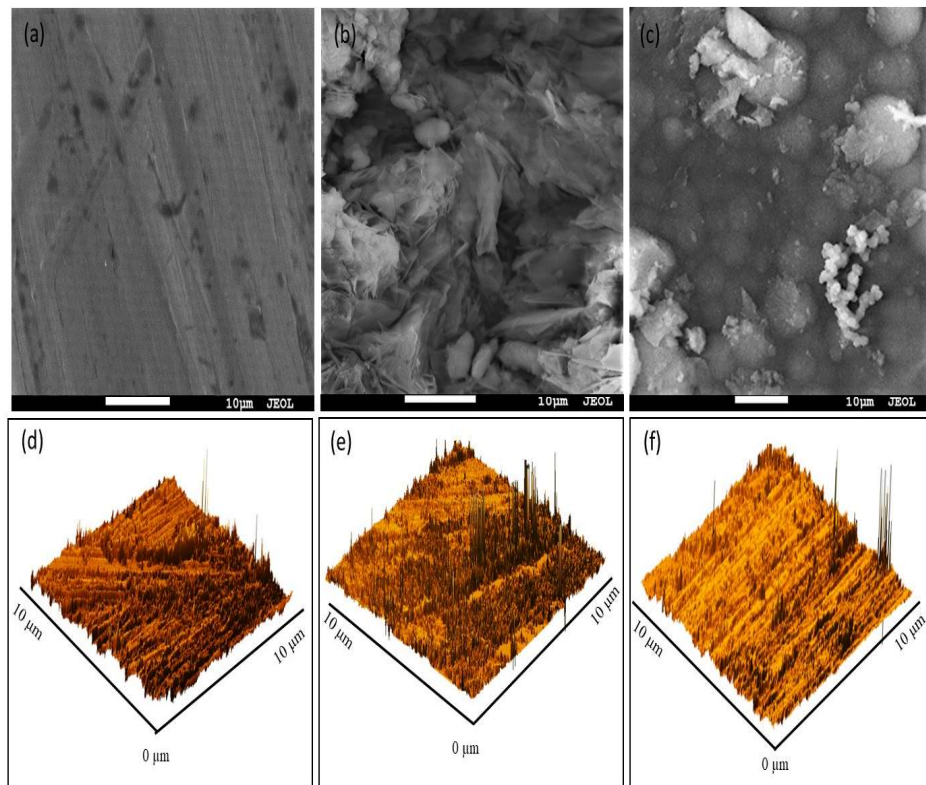


Fig. 4.27 Images showing (a) SEM micrograph of SS 316L (b) SEM micrograph of SS 316L immersed only in Hank's solution (c) SEM micrograph of SS 316L immersed in Hank's solution with IONPs (d) AFM micrograph of SS 316L (e) AFM micrograph of SS 316L immersed in Hank's solution (f) AFM micrograph of SS 316L immersed in Hank's solution containing IONPs

From the AFM analysis, the roughness values of the surface of the steel samples were obtained and it was found that the polished SS 316 L surface and the SS 316 L placed in Hank's solution, has a surface roughness value of around 39.8

nm and 880.0 nm, respectively. However, the surface roughness value of SS 316L immersed in Hank's solution in the presence of 100 ppm of IONPs was around 495.2 nm. The adsorption of IONPs from the solution established a protective layer on the SS 316L surface acting as corrosion inhibitor [228].

## 2.4 Anti- corrosive studies of IONPs synthesized from *T. arjuna* bark extract in PBS as corrosive media

### 2.4.1 Weight loss measurements

The I.E of IONPs against the corrosion of SS 316 L in the presence of PBS was analysed with the help of weight loss measurement study. The values obtained are shown in table 4.11. From the obtained data, it was concluded that by increasing the concentration of IONPs in the corrosive media, the subsequent decrease in corrosion rate was seen and it was also observed that the increment in the I.E depends upon the concentration of IONPs and maximum I.E against corrosion was 88.83 % ( $\pm 0.052$ ) at 100 ppm IONPs concentration. It was assumed that the IONPs get adsorbed on the surface of the SS 316L leading to an increased efficiency against corrosion thus by decreasing the rate of corrosion [208]. The linear coefficient value obtained was 0.9929 which is near to 1 suggesting the adsorption of IONPs on SS 316L surface follows the Langmuir adsorption isotherm (fig. 4.7).

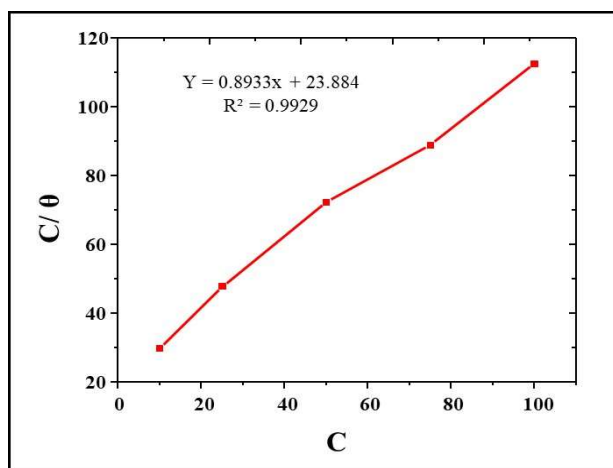


Fig. 4.28 Langmuir adsorption isotherm of *T. arjuna* synthesized IONPs on SS 316L surface with the weight loss measurements in PBS

Table 4.11 Weight loss and adsorption isotherm parameters for *T. arjuna* synthesized IONPs in different concentrations on SS 316L immersed in PBS.

Concentration (C)	$C_R$ (mmy <sup>-1</sup> )	I.E (%) $\pm$ St. Dev.	$\theta$	C/ $\theta$
PBS	0.013133	-	-	-
PBS + 10 ppm IONPs	0.008733	33.50 $\pm$ 0.599	0.3350	29.84
PBS + 25 ppm IONPs	0.006267	52.28 $\pm$ 0.545	0.5228	47.81
PBS + 50 ppm IONPs	0.004067	69.03 $\pm$ 0.298	0.6903	72.42
PBS + 75 ppm IONPs	0.002067	84.26 $\pm$ 0.360	0.8426	89.00
PBS + 100 ppm IONPs	0.001467	88.83 $\pm$ 0.052	0.8883	112.57

#### 2.4.2 Electrochemical studies

The obtained Nyquist plot is shown in fig. 4.29 (a). A maximum of 83.50 % corrosion inhibition activity was seen at 100 ppm of IONPs concentration. The IONPs get adsorbed on the surface of SS 316 L sample and formed a layer and hence reduces the flow of electrons thus by increasing the charge transfer resistance of the reaction process [230]. The polarization curves or Tafel plots were also obtained for analysing the corrosion inhibitory effect of IONPs. The data obtained from polarization analysis is shown in fig. 4.29 (b). The value obtained for  $E_{corr}$  was in 30- 35 mV range which suggests their behaviour as inhibitor of mixed type. Also, the maximum inhibition efficiency obtained was 82.37 % with 100 ppm of IONPs concentration. From the potentiodynamic study, it can be concluded that the IONPs get adsorbed on the SS 16L surface and decreased the corrosion current density hence protecting the surface of SS 316L from corrosion [235]. The obtained data electrochemical conducted is shown in table 4.12. The adsorption of IONPs on the steel substrate is also well supported by the data obtained from Bode plot and phase angle graph are given



in fig. 4.29 (c) and (d). It is clear from these graphs that the anticorrosive property of IONPs increased with the increment in the concentration of IONPs.

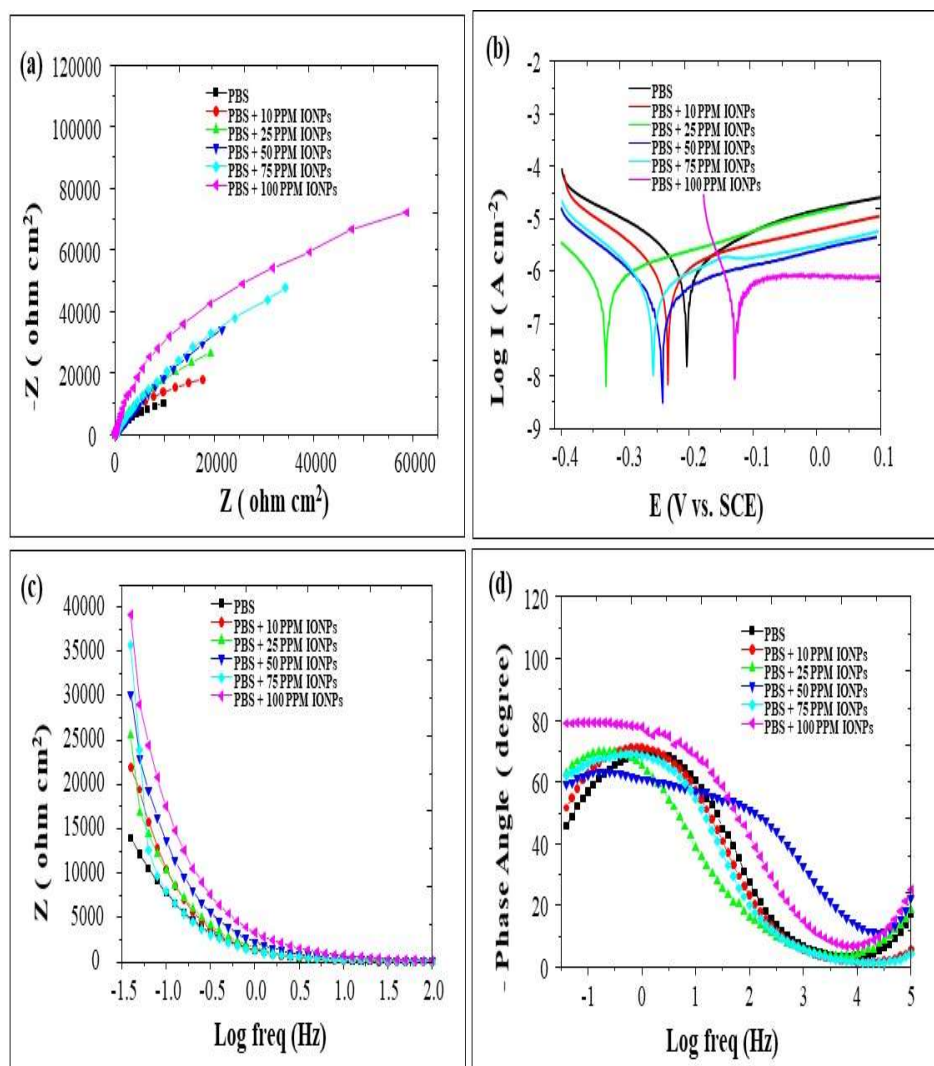


Fig. 4.29 Electrochemical studies of the effect of different concentrations of *T. arjuna* synthesized IONPs on SS 316L surface (a) Nyquist plot (b) Tafel plot (c) Bode plot and (d) phase angle plot in PBS

Table 4.12 Parameters of electrochemical analysis for SS 316L in PBS containing different concentration of *T. arjuna* synthesized IONPs.

Concentration (C)	Electrochemical parameters		Potentiodynamic parameters	
	R <sub>ct</sub> (Ω cm <sup>-2</sup> )	I. E (%)	I <sup>0</sup> <sub>corr</sub> (A cm <sup>-2</sup> ) * 10 <sup>-7</sup>	I. E (%)
PBS	9677.657	-	6.24	-
PBS + 10 ppm IONPs	17675.58	45.24	3.74	40.06
PBS + 25 ppm IONPs	19267.59	49.77	3.24	48.07
PBS + 50 ppm IONPs	21493.46	54.97	2.90	53.52
PBS + 75 ppm IONPs	34259.72	71.75	1.52	75.64
PBS + 100 ppm IONPs	58668.96	83.50	1.10	82.37

### 2.4.3 Surface investigation studies by SEM and AFM

Fig. 4.30 (a, b, c) and (d, e, f) shows the SEM and AFM images of polished SS 316 L sample, SS 316 L sample immersed in PBS and SS 316 L sample immersed in PBS containing 100 ppm of IONPs, respectively. From the analysis of images by SEM, it can be seen that the SS 316 L sample which was immersed in PBS showed very rough and damaged surface in comparison to the SS 316 L sample containing 100 ppm IONPs in PBS [237]. From the AFM analysis, the roughness values of the surface of the steel samples were obtained and it was found that the polished SS 316 L surface and the SS 316 L placed in PBS only, has a surface roughness value of around 39.8 nm and 949.0 nm respectively while the surface roughness value of SS 316L immersed in PBS with 100 ppm of IONPs was around 485.6 nm. This decrease in roughness of surface is due to the protecting action of IONPs against corrosion by blocking the transfer of electrons and hence protecting the SS 316L surface from the attack of corrosive solution [238].

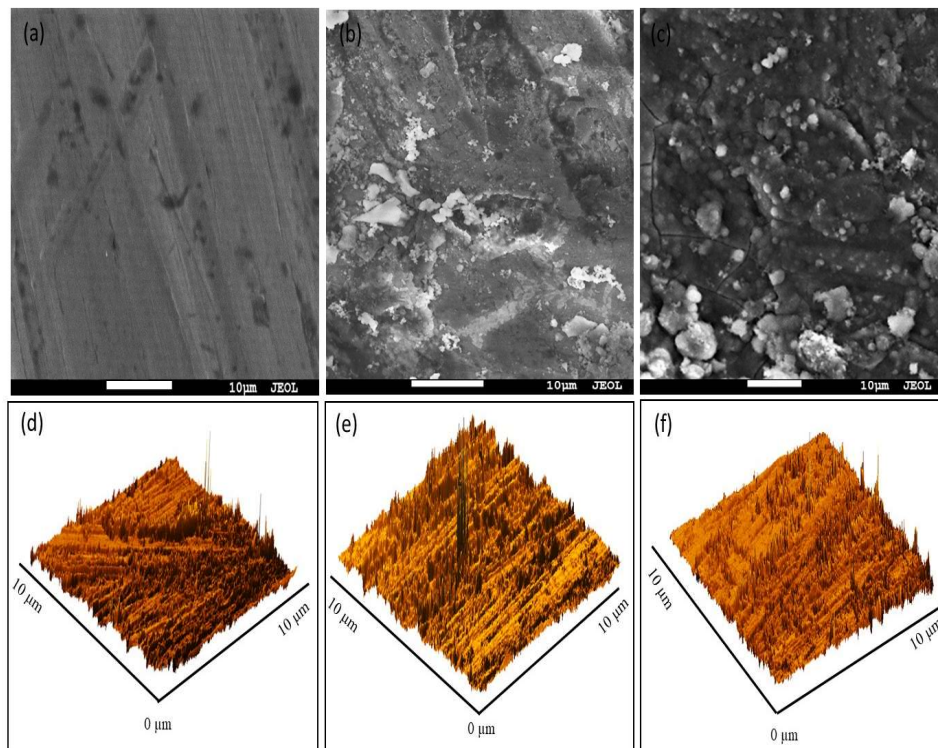


Fig. 4.30 Images showing (a) SEM micrograph of SS 316L (b) SEM micrograph of SS 316L immersed only in PBS (c) SEM micrograph of SS 316L immersed in PBS with IONPs (d) AFM micrograph of SS 316L (e) AFM micrograph of SS 316L immersed only in PBS (f) AFM micrograph of SS 316L immersed in PBS with IONPs

### 3. Iron oxide NPs (IONPs) synthesized from *F. benghalensis* leaves extract

#### 3.1 Characterization studies for synthesized NPs

##### 3.1.1 UV-vis spectroscopy

After the initiation of reaction for the synthesis of IONPs, UV –Vis spectroscopy was the first study which was done for the initial identification of NPs. The yellow color of the ferric chloride solution readily changed to dark brown after the addition of *F. benghalensis* leaves extract as recorded from visual observation indicating the formation of NPs [183]. The adsorption

maxima were recorded in between the range of 250- 300 nm [184]. Factors like concentration of ferric chloride salt solution, volume of plant extract, effect of pH and various incubation temperature were taken into concentration. With the increase in the concentration of ferric chloride salt in the solution, there is also increment in the intensity of absorption peak. The high peak intensity generally states that there is formation of more NPs at that concentration but it also shows their tendency to aggregate [185] and formation of precipitate like material. It was observed visually that the NPs synthesized with more than 50mM ferric chloride concentration, aggregated and settled down. Hence, 50 mM was chosen as optimum ferric chloride concentration for the synthesis of stable NPs which were uniformly dispersed thus making a stable colloidal solution. Volume of plant extract was also varied from 0.5 ml to 4 ml and it was found that the colloidal solution of NPs without the formation of any precipitates or aggregated mass was obtained at 4 ml of plant extract volume. Also, pH from 3 to 9 was varied to get the idea of the pH of synthesized NPs [186]. It was found that pH at 7 was optimal for synthesizing the stable NPs. Different incubation temperatures were also tested to find the optimum temperature for the effective synthesis of NPs [187, 188]. The optimum temperature was found out to be 35°C as even after 2 hour of incubation time for the reaction mixture, there is increase in the peak intensity but the peak intensity decreased after 2-hour incubation in all the other temperatures. Also, an increase in aggregation was also observed at higher temperatures. The aggregation of NPs indicated by higher peak intensities was also reported in the literature [189]. The optimum reaction parameters are necessary to enable the effective synthesis of NPs with high stability. Hence, for the synthesis of IONPs, 10 mM ferric chloride concentration, 4 ml volume of plant extract, pH at 6 and 25°C temperature were taken as optimum parameters. Also, the NPs synthesized with the identified optimum parameters were also subjected to UV –vis spectroscopy at different incubation time to check the rate of NPs synthesis and maximum reduction of ferric chloride [190]. It was found that, after 10 min of incubation time, there is no or very minimum change in the synthesis mechanism as there is decrease in the peak intensity with increasing incubation time indicating the maximum

reduction time for ferric chloride salt solution at 15 minutes [191]. Fig. 4.31 shows the UV-vis spectra of synthesized IONPs at different parameters.

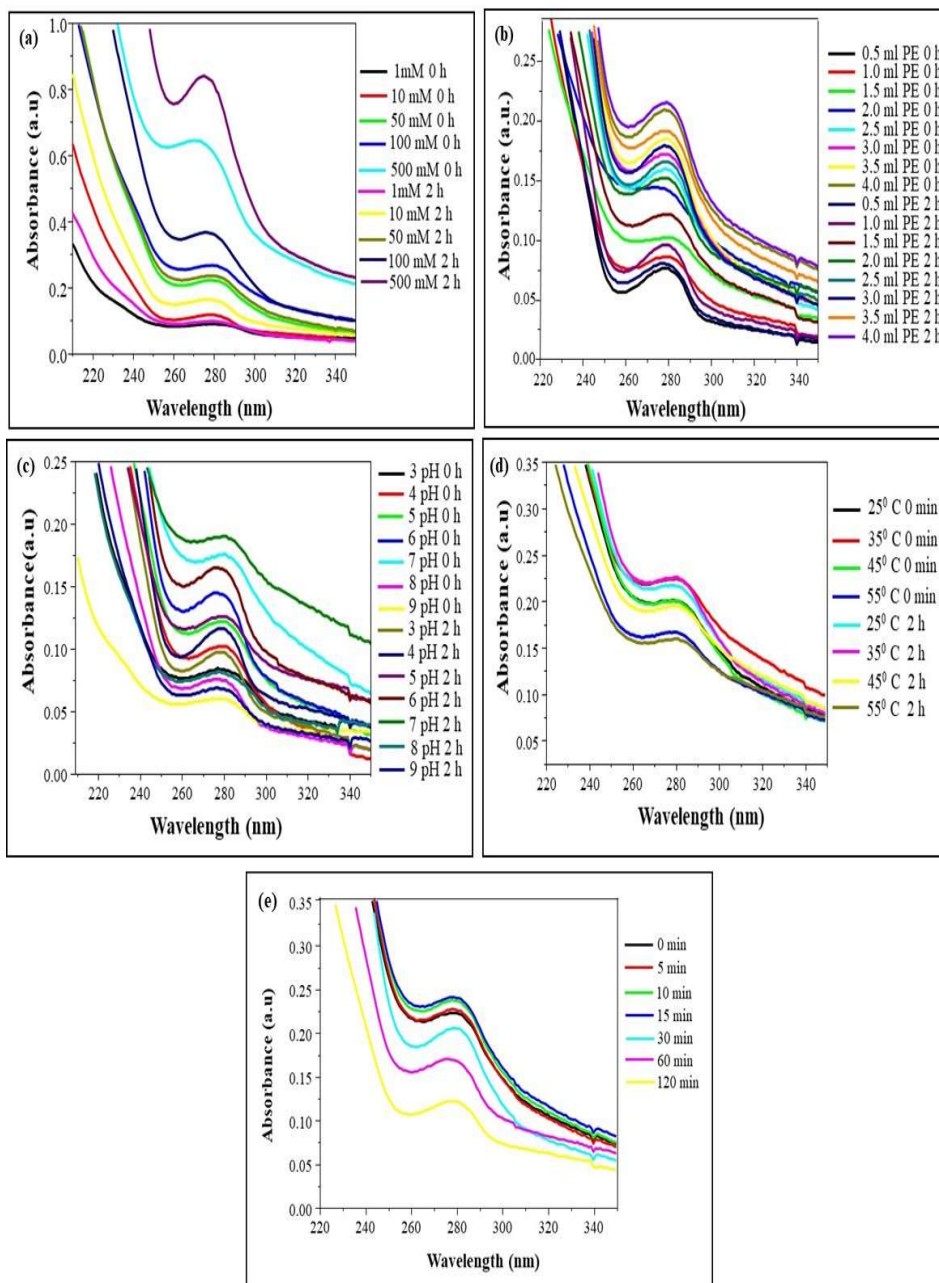


Fig. 4.31 UV-vis spectroscopy of IONPs synthesized from *F. benghalensis* leaves extract at (a) different Ferric chloride concentrations (b) different plant extract concentrations (c) different pH (d) different temperatures (e) different incubation time.

Hence, for the other characterization studies, NPs were synthesized after giving an incubation time of 10 minutes to the reaction mixture for maximum reduction process.

### 3.1.2 Zeta potential and size distribution

To determine the stability of NPs in colloidal solutions, zeta potential analysis was done. Fig. 4.32 (a) shows the zeta potential graph of synthesized NPs. From the results, it was found that the NPs possess a zeta potential of -11.1 mV. The NPs having neutral charge, possess low toxicity due to less interaction with plasma membrane. Hence, neutral NPs are good choice for the applications in biological systems [193]. The size distribution analysis done by dynamic light scattering shown in fig. 4.32 (b) suggested the hydrodynamic diameter of synthesized NPs to be around of 100 nm and this also suggest that the particles are of nanometric size with broad range of size distribution in the colloidal solution.

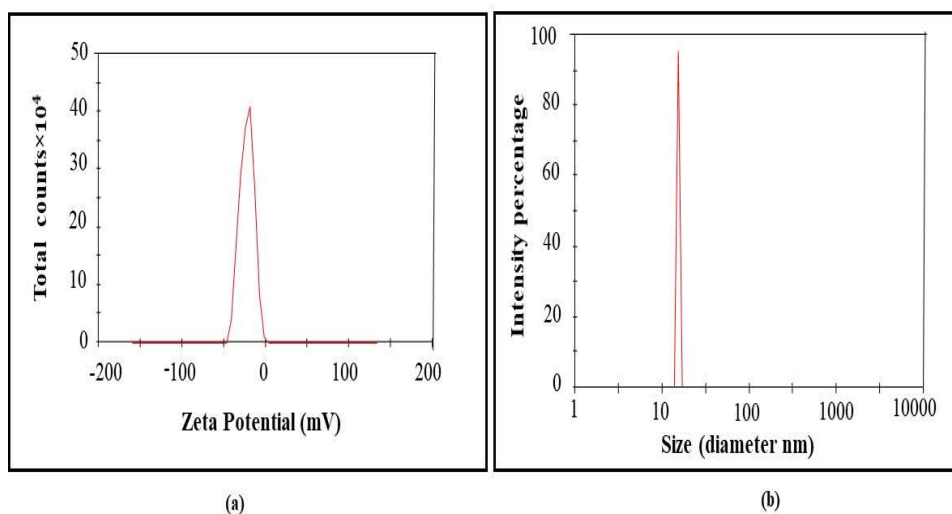


Fig. 4.32 (a) zeta potential and (b) size distribution pattern of synthesized IONPs

### 3.1.3 X-ray diffraction study

For the analysis of the physical nature of the prepared NPs, x-ray diffraction study was conducted. Fig 4.33 shows the obtained XRD pattern of prepared IONPs. There is a presence of numerous peaks in the graph which indicated formation of very small sized IONPs which are crystalline in nature [196]. The Bragg's angles or  $2\theta$  are shown by XRD graph at 24.1, 33.1, 35.608, 39.3, 40.8, 43.4, 49.4, 54.0, 56.1, 57.4, 62.4, 63.9 corresponding to 012, 104, 110, 116, 113, 202, 120, 116, 211, 122, 214, 300, 125 lattice planes respectively. Also the chemical formula of synthesized NPs as given by XRD is  $Fe_2O_3$  with the mineral form name hematite and the structural lattice of iron oxide NPs was found to be rhombohedral axes.

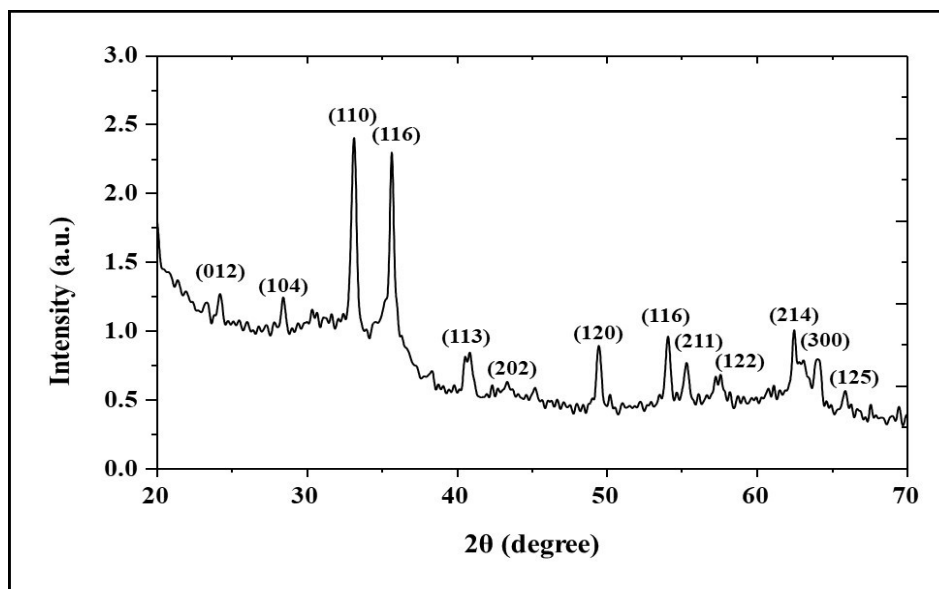


Fig. 4.33 X-ray diffraction pattern of *F. benghalensis* synthesized IONPs

### 3.1.4 SEM and TEM studies

The spherical shape of 5- 20 nm in size was clearly visible from the SEM images shown in fig. 4.34(a). From the SEM images it can be seen that there is clustering of NPs due to very low surface charge as analyzed from the zeta potential study. The agglomeration of synthesized NPs may be due to the

presence of strong H- bonding between the adjacent NPs [197]. The EDX spectra revealed iron and oxygen peaks present in the analyzed samples which confirm that the synthesized NPs were of iron oxide as shown in fig. 4.34(b). TEM analysis was done for the identification of exact morphological features and size characteristics and it was found that the IONPs were of approximately 10 nm in size as given in fig. 4.34(c). Hence, the spherical shaped, 5- 20 nm in diameter synthesized IONPs were obtained from the leaves extract of *F. benghalensis* with agglomeration properties which are helpful in their effective applicability [198].

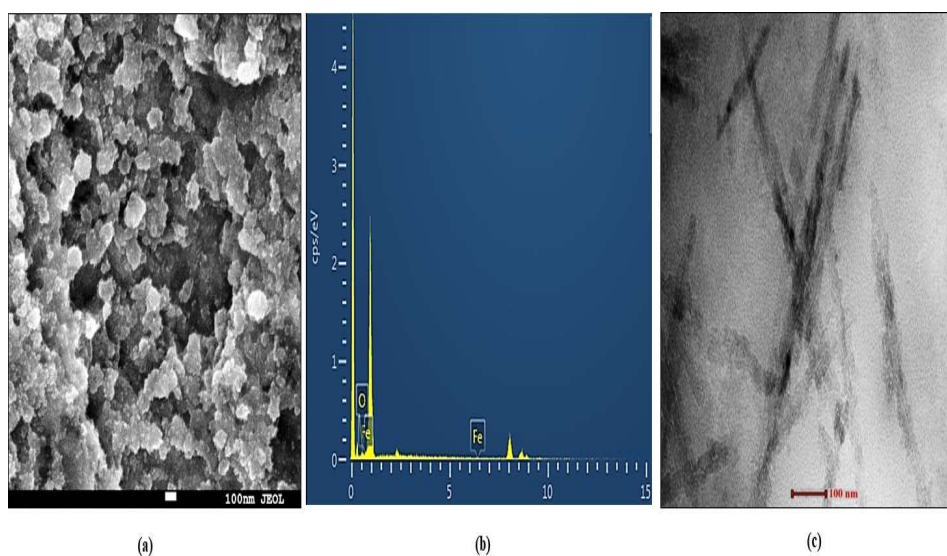


Fig. 4.34 (a) SEM image (b) EDX spectra and (c) TEM image of IONPs

### 3.1.5 Atomic force microscopy (AFM)

Three dimensional topographical features of synthesized IONPs was determined by AFM and the results are given in fig. 4.35 (a, b, c). It can be seen that there is presence of spherical IONPs with few aggregated IONPs. Spherical shape of IONPs is clearly visible from the 2-D AFM image. The agglomerated or clustered NPs can be seen which can be attributed to the presence of strong intermolecular bonding which takes place between the phytochemical constituents on the IONPs surface thus providing it a characteristic property which can be explored for various applications [199, 200].



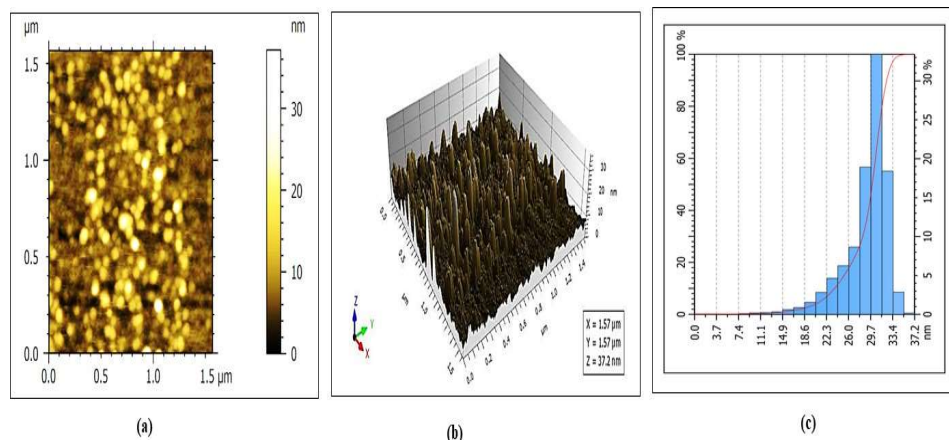


Fig. 4.35 Atomic force microscope images of (a) 2- D image (b) 3-D image and (c) size distribution maxima of synthesized IONPs

### 3.1.6 Fourier Transform Infrared Spectroscopy

The different FTIR peaks observed for the *F. benghalensis* leaves extract and for the IONPs are shown in fig. 4.36. From the FTIR spectra, it can be seen that there are peaks present at 3336.10 corresponds to the presence of stretching of O-H bonds, 2355.16 corresponding to C-N vibration which occur due to the presence of proteins, 1608.68 suggesting the occurrence of C-H vibrations, 1313.56 due to stretching of C=O and at 1030.02 which corresponds to the presence of strong C-H bonding [205]. Also the observed spectra for IONPs showed various peaks corresponding to the FTIR spectra of *F. benghalensis* leaves extract. The peaks for IONPs were observed at 3336.66, 2359.02, 1556.06, 1274.98 and 1047.38  $\text{cm}^{-1}$  which indicated the action of various phyto functional groups participating in the IONPs formation. The interaction of compounds from the leaves extract of *F. benghalensis* with the IONPs causes a shift in the wavelength corresponding to the functional group movement from plant extract to the surface of IONPs in order to facilitate the capping and stabilizing process [206,207].

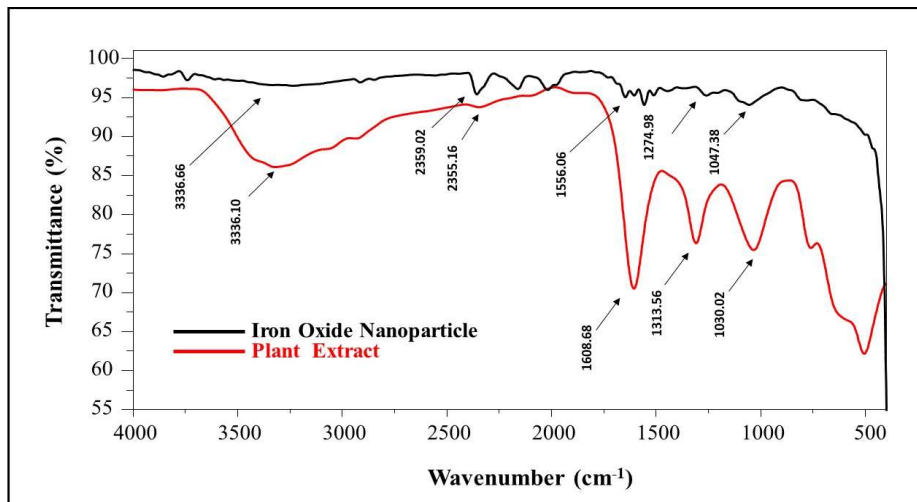


Fig. 4.36 FTIR spectra of synthesized IONPs along with the FTIR spectra of *F. benghalensis* plant extract

### 3.2 Anti- corrosive studies of IONPs synthesized from *Ficus benghalensis* leaves extract in Ringer’s solution as corrosive media

#### 3.2.1 Weight loss measurements

The I.E of IONPs against the corrosion of SS 316 L in the presence of Ringer’s solution as corrosive media was analysed with the help of weight loss measurement study. The values obtained are shown in table 4.13. From the obtained data, it was concluded that by increasing the concentration of IONPs, the subsequent decrease in corrosion rate was seen and it was also observed that the increment in the I.E was depended on concentration of IONPs and maximum I.E against corrosion was 85.31% ( $\pm 0.381$ ) at 100 ppm IONPs concentration. It was assumed that the IONPs get adsorbed on the surface of the SS 316L leading to an increased efficiency against corrosion thus by decreasing the rate of corrosion [208]. The linear coefficient value obtained was 0.9953 which is near to 1 suggesting the adsorption of IONPs on SS 316L surface follows the pattern of Langmuir adsorption isotherm (fig. 4.37).

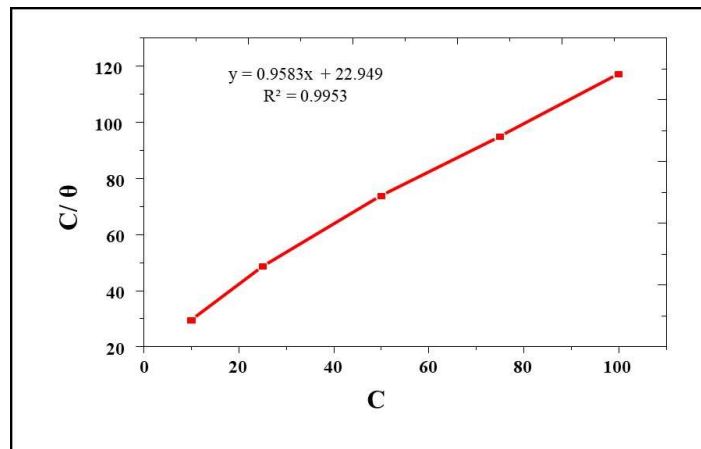


Fig. 4.37 Langmuir adsorption isotherm of *F. benghalensis* synthesized IONPs on SS 316L surface with the weight loss measurements in Ringer's solution

Table 4.13 Weight loss and adsorption isotherm parameters for *F. benghalensis* synthesized IONPs in different concentrations on SS 316L immersed in Ringer's solution

Concentration (C)	$C_R$ ( $\text{mm}^{-1}$ )	I.E (%) $\pm$ St. Dev.	$\theta$	$C/\theta$
Ringer's solution	0.0118	-	-	-
Ringer's solution + 10 ppm IONPs	0.0078	$33.89 \pm 0.020$	0.3389	29.50
Ringer's solution + 25 ppm IONPs	0.0057	$51.41 \pm 0.615$	0.5141	48.62
Ringer's solution + 50 ppm IONPs	0.0038	$67.79 \pm 1.050$	0.6779	73.75
Ringer's solution + 75 ppm IONPs	0.0024	$79.09 \pm 0.308$	0.7909	94.82
Ringer's solution + 100 ppm IONPs	0.0017	$85.31 \pm 0.381$	0.8531	117.21

### 3.2.2 Electrochemical study

The obtained Nyquist plot is shown in fig. 4.38(a). A maximum 77.12 % inhibitory activity against corrosion at 100 ppm of IONPs concentration. The polarization curves or Tafel plots were also obtained for analysing the corrosion inhibitory effect of IONPs. The data obtained from polarization analysis is

shown in fig. 4.38 (b). The value obtained for  $E_{corr}$  was in between the range of 30- 35 mV. From the reported literature it is concluded that the IONPs behaved as inhibitor of mixed type i.e. protection from corrosion at both anode and cathode because it is considered that less than 85mV shift in the corrosion potential leads to mixed type of inhibition [212]. Also the maximum inhibition efficiency obtained was 82.20 % with 100 ppm of IONPs concentration. Hence, to protect the metal surface from dissolution, inhibitors are used. The obtained data for conducted electrochemical studies are shown in table 4.14. The adsorption of IONPs on the steel substrate is also well supported by the data obtained from bode plot and phase angle graph as given in fig. 4.38 (c) and (d). The phase angle values obtained suggest the resistive nature against corrosion due to the presence of different concentration of IONPs.

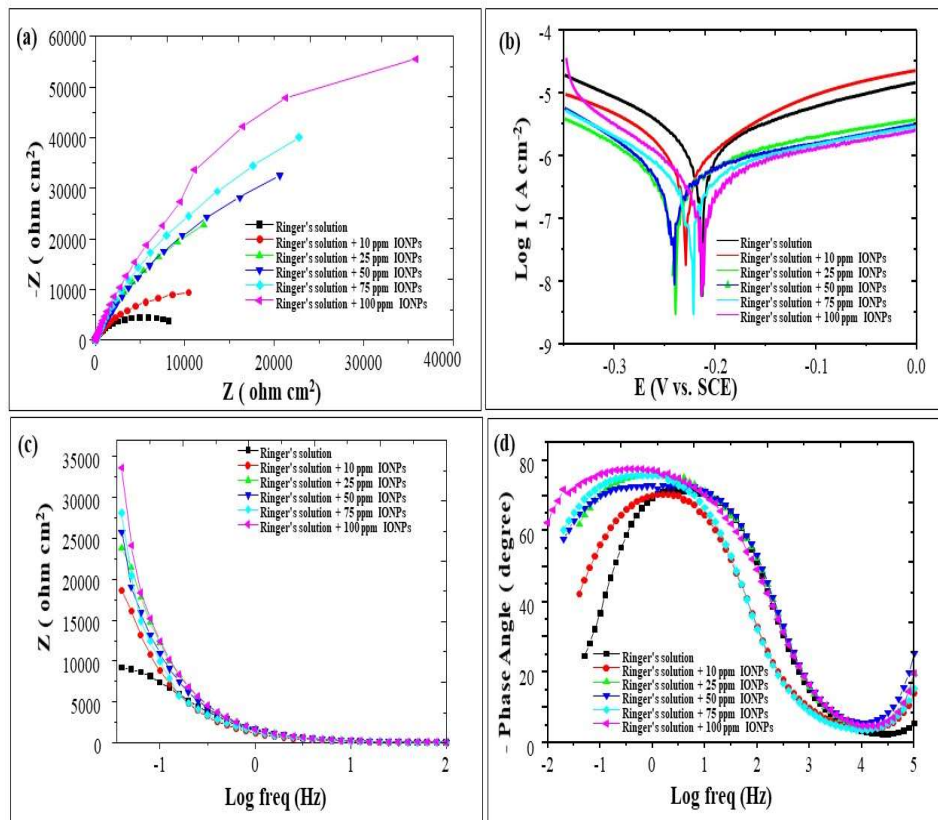


Fig. 4.38 Electrochemical studies of the effect of different concentrations  $F. benghalensis$  synthesized IONPs on SS 316L surface (a) Nyquist plot (b) Tafel plot (c) Bode plot and (d) phase angle plot in Ringer's solution

From the obtained data, it is suggested that the anticorrosive property of IONPs increased with the increment in the concentration of IONPs. Also the formation of protective barrier leads to a decrease in the value of capacitance hence making the surface of the steel less prone to dissolution thus by preventing the corrosion process in the harmful corrosive environments [216].

Table 4.14 Parameters of electrochemical analysis for SS 316L in Ringer's solution containing different concentration of *F. benghalensis* synthesized IONPs

Concentration (C)	Electrochemical parameters		Potentiodynamic parameters	
	$R_{ct}$ ( $\Omega \text{ cm}^{-2}$ )	I. E (%)	$I_{corr}^0$ ( $\text{A cm}^{-2}$ ) * $10^{-7}$	I. E (%)
Ringer's solution	8200.286	-	9.89	-
Ringer's solution + 10 ppm IONPs	10418.11	21.28	6.94	29.82
Ringer's solution + 25 ppm IONPs	12131.93	32.40	6.12	38.11
Ringer's solution + 50 ppm IONPs	20578.48	60.15	3.49	64.71
Ringer's solution + 75 ppm IONPs	22762.14	63.97	3.13	68.35
Ringer's solution + 100 ppm IONPs	35797.29	77.12	1.76	82.20

### 3.2.3 Surface investigation studies by SEM and AFM

Fig. 4.39 (a, b, c) and (d, e, f) shows the SEM and AFM images of polished SS 316 L sample, SS 316 L sample immersed in Ringer's solution and SS 316 L sample immersed in Ringer's solution containing 100 ppm of IONPs, respectively. From the analysis of images by SEM, it can be seen that the SS 316 L sample which was immersed in Ringer's solution showed very rough and

damaged surface in comparison to the SS 316 L sample containing 100 ppm IONPs in Ringer's solution [217]. From the AFM analysis, the roughness values of the surface of the steel samples were obtained and it was found that the polished SS 316 L surface and the SS 316 L placed in Ringer's solution only, has a surface roughness value of around 39.8 nm and 999.0 nm, respectively. The surface roughness value was around 472.4 nm in case of SS 316L immersed in Ringer's solution containing 100 ppm of IONPs. This decrease in roughness of surface can be attributed to the formation of a protective coating which helped in blocking the transfer of electrons and hence protecting the SS 316L surface from the attack of corrosive solution [218].

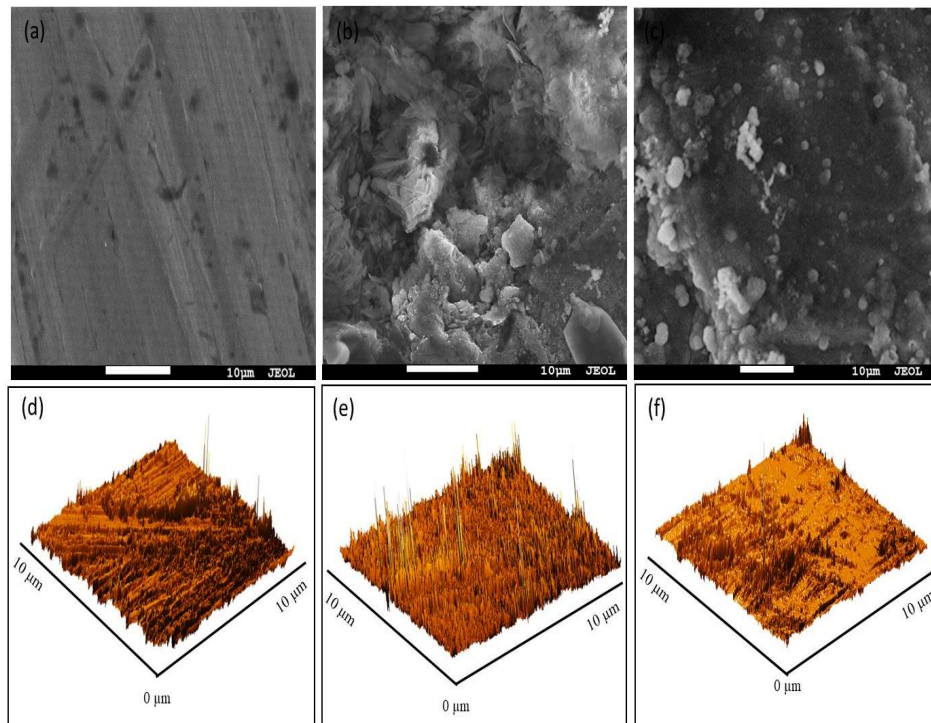


Fig. 4.39 Images showing (a) SEM micrograph of SS 316L (b) SEM micrograph of SS 316L immersed in Ringer's solution (c) SEM micrograph of SS 316L immersed in Ringer's solution with IONPs (d) AFM micrograph of SS 316L (e) AFM micrograph of SS 316L immersed in Ringer's solution (f) AFM micrograph of SS 316L immersed in Ringer's solution with IONPs

### 3.3 Anti- corrosive studies of IONPs synthesized from *F. benghalensis* leaves extract in Hank's solution as corrosive media

#### 3.3.1 Weight loss measurements

The I.E of IONPs against the corrosion of SS 316 L in the presence of Hank's solution as corrosive media was analysed with the help of weight loss measurement study. The values obtained are shown in table 1. From the obtained data, it was concluded that by increasing the concentration of IONPs in the corrosive media, the subsequent decrease in corrosion rate was seen and it was also observed that the increment in the I.E depend upon concentration of IONPs and maximum I.E against corrosion was 72.57 % ( $\pm 0.265$ ) at 100 ppm IONPs concentration. It was assumed that the IONPs get adsorbed on the surface of the SS 316L leading to an increased efficiency against corrosion thus by decreasing the rate of corrosion [208]. The linear coefficient value obtained was 0.9917 which is near to 1 suggesting the adsorption of IONPs on SS 316L surface follows the pattern of Langmuir adsorption isotherm (fig. 4.40).

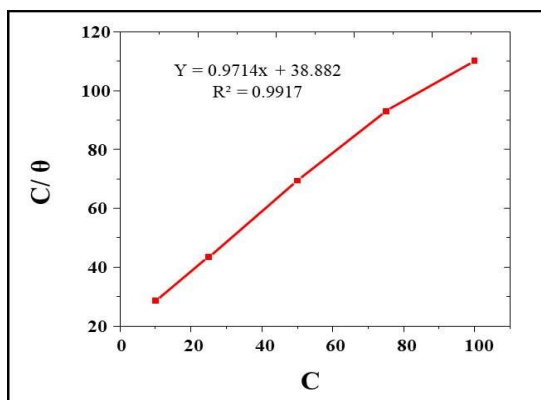


Fig. 4.40 Langmuir adsorption isotherm of *F. benghalensis* synthesized IONPs on SS 316L surface with the weight loss measurements in Hank's solution

Table 4.15 Weight loss and adsorption isotherm parameters for *F. benghalensis* synthesized IONPs in different concentrations on SS 316L immersed in Hank's solution

Concentration (C)	$C_R$ (mmy <sup>-1</sup> )	I.E (%) $\pm$ St. Dev.	$\theta$	C/ $\theta$
Hank's solution	0.011667	-	-	-
Hank's solution + 10 ppm IONPs	0.009467	18.85 $\pm$ 0.153	0.1885	53.03
Hank's solution + 25 ppm IONPs	0.006733	42.28 $\pm$ 0.375	0.4228	59.12
Hank's solution + 50 ppm IONPs	0.004867	58.28 $\pm$ 0.357	0.5828	85.78
Hank's solution + 75 ppm IONPs	0.0038	67.42 $\pm$ 0.222	0.6742	111.22
Hank's solution + 100 ppm IONPs	0.0032	72.57 $\pm$ 0.265	0.7257	137.79

### 3.3.2 Electrochemical studies

The obtained Nyquist plot is shown in fig. 4.41 (a). The calculated corrosion inhibition efficiency reached up to a maximum of 69.85 % at 100 ppm of IONPs concentration and the data obtained shown in fig. 4.41 (b). The value obtained for  $E_{corr}$  was in the range, 30- 35 mV. The maximum inhibition efficiency obtained was 71.77 % with 100 ppm of IONPs concentration. Hence, to protect the metal surface from dissolution, inhibitors are used. The inhibitors target the anodic and cathodic sites actively by inhibiting the mechanism of charge transfer in the electrochemical set up. From the potentiodynamic study, it can be concluded that the IONPs get adsorbed on the SS 316L surface and decreased the corrosion current density hence protecting the surface of SS 316L from corrosion [225]. The obtained data for studied electrochemical parameters are shown in table 4.16. The adsorption of IONPs on the steel substrate is also well supported by the data obtained from Bode plot and phase angle graph shown in fig. 4.41 (c) and (d). The phase angle values obtained suggest the resistive nature against corrosion due to the presence of different concentration on IONPs. It is



clear from the graphs that the anticorrosive property of IONPs increased with the increase in the concentration of IONPs.

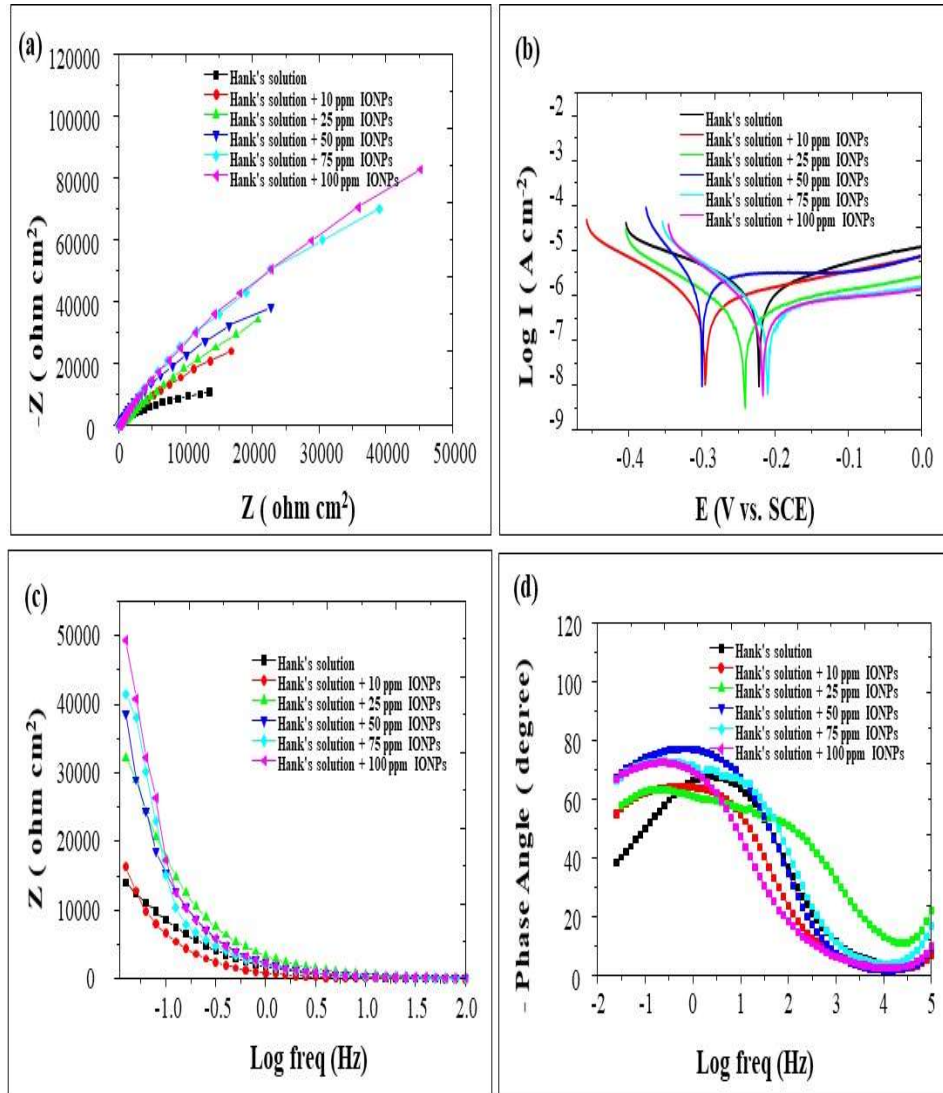


Fig. 4.41 Electrochemical studies of the effect of different concentrations *F. benghalensis* synthesized IONPs on SS 316L surface (a) Nyquist plot (b) Tafel plot (c) Bode plot and (d) phase angle plot in Hank's solution

Table 4.16 Parameters of electrochemical analysis for SS 316L in Hank's solution containing different concentration of *F. benghalensis* synthesized IONPs.

Concentration (C)	Electrochemical parameters		Potentiodynamic parameters	
	$R_{ct}$ ( $\Omega \text{ cm}^{-2}$ )	I. E (%)	$I_{corr}^0$ ( $\text{A cm}^{-2}$ ) * $10^{-7}$	I. E (%)
Hank's solution	13609.77	-	8.75	-
Hank's solution + 10 ppm IONPs	16884.19	19.39	7.08	19.08
Hank's solution + 25 ppm IONPs	20793.46	34.54	6.11	30.17
Hank's solution + 50 ppm IONPs	22795.98	40.29	5.23	40.22
Hank's solution + 75 ppm IONPs	39051.23	65.14	3.29	62.40
Hank's solution + 100 ppm IONPs	45147.93	69.85	2.47	71.77

### 3.3.3 Surface investigation studies by SEM and AFM

Fig. 4.42 (a, b, c) and (d, e, f) shows the SEM and AFM images of polished SS 316 L sample, SS 316 L sample immersed in Hank's solution and SS 316 L sample immersed in Hank's solution containing 100 ppm of IONPs, respectively. SEM studies reveal that the SS 316 L sample which was exposed only to Hank's solution showed very rough and damaged surface in comparison to the SS 316 L sample containing 100 ppm IONPs in Hank's solution [227].

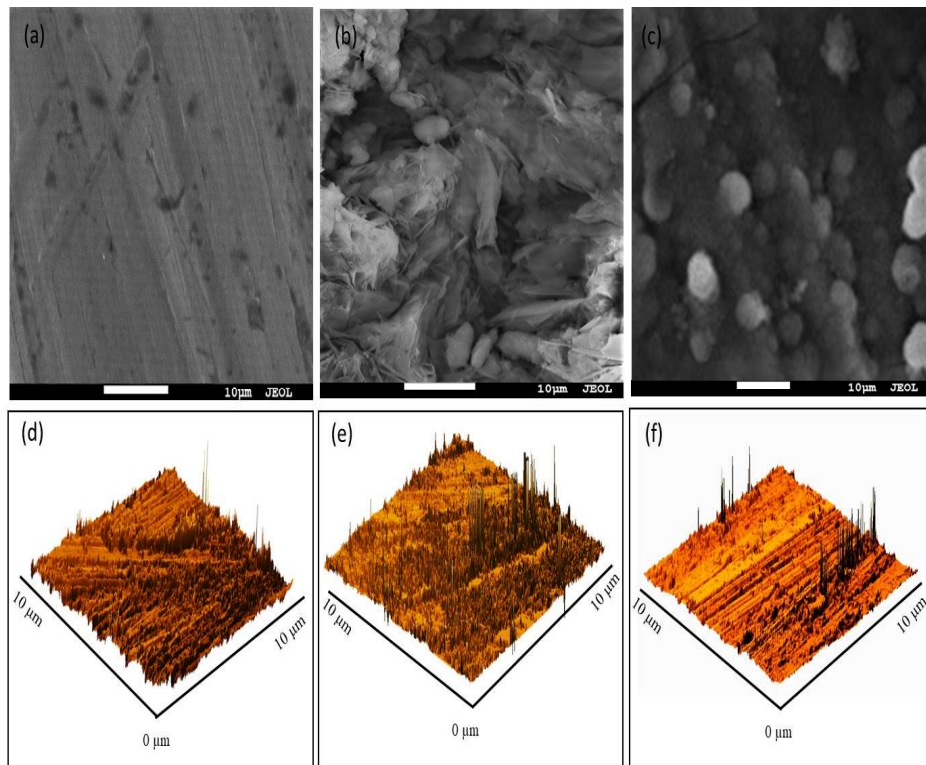


Fig. 4.42 Images showing (a) SEM micrograph of SS 316L (b) SEM micrograph of SS 316L immersed only in Hank's solution (c) SEM micrograph of SS 316L immersed in Hank's solution with IONPs (d) AFM micrograph of SS 316L (e) AFM micrograph of SS 316L immersed only in Hank's solution (f) AFM micrograph of SS 316L immersed in Hank's solution with IONPs.

From the AFM analysis, the roughness values of the surface of the steel samples were obtained and it was found that the polished SS 316 L surface and the SS 316 L placed in Hank's solution only, has a surface roughness value of around 39.8 nm and 880.0 nm, respectively while the surface roughness value was around 519.0 nm of SS 316L immersed in Hank's solution in the presence of 100 ppm of IONPs. This decrease in roughness of surface can be attributed to the formation of a protective coating which helped in blocking the transfer of electrons and hence protecting the SS 316L surface from the attack of corrosive solution [228].

### 3.4 Anti- corrosive studies of IONPs synthesized from *F. benghalensis* leaves extract in PBS as corrosive media

#### 3.4.1 Weight loss measurements

The I.E of IONPs against the corrosion of SS 316 L in the presence of PBS as corrosive media was analysed with the help of weight loss measurement study.

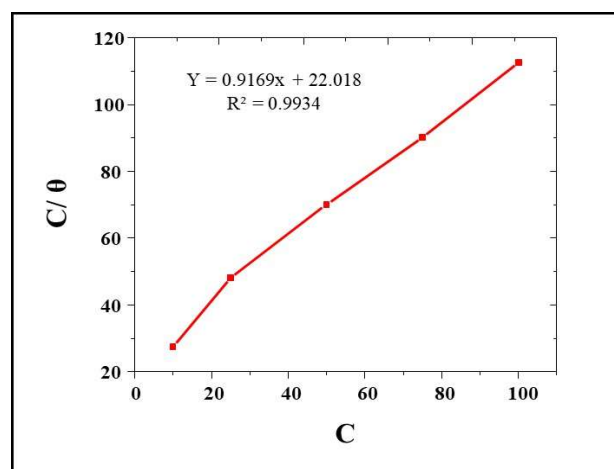


Fig. 4.43 Langmuir adsorption isotherm of *F. benghalensis* synthesized IONPs on SS 316L surface with the weight loss measurements in PBS

From the obtained data, it was concluded that by increasing the concentration of IONPs, the subsequent decrease in corrosion rate was seen and it was also observed that the increment in the I.E was depended on concentration of IONPs and maximum I.E against corrosion was 88.78 % ( $\pm 0.140$ ) at 100 ppm IONPs concentration. It was assumed that the IONPs get adsorbed on the surface of the SS 316L leading to an increased efficiency against corrosion thus decreasing the rate of corrosion [208]. The linear coefficient value obtained was 0.9934 which is near to 1 suggesting the adsorption of IONPs on SS 316L surface follows the Langmuir adsorption isotherm (fig. 4.43). The values obtained are shown in table 4.17.

Table 4.17 Weight loss and adsorption isotherm parameters for *F. benghalensis* synthesized IONPs in different concentrations on SS 316L immersed in PBS

Concentration (C)	$C_R$ (mmy <sup>-1</sup> )	I.E (%) $\pm$ St. Dev.	$\theta$	C/ $\theta$
PBS	0.0154	-	-	-
PBS + 10 ppm IONPs	0.0098	36.36 $\pm$ 0.045	0.3636	27.50
PBS + 25 ppm IONPs	0.0074	51.94 $\pm$ 0.807	0.5194	48.12
PBS + 50 ppm IONPs	0.0044	71.42 $\pm$ 0.365	0.7142	70.00
PBS + 75 ppm IONPs	0.0026	83.11 $\pm$ 0.277	0.8311	90.23
PBS + 100 ppm IONPs	0.001727	88.78 $\pm$ 0.140	0.8878	112.62

### 3.4.2 Electrochemical studies

The obtained Nyquist plot is shown in fig. 4.44 (a). A maximum of 76.16 % I.E was observed at 100 ppm of IONPs concentration. The IONPs get adsorbed on the surface of SS 316 L sample and formed a layer and hence reduces the flow of electrons thus by increasing the charge transfer resistance of the reaction process [230]. The polarization curves or Tafel plots were also obtained for analysing the corrosion inhibitory effect of IONPs. The data obtained from polarization analysis is shown in fig. 4.44 (b). The value obtained for  $E_{corr}$  was in between the range of 30- 35 mV. The maximum inhibition efficiency obtained was 77.24 % with 100 ppm of IONPs concentration. IONPs contains functional groups on their surface which have heteroatoms present in them. These heteroatoms help in the adsorption of IONPs at the SS 316L surface by making strong coordination bonds. The obtained data for the conducted studies is shown in table 4.18. The adsorption of IONPs on the steel substrate is also well supported by the data obtained from Bode plot and phase angle graph shown in fig. 4.44 (c) and (d). The phase angle values obtained suggest the

resistive nature against corrosion due to the presence of different concentration of IONPs. From the obtained data from these graphs it is suggested that the anticorrosive property of IONPs increased with the increment in the concentration of IONPs. Also the formation of protective barrier leads to a decrease in the value of capacitance hence making the surface of the steel less prone to dissolution thus by preventing the corrosion process in the harmful corrosive environments [236].

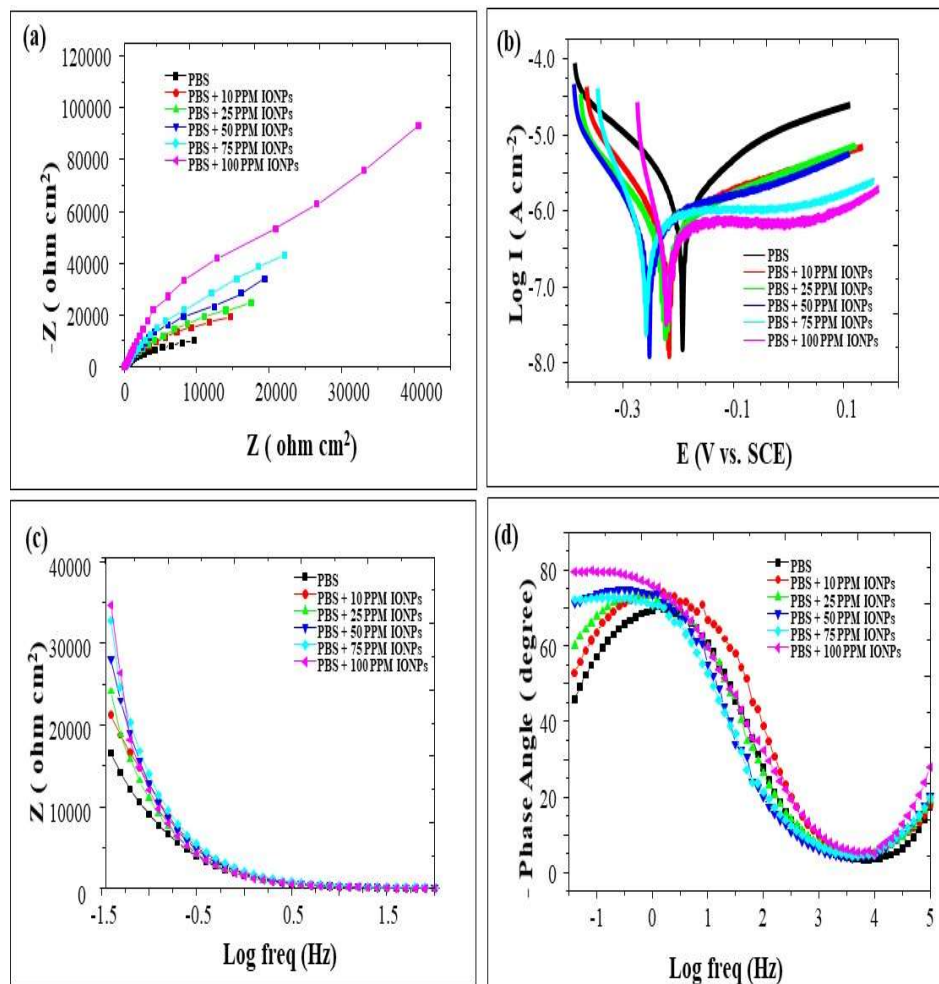


Fig. 4.44 Electrochemical studies of the effect of different concentrations *F. benghalensis* synthesized IONPs on SS 316L surface (a) Nyquist plot (b) Tafel plot (c) Bode plot and (d) phase angle plot in PBS

Table 4.18 Parameters of electrochemical analysis for SS 316L in PBS containing different concentration of *F. benghalensis* synthesized IONPs.

Concentration (C)	Electrochemical parameters		Potentiodynamic parameters	
	R <sub>ct</sub> (Ω cm <sup>-2</sup> )	IE (%)	I <sub>corr</sub> <sup>0</sup> (A cm <sup>-2</sup> ) * 10 <sup>-7</sup>	IE (%)
PBS	9677.657	-	6.24	-
PBS + 10 ppm IONPs	14646.80	33.92	3.62	41.98
PBS + 25 ppm IONPs	17529.46	44.79	2.78	55.44
PBS + 50 ppm IONPs	19373.4	50.04	2.32	62.82
PBS + 75 ppm IONPs	22154.21	56.31	1.89	69.71
PBS + 100 ppm IONPs	40608.7	76.16	1.42	77.24

### 3.4.3 Surface investigation studies by SEM and AFM

The SEM and AFM images of polished SS 316 L sample, SS 316 L sample immersed in PBS and SS 316 L sample immersed in PBS containing 100 ppm of IONPs are shown in fig. 4.45 (a, b, c) and (d, e, f), respectively. From the analysis of images by SEM, it can be seen that the SS 316 L sample which was immersed in PBS showed very rough and damaged surface in comparison to the SS 316 L sample containing 100 ppm IONPs in PBS [237]. This difference in the surface images of the steel samples is attributed to the presence of protective barrier on the surface of steel formed by the presence of IONPs. From the AFM analysis, the roughness values of the surface of the steel samples were obtained and it was found that the polished SS 316 L surface and the SS 316 L placed in PBS only, has a surface roughness value of around 39.8 nm and 949.0 nm, respectively. However, the surface roughness value of SS 316L immersed in PBS with 100 ppm of IONPs was around 565.0 nm. This decrease in roughness of surface can be attributed to the formation of a protective coating which helped

in blocking the transfer of electrons and hence protecting the SS 316L surface from the attack of corrosive solution [238].

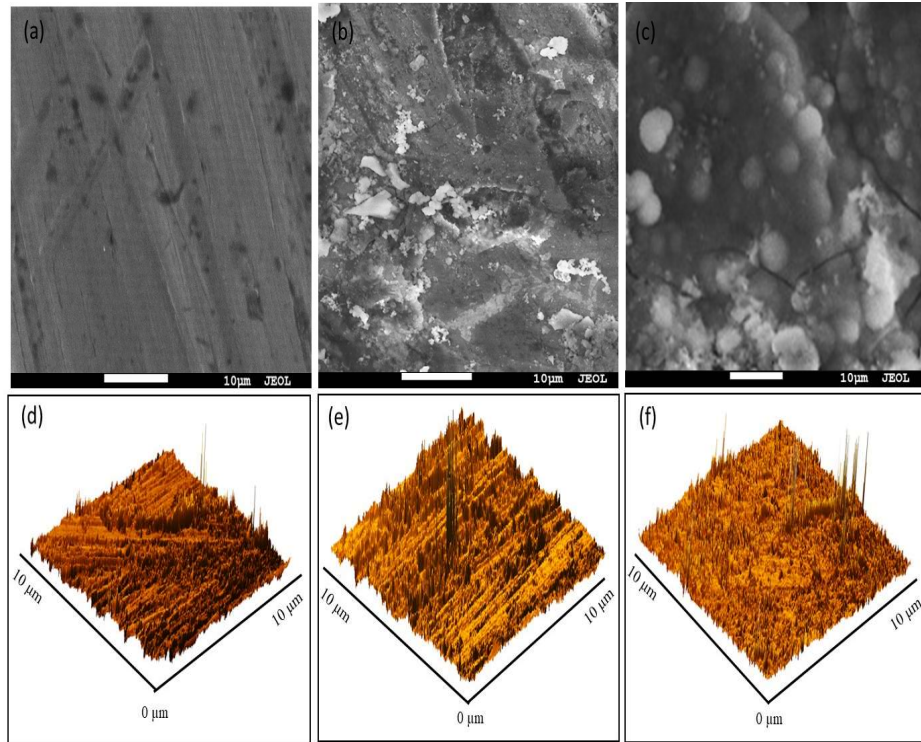


Fig. 4.45 Images showing (a) SEM micrograph of SS 316L (b) SEM micrograph of SS 316L immersed only in PBS (c) SEM micrograph of SS 316L immersed in PBS with IONPs (d) AFM micrograph of SS 316L (e) AFM micrograph of SS 316L immersed only in PBS (f) AFM micrograph of SS 316L immersed in PBS with IONPs.

#### **Comparative analysis of the presented study with some already reported work**

Table 4.19 presents some already reported findings in the area of corrosion protection with the help of different nanomaterials. Many studies have been conducted in the physiological solutions as corrosive media to gain an insight into the protection mechanism of different implant materials against corrosion.



Table 4.19 Comparative literature studies with the already reported finding

Corrosive media	Inhibitor/ substrate	Studies conducted	Remarks	Refer-ence
<b>Ringer's solution</b>	IONPs from <i>S. chirata</i> / SS 316L  IONPs from <i>T. arjuna</i> / SS 316L  IONPs from <i>F. benghalensis</i> / SS 316L	Weight loss, electrochemical impedance and potentiodynamic polarization, surface characterization	More than 75% corrosion inhibition efficiency was observed at 100 ppm IONPs conc. Surface characterization showed remarkable decrease in corrosion in IONPs containing solution	-
	ZnO NPs / titanium	Potentiodynamic and electrochemical impedance	Significant decrease in corrosion current density was observed at a conc. of 15g/L, 93% reduction in corrosion	241
	ZnO NPs/ titanium	Potentiodynamic polarization and wet angle test	Maximum corrosion inhibition was observed at 1g/L NPs conc. Also, ZnO nanoparticles increased the thickness, wetting angle and roughness of the coating formed	242
	Fe <sub>3</sub> O <sub>4</sub> loaded bioglass-chitosan nanocomposite/AZ 91 Mg alloy	Potentiodynamic polarization	The nanocomposite showed remarkable decrease in corrosion potential at a conc. Of 1% nanocomposite	243

<b>Hank's solution</b>	IONPs from <i>S. chirata</i> / SS 316L  IONPs from <i>T. arjuna</i> / SS 316L  IONPs from <i>F. benghalensis</i> / SS 316L	Weight loss, electrochemical impedance and potentiodynamic polarization, surface characterization	IONPs from <i>S. chirata</i> showed max. inhibition potential of 76.83% at 100 ppm conc., 80.06% max. inhibition potential was shown by <i>T.arjuna</i> IONPs and 69.85% was shown by <i>F. benghalensis</i> IONPs	-
	ZrO <sub>2</sub> NPs / Ti-6Al-4V	Potentiodynamic and electrochemical impedance	Max. corrosion protection was observed at 3g/L/ ZrO <sub>2</sub> NPs conc.	244
	ZnO NPs / AZ31 Mg alloy	Potentiodynamic and electrochemical impedance	6g/L ZnO NPs conc. showed max. inhibition at 0.08 $\mu\text{A}/\text{cm}^2$ corrosion current density and corrosion resistance of $1.05 \times 10^6 \Omega.\text{cm}^2$	245
	Chitosan-gold(AuNPs/ CS) NPs / titanium	Cyclic voltammetry and OCP, Potentiodynamic and electrochemical impedance	Higher impedance values and phase angles were observed for solution containing AuNPs /CS biocomposite and protective coating was formed on the titanium surface, max. inhibition was around 98%	246
<b>Phosphate buffer solution (PBS)</b>	IONPs from <i>S. chirata</i> / SS 316L	Weight loss, electrochemical impedance and	IONPs from <i>S. chirata</i> showed max. inhibition potential of	-

<p>IONPs from <i>T. arjuna</i>/ SS 316L</p> <p>IONPs from <i>F. benghalensis</i> / SS 316L</p>	<p>potentiodynamic polarization, surface characterization</p>	<p>75.98% at 100 ppm conc., 83.50% max. inhibition potential was shown by <i>T.arjuna</i> IONPs and 76.16% was shown by <i>F. benghalensis</i> IONPs</p>	
<p>CS/HA/TiO<sub>2</sub> nanocomposite/ Ti-6Al-4V alloy</p>	<p>OCP, Potentiodynamic and electrochemical impedance</p>	<p>The lower negative OCP showed the stability of the nanocomposite with highest corrosion resistance value of 7.3 MΩ cm<sup>2</sup> and max. inhibition reaching 97.4%</p>	<p>247</p>
<p>ZnO NPs / WE43 Mg alloy</p>	<p>OCP, Potentiodynamic and electrochemical impedance and SEM for surface analysis</p>	<p>ZnO NPs coating was formed at -3V of 1μm thickness which prevented the alloy from corrosion with 99.9% inhibition efficiency. Also SEM images showed ZnO coated surface of the alloy protecting against corrosion</p>	<p>248</p>
<p>Mn<sub>3</sub>O<sub>4</sub> NPs / tantalum</p>	<p>OCP, Potentiodynamic and electrochemical impedance</p>	<p>Mn<sub>3</sub>O<sub>4</sub> NPs provided physical barrier against the corrosion by sealing the layers together. Also, generation of ROS is suppressed</p>	<p>249</p>

## CHAPTER 5

### SUMMARY AND CONCLUSION

The present study focused on the synthesis of iron oxide NPs (IONPs) via green route using plant extracts of *Swertia chirata*, *Terminalia arjuna* and *Ficus benghalensis*. The Bottom up approach for NPs synthesis was employed for the effective generation of IONPs. The formation of IONPs was first confirmed by UV-Vis spectra and it was found that 10Mm concentration of ferric chloride salt was optimum for the synthesis of IONPs by *S. chirata* and 50 mM by *T. arjuna* and *F. benghalensis*. The volume of plant extract required for the formation of IONPs was found to be optimum at 4 ml for all the three plants. The pH of the synthesized IONPs was found to be around 6 and 7. The optimum temperature for the effective synthesis of IONPs was found to be around 25°C and 35°C. The incubation time for the reduction of ferric chloride salt was found to be 10 min and 15 min. The IONPs prepared from each plant were found to be neutrally charged with good stability in colloidal solution. The hydrodynamic size for the IONPs also helped in determining their stability in solutions suggesting their good dispersion in aqueous solution. The IONPs synthesized from *S. chirata* were found to be amorphous in nature and with orthorhombic structural lattice while the IONPs synthesized from *T. arjuna* and *F. benghalensis* were crystalline in nature with cubic and rhombohedral crystal lattice respectively. The IONPs were found spherical in shape with average size of IONPs was below 50 nm. The different types of phytochemical groups were found to be participating in the formation of IONPs.

For the anticorrosive analysis of prepared IONPs, various studies were conducted which include weight loss measurement study, electrochemical studies and adsorption studies included SEM and AFM analysis of surface of the SS 316L untreated and treated with optimum amount of IONPs. From the corrosion studies, it was found that the synthesized IONPs effectively resisted the corrosion attack in different corrosive media. The corrosive media used in

this study were Ringer's solution, Hank's solution and Phosphate Buffer Saline (PBS). The average corrosion inhibition efficiency of IONPs against the three corrosive solution was found to be more than 70% which proved their efficacy to be used as anticorrosive agent. The electrochemical studies suggested that the IONPs behaved as mixed type of inhibitors which protected the steel at both the anodic and cathodic sites thus by resisting the corrosion process. Further, it can be suggested that the mechanism of inhibition was of both types which means that the protection was due to chemisorption and physisorption. Further, the adsorption study concluded that the IONPs formed a protective barrier on the steel surface which helped in resisting the destruction of surface of the SS 316L when the steel samples were subjected to corrosive solutions. The SEM and AFM studies were conducted to compare the deterioration of surface of SS 316L samples when they are immersed in corrosion solution and corrosive solution containing optimum amount of IONPs. These samples were compared with the clean and polished SS 316L surface which was not exposed to corrosive solutions. The surface roughness values were obtained in the case of AFM which suggested a significance decrease in the roughness of surface of SS 316L when they are immersed in corrosive solution containing IONPs as compared to surface of SS 316L when they are immersed in corrosive solution only. Hence, it can be summarized that the green synthesized IONPs with the help of *S. chirata*, *T. arjuna* and *F. benghalensis* were successfully prepared and characterized. The IONPs were effective against corrosion attack and hence can be utilized as potent anticorrosive agents.

### **Conclusion**

Corrosion is an inevitable process that cannot be stopped completely. The process of corrosion leads to the destruction of metals. The losses occurring due to corrosion costs very large to the economy. The metals and alloys start corroding when they come in contact with the external environment containing corrosive agents. These corrosive agents disturb the electrochemical balance on the surface of metals and the corrosion process is initiated. The stainless steel of 300 series are regarded as highly corrosion resistant and SS 316L is specially

designed to be used in biomedical devices, marine equipments, in aerospace and defense equipments for their corrosion resistant but these metallic materials also corrode when they are continuously exposed to the corrosive agents. In the case of SS 316L, which is mostly used in biomedical devices and sometimes regarded as surgical steel or biomedical steel comes in contact with the various physiological fluids which is not a habitable place for the metallic materials or biomaterials in terms of corrosion. To protect the materials from corrosion, suitable strategies are employed, out of which the corrosion inhibitors are the most significant and promising in combating corrosion attack. The present study was based on identifying the synthesized IONPs as suitable inhibitors for corrosion in various physiological media. Overall, it can be concluded that the novel green plant extract based synthesized IONPs effectively prevented the SS 316L metal from deterioration by the corrosion attack.

#### **Scope of future work**

This research work utilized the IONPs synthesized from green route for their anticorrosive behaviour in different corrosive media. Different studies were conducted to understand the effect of IONPs as corrosion inhibitors. This work can further be explored as:

- Different type of metals can be used to evaluate the corrosion inhibiting potential of IONPs for broader applicability.
- Broad range of corrosive media can be taken into consideration for better understanding of the anticorrosive properties of synthesized IONPs on large scale.
- More studies to analyze the characteristic properties of IONPs can be done.
- IONPs can also be subjected to toxicity evaluation studies to increase their application in various fields.

## BIBLIOGRAPHY

- [1]. Shreir, L. L. (Ed.). (2013). Corrosion: metal/environment reactions. Newnes.
- [2]. Saini, M., Singh, Y., Arora, P., Arora, V., & Jain, K. (2015). Implant biomaterials: A comprehensive review. *World Journal of Clinical Cases: WJCC*, 3(1), 52.
- [3]. Soman, S., & Ajitha, A. R. (2018). Life cycle assessment of metallic biomaterials. *Fundamental Biomaterials: Metals*, 411-423.
- [4]. Breme, H., Biehl, V., Reger, N., & Gawalt, E. (2016). A metallic biomaterial: Introduction. In *Handbook of Biomaterial Properties*, Springer, New York, 151-158.
- [5]. Dikici, B., Esen, Z., Duygulu, O., & Gungor, S. (2015). Corrosion of metallic biomaterials. In *Advances in Metallic Biomaterials*, Springer, Berlin, Heidelberg, 275-303.
- [6]. Chen, Q., & Thouas, G. A. (2015). *Metallic implant biomaterials. Materials Science and Engineering: R: Reports*, 87, 1-57.
- [7]. Hasirci, V., & Hasirci, N. (2018). *Fundamentals of biomaterials*. Verlag: Springer New York.
- [8]. Virtanen, S. (2008). Corrosion of Biomedical Implant Materials. *Corrosion Reviews*, 26(2-3), 147-171.
- [9]. Mudali, U. K., Sridhar, T. M., Eliaz, N., & Raj, B. (2003). Failures of stainless steel orthopedic devices-causes and remedies. *Corrosion Reviews*, 21(2-3), 231-268.
- [10]. Pound, B. G. (2014). Corrosion behavior of metallic materials in biomedical applications. I. Ti and its alloys. *Corrosion Reviews*, 32(1-2), 1-20.
- [11]. Witte, F., & Eliezer, A. (2012). *Biodegradable Metals. Degradation of Implant Materials*, 93-109
- [12]. Gilbert, J. L., & Mali, S. A. (2012). Medical implant corrosion: Electrochemistry at metallic biomaterial surfaces. In *Degradation of implant materials*, Springer, New York, NY, 1-28.

- [13]. Black, J. (2005). *Biological performance of materials: fundamentals of biocompatibility*. CRC Press.
- [14]. Laing, P. G. (1977). 9.0-Hematoma. *NBS Special Publication*, (472-475), 31.
- [15]. Williams, D. F. (2003). Biomaterials and tissue engineering in reconstructive surgery. *Sadhana*, 28(3-4), 563-574.
- [16]. Simoes, T. A., Bryant, M. G., Brown, A. P., Milne, S. J., Ryan, M., Neville, A., & Brydson, R. (2016). Evidence for the dissolution of molybdenum during tribocorrosion of Co-Cr-Mo hip implants in the presence of serum protein. *Acta Biomaterialia*, 45, 410-418.
- [17]. Galal, A., Atta, N. F., & Al-Hassan, M. H. S. (2005). Effect of some thiophene derivatives on the electrochemical behavior of AISI 316 austenitic stainless steel in acidic solutions containing chloride ions: I. Molecular structure and inhibition efficiency relationship. *Materials Chemistry and Physics*, 89(1), 38-48.
- [18]. A Negm, N., A Yousef, M., & M Tawfik, S. (2013). Impact of synthesized and natural compounds in corrosion inhibition of carbon steel and aluminium in acidic media. *Recent Patents on Corrosion Science*, 3(1), 58-68.
- [19]. Hussain, I., Singh, N. B., Singh, A., Singh, H., & Singh, S. C. (2016). Green synthesis of nanoparticles and its potential application. *Biotechnology Letters*, 38(4), 545-560.
- [20]. Barik, T. K., Maity, G. C., Gupta, P., Mohan, L., & Santra, T. S. (2021). Nanomaterials: An Introduction. *Nanomaterials and Their Biomedical Applications*, 16, 1-27.
- [21]. Kumbhakar, P., Ray, S. S., & Stepanov, A. L. (2014). Optical properties of nanoparticles and nanocomposites. *Journal of Nanomaterials*, 2014, 181365-181365.
- [22]. Rathish, R. J., Joany, R. D. R., Pandiarajan, M., & Rajendran, S. (2013). Corrosion resistance of nanoparticle-incorporated nano coatings. *European Chemical Bulletin*, 2(12), 965-970.
- [23]. Jain, P., Patidar, B., & Bhawsar, J. (2020). Potential of nanoparticles as a corrosion inhibitor: a review. *Journal of Bio-and Tribo-Corrosion*, 6(2), 1-12.



- [24]. Mochochoko, T., Oluwafemi, O. S., Jumbam, D. N., & Songca, S. P. (2013). Green synthesis of silver nanoparticles using cellulose extracted from an aquatic weed; water hyacinth. *Carbohydrate Polymers*, 98(1), 290-294.
- [25]. Solomon, M. M., Gerengi, H., & Umoren, S. A. (2017). Carboxymethyl cellulose/silver nanoparticles composite: synthesis, characterization and application as a benign corrosion inhibitor for St37 steel in 15% H<sub>2</sub>SO<sub>4</sub> medium. *ACS Applied Materials & Interfaces*, 9(7), 6376-6389..
- [26]. Voevodin, N. N., Balbyshev, V. N., Khobaib, M., & Donley, M. S. (2003). Nanostructured coatings approach for corrosion protection. *Progress in Organic Coatings*, 47(3-4), 416-423.
- [27]. Schweitzer, P. A. (2003). In *Metallic materials: physical, mechanical, and corrosion properties*, 19, CRC press.
- [28]. Omran, B. A., & Abdel-Salam, M. O. (2020). Basic Corrosion Fundamentals, Aspects and Currently Applied Strategies for Corrosion Mitigation. In *A New Era for Microbial Corrosion Mitigation Using Nanotechnology*, Springer, Cham, 1-45.
- [29]. Guérin, M., Andrieu, E., Odemer, G., Alexis, J., & Blanc, C. (2014). Effect of varying conditions of exposure to an aggressive medium on the corrosion behavior of the 2050 Al–Cu–Li alloy. *Corrosion Science*, 85, 455-470.
- [30]. Alamri, A. H. (2020). Localized Corrosion and Mitigation Approach of Steel Materials Used in Oil and Gas Pipelines-An overview. *Engineering Failure Analysis*, 104735.
- [31]. Dwivedi, D., Lepková, K., & Becker, T. (2017). Carbon steel corrosion: a review of key surface properties and characterization methods. *RSC Advances*, 7(8), 4580-4610.
- [32]. Balamurugan, A., Rajeswari, S., Balossier, G., Rebelo, A. H. S., & Ferreira, J. M. F. (2008). Corrosion aspects of metallic implants—An overview. *Materials and Corrosion*, 59(11), 855-869.
- [33]. Lee, J. Y., Nagalingam, A. P., & Yeo, S. H. (2020). A review on the state-of-the-art of surface finishing processes and related ISO/ASTM standards for metal additive manufactured components. *Virtual and Physical Prototyping*, 1-29.

- [34]. Eliaz, N. (2019). Corrosion of metallic biomaterials: A review. *Materials*, 12(3), 407.
- [35]. Li, C., Guo, C., Fitzpatrick, V., Ibrahim, A., Zwierstra, M. J., Hanna, P., ... & Kaplan, D. L. (2020). Design of biodegradable, implantable devices towards clinical translation. *Nature Reviews Materials*, 5(1), 61-81.
- [36]. Souza, J. C., Henriques, M., Teughels, W., Ponthiaux, P., Celis, J. P., & Rocha, L. A. (2015). Wear and corrosion interactions on titanium in oral environment: literature review. *Journal of Bio-and Tribo-Corrosion*, 1(2), 13.
- [37]. Prasad, K., Bazaka, O., Chua, M., Rochford, M., Fedrick, L., Spoor, J., ... & Bazaka, K. (2017). Metallic biomaterials: Current challenges and opportunities. *Materials*, 10(8), 884.
- [38]. Zhen, Z. H. E. N., Xi, T. F., & Zheng, Y. F. (2013). A review on in vitro corrosion performance test of biodegradable metallic materials. *Transactions of Nonferrous Metals Society of China*, 23(8), 2283-2293.
- [39]. Williams, D. F. (1994). Titanium: epitome of biocompatibility or cause for concern. *The Journal of Bone and Joint Surgery. British Volume*, 76(3), 348-349.
- [40]. Okazaki, Y., & Gotoh, E. (2008). Metal release from stainless steel, Co–Cr–Mo–Ni–Fe and Ni–Ti alloys in vascular implants. *Corrosion Science*, 50(12), 3429-3438.
- [41]. Virtanen, S. (2012). Degradation of titanium and its alloys. In *Degradation of Implant Materials* Springer, New York, NY. 29-55.
- [42]. Bahn, A. (2017). Water, 7 electrolytes, and acid-base balance. *Essentials of Human Nutrition*, 113.
- [43]. Blackwood, D. J. (2003). Biomaterials: past successes and future problems. *Corrosion Reviews*, 21(2-3), 97-124.
- [44]. Hansen, D. C. (2008). Metal corrosion in the human body: the ultimate bio-corrosion scenario. *The Electrochemical Society Interface*, 17(2), 31.
- [45]. Smith, G. K. (1977). Discussions of the possible systemic roles of metallic corrosion products should properly begin with a brief review of the phenomena that are collectively termed corrosion. In *Retrieval and Analysis of Orthopaedic Implants: Proceedings of a Symposium Held at the National Bureau of Standards*,

Gaithersburg, Maryland, March 5, 1976, 472, 23. US Department of Commerce, National Bureau of Standards.

- [46]. Kamachi, M., & Baldev, R. (2008). In *Corrosion Science and Technology: Mechanism, Mitigation and Monitoring*.
- [47]. Geetha, M., Singh, A. K., Asokamani, R., & Gogia, A. K. (2009). Ti based biomaterials, the ultimate choice for orthopaedic implants—a review. *Progress in Materials Science*, 54(3), 397-425.
- [48]. Congmin, X. U., Zhang, Y., Cheng, G., & Wensheng, Z. H. U. (2006). Corrosion and electrochemical behavior of 316L stainless steel in sulfate-reducing and iron-oxidizing bacteria solutions. *Chinese Journal of Chemical Engineering*, 14(6), 829-834.
- [49]. Amel-Farзад, H., Peivandi, M. T., & Yusof-Sani, S. M. R. (2007). In-body corrosion fatigue failure of a stainless steel orthopaedic implant with a rare collection of different damage mechanisms. *Engineering Failure Analysis*, 14(7), 1205-1217.
- [50]. Aksakal, B., Yildirim, Ö. S., & Gul, H. (2004). Metallurgical failure analysis of various implant materials used in orthopedic applications. *Journal of Failure Analysis and Prevention*, 4(3), 17-23.
- [51]. Hiromoto, S., Onodera, E., Chiba, A., Asami, K., & Hanawa, T. (2005). Microstructure and corrosion behaviour in biological environments of the new forged low Ni Co–Cr–Mo alloys. *Biomaterials*, 26(24), 4912-4923.
- [52]. Singh, R., & Dahotre, N. B. (2007). Corrosion degradation and prevention by surface modification of biometallic materials. *Journal of Materials Science: Materials in Medicine*, 18(5), 725-751.
- [53]. Silver, F. H., & Doillon, C. (1998). Biocompatibility: polymers: interactions of biological and implantable materials. *New York: John Wiley & Sons*, 1, 254-580.
- [54]. Witte, F., Fischer, J., Nellesen, J., Crostack, H. A., Kaese, V., Pisch, A., Beckmann, F. & Windhagen, H. (2006). In vitro and in vivo corrosion measurements of magnesium alloys. *Biomaterials*, 27(7), 1013-1018.
- [55]. Marino, C. E., & Mascaro, L. H. (2004). EIS characterization of a Ti-dental implant in artificial saliva media: dissolution process of the oxide barrier. *Journal of Electroanalytical Chemistry*, 568, 115-120.

- [56]. Chu, P. K. (2007). Enhancement of surface properties of biomaterials using plasma-based technologies. *Surface and Coatings Technology*, 201(19-20), 8076-8082.
- [57]. Baxmann, M., Pfaff, A. M., Schilling, C., Grupp, T. M., & Morlock, M. M. (2017). Biomechanical evaluation of the fatigue performance, the taper corrosion and the metal ion release of a dual taper hip prosthesis under physiological environmental conditions. *Biotribology*, 12, 1-7.
- [58]. Hallab, N., Merritt, K., & Jacobs, J. J. (2001). Metal sensitivity in patients with orthopaedic implants. *Journal of Bone and Joint Surgery*, 83(3), 428.
- [59]. Black, J. (1977). location determines the pH, pO<sub>2</sub>, and mechanical stresses encountered by the implant. We are. *NBS Special Publication*, 23, 472-475.
- [60]. Keegan, G. M., Learmonth, I. D., & Case, C. (2008). A systematic comparison of the actual, potential, and theoretical health effects of cobalt and chromium exposures from industry and surgical implants. *Critical Reviews in Toxicology*, 38(8), 645-674.
- [61]. Rani, B. E., & Basu, B. B. J. (2012). Green inhibitors for corrosion protection of metals and alloys: an overview. *International Journal of Corrosion*, 2012.
- [62]. Harvey, T. J., Walsh, F. C., & Nahlé, A. H. (2018). A review of inhibitors for the corrosion of transition metals in aqueous acids. *Journal of Molecular Liquids*, 266, 160-175.
- [63]. Al-Amiery, A. A., Kadhum, A. A. H., Kadhum, A., Mohamad, A. B., How, C. K., & Junaedi, S. (2014). Inhibition of mild steel corrosion in sulfuric acid solution by new Schiff base. *Materials*, 7(2), 787-804.
- [64]. Ibanga, I. J. (2015). Corrosion inhibition of mild steel using *Delonix regia* plant extract, 1-62.
- [65]. Pehkonen, S. O., & Yuan, S. (2018). *Tailored thin coatings for corrosion inhibition using a molecular approach*. Academic Press.
- [66]. Javaherdashti, R., & Sarjahani, R. (2021). An Overview of the Effect of Graphene as a Metal Protector Against Microbiologically Influenced Corrosion (MIC). *Corrosion Protection of Metals and Alloys Using Graphene and Biopolymer Based Nanocomposites*, 149-168.

- [67]. Oguzie, E. E. (2007). Corrosion inhibition of aluminium in acidic and alkaline media by *Sansevieria trifasciata* extract. *Corrosion Science*, 49(3), 1527-1539.
- [68]. Oguzie, E. E. (2008). Corrosion inhibitive effect and adsorption behaviour of *Hibiscus sabdariffa* extract on mild steel in acidic media. *Portugaliae Electrochimica Acta*, 26(3), 303-314.
- [69]. Dar, M. A. (2011). A review: plant extracts and oils as corrosion inhibitors in aggressive media. *Industrial Lubrication and Tribology*. 63(4): 227- 233
- [70]. Left, D. B., Zertoubi, M., Essaqui, A., Khoudali, S., Irhzo, A., & Azzi, M. (2018). Amelioration of reinforcement steel protection in simulated fresh concrete pore solution by adding the *Warionia saharae* extract. *Journal of Materials and Environmental Science*, 9(9), 2692-2702.
- [71]. Sangeetha, M., Rajendran, S., Sathiyabamaa, J., & Krishnavenic, A. (2013). Inhibition of corrosion of aluminium and its alloys by extracts of green inhibitors. *Portugaliae Electrochimica Acta*, 31(1), 44-45.
- [72]. Khanari, K., Finšgar, M., Hrnčič, M. K., Maver, U., Knez, Ž., & Seiti, B. (2017). Green corrosion inhibitors for aluminium and its alloys: a review. *RSC Advances*, 7(44), 27299-27330.
- [73]. Mourya, P., Banerjee, S., & Singh, M. M. (2014). Corrosion inhibition of mild steel in acidic solution by *Tagetes erecta* (Marigold flower) extract as a green inhibitor. *Corrosion Science*, 85, 352-363.
- [74]. Ogwo, K. D., Osuwa, J. C., Udoinyang, I. E., & Nnanna, L. A. (2017). Corrosion inhibition of mild steel and aluminium in 1 M hydrochloric acid by leaves extracts of *Ficus sycomorus*. *Physical Science International Journal*, 14, 1-10.
- [75]. Faustin, M., Maciuk, A., Salvin, P., Roos, C., & Lebrini, M. (2015). Corrosion inhibition of C38 steel by alkaloids extract of *Geissospermum laeve* in 1 M hydrochloric acid: electrochemical and phytochemical studies. *Corrosion Science*, 92, 287-300.
- [76]. Emran, K. M., Al-Ahmadi, A. O., Torjoman, B. A., Ahmed, N. M., & Sheekh, S. N. (2015). Corrosion and corrosion inhibition of cast Iron in hydrochloric acid (HCl) solution by cantaloupe (*Cucumis melo*) as green inhibitor. *African Journal of Pure and Applied Chemistry*, 9(3), 39-49.

- [77]. Fouda, A. S., Elmorsi, M. A., & Abou-Elmagd, B. S. (2017). Adsorption and inhibitive properties of methanol extract of *Eeuphorbia Heterophylla* for the corrosion of copper in 0.5 M nitric acid solutions. *Polish Journal of Chemical Technology*, 19(1), 95-103.
- [78]. Abd-El-Naby, B. A., Abdullatef, O. A., Abd-El-Gabr, A. M., Shaker, M. A., & Esmail, G. (2012). Effect of some natural extracts on the corrosion of zinc in 0.5 M NaCl. *International Journal of Electrochemical Science*, 7, 5864-5879.
- [79]. Singh, A., Ahamad, I., & Quraishi, M. A. (2016). *Piper longum* extract as green corrosion inhibitor for aluminium in NaOH solution. *Arabian Journal of Chemistry*, 9, S1584-S1589.
- [80]. Benelmekki, M., Vernieres, J., Kim, J. H., Diaz, R. E., Grammatikopoulos, P., & Sowwan, M. (2015). On the formation of ternary metallic-dielectric multicore-shell nanoparticles by inert-gas condensation method. *Materials Chemistry and Physics*, 151, 275-281.
- [81]. Tseng, K. H., Chou, C. J., Liu, T. C., Haung, Y. H., & Chung, M. Y. (2016). Preparation of Ag-Cu composite nanoparticles by the submerged arc discharge method in aqueous media. *Materials Transactions*, 57(3), 294-301.
- [82]. Hiragino, Y., Tanaka, T., Takeuchi, H., Takeuchi, A., Lin, J., Yoshida, T., & Fujita, Y. (2016). Synthesis of nitrogen-doped ZnO nanoparticles by RF thermal plasma. *Solid-State Electronics*, 118, 41-45.
- [83]. Duan, H., Wang, D., & Li, Y. (2015). Green chemistry for nanoparticle synthesis. *Chemical Society Reviews*, 44(16), 5778-5792.
- [84]. Tarasenko, N. V., Butsen, A. V., Nevar, E. A., & Savastenko, N. A. (2006). Synthesis of nanosized particles during laser ablation of gold in water. *Applied Surface Science*, 252(13), 4439-4444.
- [85]. Korbekandi, H., Irvani, S., & Abbasi, S. (2009). Production of nanoparticles using organisms. *Critical Reviews in Biotechnology*, 29(4), 279-306.
- [86]. Mittal, A. K., Chisti, Y., & Banerjee, U. C. (2013). Synthesis of metallic nanoparticles using plant extracts. *Biotechnology Advances*, 31(2), 346-356.
- [87]. Elia, P., Zach, R., Hazan, S., Kolusheva, S., Porat, Z. E., & Zeiri, Y. (2014). Green synthesis of gold nanoparticles using plant extracts as reducing agents. *International Journal of Nanomedicine*, 9, 4007.

- [88]. Pal, G., Rai, P., & Pandey, A. (2019). Green synthesis of nanoparticles: A greener approach for a cleaner future. In *Green synthesis, characterization and applications of nanoparticles*, Elsevier, 1-26.
- [89]. Patra, J. K., & Baek, K. H. (2014). Green nanobiotechnology: factors affecting synthesis and characterization techniques. *Journal of Nanomaterials*, 2014.
- [90]. Ahmed, S., Ahmad, M., Swami, B. L., & Ikram, S. (2016). A review on plants extract mediated synthesis of silver nanoparticles for antimicrobial applications: a green expertise. *Journal of Advanced Research*, 7(1), 17-28.
- [91]. Gericke, M., & Pinches, A. (2006). Biological synthesis of metal nanoparticles. *Hydrometallurgy*, 83(1-4), 132-140.
- [92]. Rai, A., Singh, A., Ahmad, A., & Sastry, M. (2006). Role of halide ions and temperature on the morphology of biologically synthesized gold nanotriangles. *Langmuir*, 22(2), 736-741.
- [93]. Baer, D. R., Engelhard, M. H., Johnson, G. E., Laskin, J., Lai, J., Mueller, K., ... & Moon, D. (2013). Surface characterization of nanomaterials and nanoparticles: Important needs and challenging opportunities. *Journal of Vacuum Science & Technology A: Vacuum, Surfaces, and Films*, 31(5), 050820.
- [94]. Shukla, A. K., & Iravani, S. (Eds.). (2018). *Green synthesis, characterization and applications of nanoparticles*. Elsevier.
- [95]. Herlekar, M., Barve, S., & Kumar, R. (2014). Plant-mediated green synthesis of iron nanoparticles. *Journal of Nanoparticles*, 2014.
- [96]. Lee, N., & Hyeon, T. (2012). Designed synthesis of uniformly sized iron oxide nanoparticles for efficient magnetic resonance imaging contrast agents. *Chemical Society Reviews*, 41(7), 2575-2589.
- [97]. Panigrahi, S., Kundu, S., Ghosh, S., Nath, S., & Pal, T. (2004). General method of synthesis for metal nanoparticles. *Journal of nanoparticle Research*, 6(4), 411-414.
- [98]. Makarov, V. V., Love, A. J., Sinitsyna, O. V., Makarova, S. S., Yaminsky, I. V., Taliansky, M. E., & Kalinina, N. O. (2014). "Green" nanotechnologies: synthesis of metal nanoparticles using plants. *Acta Naturae (англоязычная версия)*, 6(1), 35-44.

- [99]. Kozma, G., Rónavári, A., Kónya, Z., & Kukovecz, A. (2016). Environmentally benign synthesis methods of zero-valent iron nanoparticles. *ACS Sustainable Chemistry & Engineering*, 4(1), 291-297.
- [100]. Ebrahiminezhad, A., Zare-Hoseinabadi, A., Berenjian, A., & Ghasemi, Y. (2017). Green synthesis and characterization of zero-valent iron nanoparticles using stinging nettle (*Urtica dioica*) leaf extract. *Green Processing and Synthesis*, 6(5), 469-475.
- [101]. Kuang, Y., Wang, Q., Chen, Z., Megharaj, M., & Naidu, R. (2013). Heterogeneous Fenton-like oxidation of monochlorobenzene using green synthesis of iron nanoparticles. *Journal of Colloid and Interface Science*, 410, 67-73.
- [102]. Wang, T., Jin, X., Chen, Z., Megharaj, M., & Naidu, R. (2014). Green synthesis of Fe nanoparticles using eucalyptus leaf extracts for treatment of eutrophic wastewater. *Science of the Total Environment*, 466, 210-213.
- [103]. Wang, Z., Fang, C., & Mallavarapu, M. (2015). Characterization of iron-polyphenol complex nanoparticles synthesized by Sage (*Salvia officinalis*) leaves. *Environmental Technology & Innovation*, 4, 92-97.
- [104]. Awwad, A. M., & Salem, N. M. (2012). A green and facile approach for synthesis of magnetite nanoparticles. *Nanoscience and Nanotechnology*, 2(6), 208-213.
- [105]. Makarov, V. V., Makarova, S. S., Love, A. J., Sinitsyna, O. V., Dudnik, A. O., Yaminsky, I. V., ... & Kalinina, N. O. (2014). Biosynthesis of stable iron oxide nanoparticles in aqueous extracts of *Hordeum vulgare* and *Rumex acetosa* plants. *Langmuir*, 30(20), 5982-5988.
- [106]. Ebrahiminezhad, A., Zare, M., Kiyandpour, S., Berenjian, A., Niknezhad, S. V., & Ghasemi, Y. (2018). Biosynthesis of xanthangum-coated INPs by using *Xanthomonas campestris*. *IET Nanobiotechnology*, 12(3), 254-258.
- [107]. Ranmadugala, D., Ebrahiminezhad, A., Manley-Harris, M., Ghasemi, Y., & Berenjian, A. (2018). Magnetic immobilization of bacteria using iron oxide nanoparticles. *Biotechnology Letters*, 40(2), 237-248.



- [108]. Prasad, A. S. (2016). Iron oxide nanoparticles synthesized by controlled bioprecipitation using leaf extract of Garlic Vine (*Mansoa alliacea*). *Materials Science in Semiconductor Processing*, 53, 79-83.
- [109]. Ali, A., Hira Zafar, M. Z., ul Haq, I., Phull, A. R., Ali, J. S., & Hussain, A. (2016). Synthesis, characterization, applications, and challenges of iron oxide nanoparticles. *Nanotechnology, Science and Applications*, 9, 49.
- [110]. Wu, W., Wu, Z., Yu, T., Jiang, C., & Kim, W. S. (2015). Recent progress on magnetic iron oxide nanoparticles: synthesis, surface functional strategies and biomedical applications. *Science and Technology of Advanced Materials*, 16(2), 023501.
- [111]. Sangaiya, P., & Jayaprakash, R. (2018). A review on iron oxide nanoparticles and their biomedical applications. *Journal of Superconductivity and Novel Magnetism*, 31(11), 3397-3413.
- [112]. Smital, K., Niharika, S., & Mansee, T. (2020). Sub-acute Toxicity Assessment of Green Synthesized Hematite Nanoparticles ( $\alpha$ -Fe<sub>2</sub>O<sub>3</sub> NPs) using Wistar Rat. *Research Journal of Biotechnology*, 15 (4), 121-135.
- [113]. Huang, D. M., Hsiao, J. K., Chen, Y. C., Chien, L. Y., Yao, M., Chen, Y. K., ... & Chen, Y. C. (2009). The promotion of human mesenchymal stem cell proliferation by superparamagnetic iron oxide nanoparticles. *Biomaterials*, 30(22), 3645-3651.
- [114]. Hou, Z., Liu, Y., Xu, J., & Zhu, J. (2020). Surface engineering of magnetic iron oxide nanoparticles by polymer grafting: synthesis progress and biomedical applications. *Nanoscale*, 12(28), 14957-14975.
- [115]. Gupta, A. K., Naregalkar, R. R., Vaidya, V. D., & Gupta, M. (2007). Recent advances on surface engineering of magnetic iron oxide nanoparticles and their biomedical applications, *Nanomedicine*, 2(1), 23-29.
- [116]. Ju, Y., Zhang, H., Yu, J., Tong, S., Tian, N., Wang, Z., ... & Hou, Y. (2017). Monodisperse Au-Fe<sub>2</sub>C Janus nanoparticles: An attractive multifunctional material for triple-modal imaging-guided tumor photothermal therapy. *ACS Nano*, 11(9), 9239-9248.
- [117]. Koduru, J. R., Kailasa, S. K., Bhamore, J. R., Kim, K. H., Dutta, T., & Vellingiri, K. (2018). Phytochemical-assisted synthetic approaches for silver

- nanoparticles antimicrobial applications: A review. *Advances in Colloid and Interface Science*, 256, 326-339.
- [118]. Pour, Z. S., Ghaemy, M., Bordbar, S., & Karimi-Maleh, H. (2018). Effects of surface treatment of TiO<sub>2</sub> nanoparticles on the adhesion and anticorrosion properties of the epoxy coating on mild steel using electrochemical technique. *Progress in Organic Coatings*, 119, 99-108.
- [119]. Hoai Vu, N. S., Hien, P. V., Mathesh, M., Hanh Thu, V. T., & Nam, N. D. (2019). Improved corrosion resistance of steel in ethanol fuel blend by titania nanoparticles and *Aganonerion polymorphum* leaf extract. *ACS Omega*, 4(1), 146-158.
- [120]. Johnson, A. S., Obot, I. B., & Ukpang, U. S. (2014). Green synthesis of silver nanoparticles using *Artemisia annua* and *Sida acuta* leaves extract and their antimicrobial, antioxidant and corrosion inhibition potentials. *Journal Journal of Materials and Environmental Science*, 5(3), 899-906.
- [121]. Okeniyi, J. O., Popoola, A. P. I., Ojewumi, M. E., Okeniyi, E. T., & Ikotun, J. O. (2018). *Tectona grandis* capped silver-nanoparticle material effects on microbial strains inducing microbiologically influenced corrosion. *International Journal of Chemical Engineering*, 2018.
- [122]. Narenkumar, J., Parthipan, P., Madhavan, J., Murugan, K., Marpu, S. B., Suresh, A. K., & Rajasekar, A. (2018). Bioengineered silver nanoparticles as potent anti-corrosive inhibitor for mild steel in cooling towers. *Environmental Science and Pollution Research*, 25(6), 5412-5420.
- [123]. Tavakoli, S., Nemati, S., Kharaziha, M., & Akbari-Alavijeh, S. (2019). Embedding CuO nanoparticles in PDMS-SiO<sub>2</sub> coating to improve antibacterial characteristic and corrosion resistance. *Colloid and Interface Science Communications*, 28, 20-28.
- [124]. Ituen, E., Mkpene, V., & Ekemini, E. (2019). Adsorptive Fe-nanoparticles mediated by *Musa sapientum* peels extract as anticorrosion additive for aqueous oilfield descaling solution. *Scientific African*, 3, e00075.
- [125]. Essien, E. A., Kavaz, D., Ituen, E. B., & Umoren, S. A. (2018). Synthesis, characterization and anticorrosion property of olive leaves extract-titanium

- nanoparticles composite. *Journal of Adhesion Science and Technology*, 32(16), 1773-1794.
- [126]. Asaad, M. A., Ismail, M., Tahir, M. M., Huseien, G. F., Raja, P. B., & Asmara, Y. P. (2018). Enhanced corrosion resistance of reinforced concrete: Role of emerging eco-friendly *Elaeis guineensis*/silver nanoparticles inhibitor. *Construction and Building Materials*, 188, 555-568.
- [127]. Xiao, M., Chen, Y. M., Biao, M. N., Zhang, X. D., & Yang, B. C. (2017). Bio-functionalization of biomedical metals. *Materials Science and Engineering: C*, 70, 1057-1070.
- [128]. Morsiya, C. (2020). A review on parameters affecting properties of biomaterial SS 316L. *Australian Journal of Mechanical Engineering*, 1-11.
- [129]. Hermenau, S., Prewett, A., & Ramachandran, R. (2010). The Biochemistry of Spinal Implants: Short-and Long-Term Considerations. *The Comprehensive Treatment of the Aging Spine E-Book: Minimally Invasive and Advanced Techniques-Expert Consult*, 459.
- [130]. Talha, M., Behera, C. K., & Sinha, O. P. (2013). A review on nickel-free nitrogen containing austenitic stainless steels for biomedical applications. *Materials Science and Engineering: C*, 33(7), 3563-3575.
- [131]. Gubicza, J., El-Tahawy, M., Huang, Y., Choi, H., Choe, H., Lábár, J. L., & Langdon, T. G. (2016). Microstructure, phase composition and hardness evolution in 316L stainless steel processed by high-pressure torsion. *Materials Science and Engineering: A*, 657, 215-223.
- [132]. Zindani, D., Kumar, K., & Davim, J. P. (2019). Metallic biomaterials—A review. *Mechanical Behaviour of Biomaterials*, 83-99.
- [133]. Pilliar, R. M. (2021). Metallic biomaterials. In *Biomedical materials* Springer, Cham. 1-47.
- [134]. Minnath, M. A. (2018). Metals and alloys for biomedical applications. In *Fundamental Biomaterials: Metals* Woodhead Publishing, 167-174.
- [135]. Luo, Y., Yang, L., & Tian, M. (2013). Application of biomedical-grade titanium alloys in trabecular bone and artificial joints. In *Biomaterials and Medical Tribology* (pp. 181-216). Woodhead Publishing.

- [136]. Hussein, M. A., Mohammed, A. S., & Al-Aqeeli, N. (2015). Wear characteristics of metallic biomaterials: a review. *Materials*, 8(5), 2749-2768.
- [137]. Ibrahim, M. Z., Sarhan, A. A., Yusuf, F., & Hamdi, M. (2017). Biomedical materials and techniques to improve the tribological, mechanical and biomedical properties of orthopedic implants—A review article. *Journal of Alloys and Compounds*, 714, 636-667.
- [138]. Hanawa, T. (2004). Metal ion release from metal implants. *Materials Science and Engineering: C*, 24(6-8), 745-752.
- [139]. Sahoo, P., Das, S. K., & Davim, J. P. (2019). Tribology of materials for biomedical applications. In *Mechanical Behaviour of Biomaterials* (pp. 1-45). Woodhead Publishing.
- [140]. Alphanđery, E. (2019). Biodistribution and targeting properties of iron oxide nanoparticles for treatments of cancer and iron anaemia disease. *Nanotoxicology*, 13(5), 573-596.
- [141]. Sangaiya, P., & Jayaprakash, R. (2018). A review on iron oxide nanoparticles and their biomedical applications. *Journal of Superconductivity and Novel Magnetism*, 31(11), 3397-3413.
- [142]. Gahlawat, G., & Choudhury, A. R. (2019). A review on the biosynthesis of metal and metal salt nanoparticles by microbes. *RSC Advances*, 9(23), 12944-12967.
- [143]. Safaepour, M., Shahverdi, A. R., Shahverdi, H. R., Khorramizadeh, M. R., & Gohari, A. R. (2009). Green synthesis of small silver nanoparticles using geraniol and its cytotoxicity against fibrosarcoma-wehi 164. *Avicenna Journal of Medical Biotechnology*, 1(2), 111-115.
- [144]. D'Britto, V. I. R. G. I. N. I. A., Devi, P. P., Prasad, B. L. V., Dhawan, A., Mantri, V. G., & Prabhune, A. S. M. I. T. A. (2012). Medicinal plant extracts used for blood sugar and obesity therapy shows excellent inhibition of invertase activity: synthesis of nanoparticles using this extract and its cytotoxic and genotoxic effects. *International Journal of Life science and Pharma Research*, 2, 61-74.
- [145]. Alphanđery, E. (2020). Bio-synthesized iron oxide nanoparticles for cancer treatment. *International Journal of Pharmaceutics*, 586, 119472.

- [146]. Dorniani, D., Hussein, M. Z. B., Kura, A. U., Fakurazi, S., Shaari, A. H., & Ahmad, Z. (2012). Preparation of Fe<sub>3</sub>O<sub>4</sub> magnetic nanoparticles coated with gallic acid for drug delivery. *International Journal of Nanomedicine*, 7, 5745.
- [147]. Gholami, L., Oskuee, R. K., Tafaghodi, M., Farkhani, A. R., & Darroudi, M. (2018). Green facile synthesis of low-toxic superparamagnetic iron oxide nanoparticles (SPIONs) and their cytotoxicity effects toward Neuro2A and HUVEC cell lines. *Ceramics International*, 44(8), 9263-9268.
- [148]. Khalil, A. T., Ovais, M., Ullah, I., Ali, M., Shinwari, Z. K., & Maaza, M. (2017). Biosynthesis of iron oxide (Fe<sub>2</sub>O<sub>3</sub>) nanoparticles via aqueous extracts of *Sageretia thea* (Osbeck.) and their pharmacognostic properties. *Green Chemistry Letters and Reviews*, 10(4), 186-201.
- [149]. Nazeer, A. A., Udhayakumar, S., Mani, S., Dhanapal, M., & Vijaykumar, S. D. (2018). Surface modification of Fe<sub>2</sub>O<sub>3</sub> and MgO nanoparticles with agrowastes for the treatment of chlorosis in *Glycine max*. *Nano Convergence*, 5(1), 1-8.
- [150]. Hafiz, S. M., Kulkarni, S. S., & Thakur, M. K. (2018). In-vivo toxicity assessment of biologically synthesized iron oxide nanoparticles in Zebrafish (*Danio rerio*). *Biosciences Biotechnology Research Asia*, 15(2), 419-425.
- [151]. Markova, Z., Novak, P., Kaslik, J., Plachtova, P., Brazdova, M., Jancula, D., ... & Varma, R. (2014). Iron (II, III)-polyphenol complex nanoparticles derived from green tea with remarkable eco-toxicological impact. *ACS Sustainable Chemistry & Engineering*, 2(7), 1674-1680.
- [152]. Pravallika, P. L., Mohan, G. K., Rao, K. V., & Shanker, K. (2019). Biosynthesis, characterization and acute oral toxicity studies of synthesized iron oxide nanoparticles using ethanolic extract of *Centella asiatica* plant. *Materials Letters*, 236, 256-259.
- [153]. Plachtová, P., Medrikova, Z., Zboril, R., Tucek, J., Varma, R. S., & Maršálek, B. (2018). Iron and iron oxide nanoparticles synthesized with green tea extract: differences in ecotoxicological profile and ability to degrade malachite green. *ACS Sustainable Chemistry & Engineering*, 6(7), 8679-8687.
- [154]. Njagi, E. C., Huang, H., Stafford, L., Genuino, H., Galindo, H. M., Collins, J. B., ... & Suib, S. L. (2011). Biosynthesis of iron and silver nanoparticles at room temperature using aqueous sorghum bran extracts. *Langmuir*, 27(1), 264-271.

- [155]. Fahmy, H. M., Aly, E. M., Mohamed, F. F., Noor, N. A., & Elsayed, A. A. (2020). Neurotoxicity of green-synthesized magnetic iron oxide nanoparticles in different brain areas of wistar rats. *Neurotoxicology*, 77, 80-93.
- [156]. Kumari, M., Rajak, S., Singh, S. P., Murty, U. S., Mahboob, M., Grover, P., & Rahman, M. F. (2013). Biochemical alterations induced by acute oral doses of iron oxide nanoparticles in Wistar rats. *Drug and Chemical Toxicology*, 36(3), 296-305.
- [157]. Kim, Y., Kong, S. D., Chen, L. H., Pisanic II, T. R., Jin, S., & Shubayev, V. I. (2013). In vivo nanoneurotoxicity screening using oxidative stress and neuroinflammation paradigms. *Nanomedicine: Nanotechnology, Biology and Medicine*, 9(7), 1057-1066.
- [158]. Wang, Y., Wang, B., Zhu, M. T., Li, M., Wang, H. J., Wang, M., ... & Zhao, Y. L. (2011). Microglial activation, recruitment and phagocytosis as linked phenomena in ferric oxide nanoparticle exposure. *Toxicology Letters*, 205(1), 26-37.
- [159]. de Oliveira, G. M. T., Kist, L. W., Pereira, T. C. B., Bortolotto, J. W., Paquete, F. L., de Oliveira, E. M. N., ... & Bogo, M. R. (2014). Transient modulation of acetylcholinesterase activity caused by exposure to dextran-coated iron oxide nanoparticles in brain of adult zebrafish. *Comparative Biochemistry and Physiology Part C: Toxicology & Pharmacology*, 162, 77-84.
- [160]. Dhakshinamoorthy, V., Manickam, V., & Perumal, E. (2017). Neuro-behavioural toxicity of iron oxide nanoparticles in mice. *Neurotoxicity Research*, 32(2), 187-203
- [161]. WCO, The World Corrosion Organization, 2011 (<http://www.corrosion.org>.)
- [162]. Kumar, V., & Van Staden, J. (2016). A review of *Swertia chirayita* (Gentianaceae) as a traditional medicinal plant. *Frontiers in Pharmacology*, 6, 308.
- [163]. Soni, N., & Singh, V. K. (2019). Efficacy and Advancement of *Terminalia arjuna* in Indian Herbal Drug Research: A Review. *Trends in Applied Sciences Research*, 14, 233-242

- [164]. Deepa, P., Sowndhararajan, K., Kim, S., & Park, S. J. (2018). A role of Ficus species in the management of diabetes mellitus: A review. *Journal of ethnopharmacology*, 215, 210-232.
- [165]. Sharma, A., Oh, M. C., Kim, J. T., Srivastava, A. K., & Ahn, B. (2020). Investigation of electrochemical corrosion behavior of additive manufactured Ti–6Al–4V alloy for medical implants in different electrolytes. *Journal of Alloys and Compounds*, 830, 154620.
- [166]. García-Galvan, F. R., Fajardo, S., Barranco, V., & Feliu, S. (2021). Experimental Apparent Stern–Geary Coefficients for AZ31B Mg Alloy in Physiological Body Fluids for Accurate Corrosion Rate Determination. *Metals*, 11(3), 391.
- [167]. Arya, S. B., Bhattacharjee, A., & Roy, M. (2018). Electrochemical corrosion behavior of Ti-10V-2Fe-3Al in different corrosive media. *Materials and Corrosion*, 69(8), 1025-1038.
- [168]. Kumar, V., & Yadav, S. K. (2009). Plant-mediated synthesis of silver and gold nanoparticles and their applications. *Journal of Chemical Technology & Biotechnology: International Research in Process, Environmental & Clean Technology*, 84(2), 151-157.
- [169]. Kumar, V., Yadav, S. C., & Yadav, S. K. (2010). Syzygium cumini leaf and seed extract mediated biosynthesis of silver nanoparticles and their characterization. *Journal of Chemical Technology & Biotechnology*, 85(10), 1301-1309.
- [170]. Kumar, V., Singh, K., Panwar, S., & Mehta, S. K. (2017). Green synthesis of manganese oxide nanoparticles for the electrochemical sensing of p-nitrophenol. *International Nano Letters*, 7(2), 123-131.
- [171]. Nahlé, A., Salim, R., El Hajjaji, F., Aouad, M. R., Messali, M., Ech-Chihbi, E., ... & Taleb, M. (2021). Novel triazole derivatives as ecological corrosion inhibitors for mild steel in 1.0 M HCl: experimental & theoretical approach. *RSC Advances*, 11(7), 4147-4162.
- [172]. Richard, A. C. (2003). Laboratory corrosion testing of medical implants. ASTM International, Newyark, Delaware, USA.

- [173]. Nandini, S., Ronald, N., Adimule, S. P., & Krishnamurthy, P. (2021). Anticorrosive Effects of Derivatives of 4-{[4-(Dimethylamino) Benzyldene] amino}-1, 2, 4-Triazole on 316 Stainless Steel in HCl Medium: Experimental and Computational Study. *Journal of Failure Analysis and Prevention*, 21, 1057-1076.
- [174]. Aralu, C. C., Chukwuemeka-Okorie, H. O., & Akpomie, K. G. (2021). Inhibition and adsorption potentials of mild steel corrosion using methanol extract of *Gongronema latifoliuim*. *Applied Water Science*, 11(2), 1-7.
- [175]. Odewole, O. A., Ibeji, C. U., Oluwasola, H. O., Oyeneyin, O. E., Akpomie, K. G., Ugwu, C. M., ... & Bakare, T. E. (2021). Synthesis and anti-corrosive potential of Schiff bases derived 4-nitrocinnamaldehyde for mild steel in HCl medium: Experimental and DFT studies. *Journal of Molecular Structure*, 1223, 129214.
- [176]. Kamga, F. T. (2019). Modeling adsorption mechanism of paraquat onto Ayous (*Triplochiton scleroxylon*) wood sawdust. *Applied Water Science*, 9(1), 1-7.
- [177]. Bhatt, Y., Kumari, P., Sunil, D., Rao, S. A., Shetty, P., & Kagatkar, S. (2021). The impact of naphthalimide derivative on the mitigation of mild steel corrosion in sulfamic acid medium: experimental and theoretical insights. *Chemical Papers*, 75, 3831-3845.
- [178]. Ananthi, G. B. G., Sivakumar, N., & Deepak, M. S. (2021). Experimental study of biopolymer in corrosion resistance for industrial exposure condition. *Materials Today: Proceedings*, 44, 651-658.
- [179]. El-Sheekh, M. M., El-Kassas, H. Y., Shams El-Din, N. G., Eissa, D. I., & El-Sherbiny, B. A. (2021). Green synthesis, characterization applications of iron oxide nanoparticles for antialgal and wastewater bioremediation using three brown algae. *International Journal of Phytoremediation*, 1-15.
- [180]. Abdelaziz, S., Benamira, M., Messaadia, L., Boughoues, Y., Lahmar, H., & Boudjerda, A. (2021). Green corrosion inhibition of mild steel in HCl medium using leaves extract of *Arbutus unedo* L. plant: an experimental and computational approach. *Colloids and Surfaces A: Physicochemical and Engineering Aspects*, 619, 126496.
- [181]. ASTM F2129-17b, (2017). Standard Test Method for Conducting Cyclic Potentiodynamic Polarization Measurements to Determine the Corrosion



Susceptibility of Small Implant Devices, ASTM International, West Conshohocken, PA.

- [182]. Goyal, M., Vashist, H., Kumar, S., Bahadur, I., Benhiba, F., & Zarrouk, A. (2020). Acid corrosion inhibition of ferrous and non-ferrous metal by nature friendly Ethoxycarbonylmethyltriphenylphosphonium Bromide (ECMTPB): Experimental and MD simulation evaluation. *Journal of Molecular Liquids*, 315, 113705.
- [183]. Pattanayak, M., & Nayak, P. L. (2013). Green synthesis and characterization of zero valent iron nanoparticles from the leaf extract of *Azadirachta indica* (Neem). *World Journal of Nano Science & Technology*, 2(1), 06-09.
- [184]. Behera, S. S., Patra, J. K., Pramanik, K., Panda, N., & Thatoi, H. (2012). Characterization and Evaluation of Antibacterial Activities of Chemically Synthesized Iron Oxide Nanoparticles. *World Journal of Nano Science and Engineering*, 2(4), 196-200.
- [185]. Prathna, T. C., Chandrasekaran, N., & Mukherjee, A. (2011). Studies on aggregation behaviour of silver nanoparticles in aqueous matrices: effect of surface functionalization and matrix composition. *Colloids and Surfaces A: Physicochemical and Engineering Aspects*, 390(1-3), 216-224.
- [186]. Iravani, S., & Zolfaghari, B. (2013). Green synthesis of silver nanoparticles using *Pinus eldarica* bark extract. *Biomed Research International*, 2013, 1-5.
- [187]. Kumar, V., & Yadav, S. K. (2012). Synthesis of different-sized silver nanoparticles by simply varying reaction conditions with leaf extracts of *Bauhinia variegata* L. *IET Nanobiotechnology*, 6(1), 1-8.
- [188]. Eya'ane Meva, F., Segnou, M. L., Ebongue, C. O., Ntumba, A. A., Kedi, P. B. E., Deli, V., Etoh M. A & Mpondo, E. M. (2016). Spectroscopic synthetic optimizations monitoring of silver nanoparticles formation from *Megaphrynium macrostachyum* leaf extract. *Revista Brasileira de Farmacognosia*, 26, 640-646.
- [189]. Kumar, V., Yadav, S. C., & Yadav, S. K. (2010). *Syzygium cumini* leaf and seed extract mediated biosynthesis of silver nanoparticles and their characterization. *Journal of Chemical Technology & Biotechnology*, 85(10), 1301-1309.

- [190]. Awwad, A. M., Salem, N. M., & Abdeen, A. O. (2013). Green synthesis of silver nanoparticles using carob leaf extract and its antibacterial activity. *International Journal of Industrial Chemistry*, 4(1), 1-6.
- [191]. Clogston, J. D., & Patri, A. K. (2011). Zeta potential measurement. In *Characterization of nanoparticles intended for drug delivery*, 697, 63-70. Humana press.
- [192]. Li, S. D., & Huang, L. (2008). Pharmacokinetics and biodistribution of nanoparticles. *Molecular Pharmaceutics*, 5(4), 496-504.
- [193]. Sonavane, G., Tomoda, K., & Makino, K. (2008). Biodistribution of colloidal gold nanoparticles after intravenous administration: effect of particle size. *Colloids and Surfaces B: Biointerfaces*, 66(2), 274-280.
- [194]. Levchenko, T. S., Rammohan, R., Lukyanov, A. N., Whiteman, K. R., & Torchilin, V. P. (2002). Liposome clearance in mice: the effect of a separate and combined presence of surface charge and polymer coating. *International journal of pharmaceutics*, 240(1-2), 95-102.
- [195]. Kumar, V., Singh, K., Panwar, S., & Mehta, S. K. (2017). Green synthesis of manganese oxide nanoparticles for the electrochemical sensing of p-nitrophenol. *International Nano Letters*, 7(2), 123-131.
- [196]. Bibi, I., Kamal, S., Ahmed, A., Iqbal, M., Nouren, S., Jilani, K., Nazar, N., Amir, M., Abbas, A., Ata, S., & Majid, F. (2017). Nickel nanoparticle synthesis using *Camellia Sinensis* as reducing and capping agent: Growth mechanism and photo-catalytic activity evaluation. *International journal of biological macromolecules*, 103, 783-790.
- [197]. Karpagavinayagam, P., & Vedhi, C. (2019). Green synthesis of iron oxide nanoparticles using *Avicennia marina* flower extract. *Vacuum*, 160, 286-292.
- [198]. Igwe, O., & Nwamezie, F. (2018). Green synthesis of iron nanoparticles using flower extract of *Piliostigma thonningii* and their antibacterial activity evaluation. *Chemistry International*, 4(1), 60-66.
- [199]. Hemben, A., Chianella, I., & Leighton, G. J. T. (2021). Surface Engineered Iron Oxide Nanoparticles Generated by Inert Gas Condensation for Biomedical Applications. *Bioengineering*, 8(3), 38.

- [200]. Sravanthi, K., Ayodhya, D., & Swamy, P. Y. (2018). Green synthesis, characterization of biomaterial-supported zero-valent iron nanoparticles for contaminated water treatment. *Journal of Analytical Science and Technology*, 9(1), 1-11.
- [201]. Onwudiwe, D. C., Ravele, M. P., & Elemike, E. E. (2020). Eco-friendly synthesis, structural properties and morphology of cobalt hydroxide and cobalt oxide nanoparticles using extract of *Litchi chinensis*. *Nano-Structures & Nano-Objects*, 23, 100470.
- [202]. Ahluwalia, V., Elumalai, S., Kumar, V., Kumar, S., & Sangwan, R. S. (2018). Nano silver particle synthesis using *Swertia paniculata* herbal extract and its antimicrobial activity. *Microbial Pathogenesis*, 114, 402-408.
- [203]. Akhter, S. M. H., Mahmood, Z., Ahmad, S., & Mohammad, F. (2018). Plant-mediated green synthesis of zinc oxide nanoparticles using *Swertia chirayita* leaf extract, characterization and its antibacterial efficacy against some common pathogenic bacteria. *Bionanoscience*, 8(3), 811-817.
- [204]. Mohammed, A. E., Al-Qahtani, A., Al-Mutairi, A., Al-Shamri, B., & Abed, K. (2018). Antibacterial and cytotoxic potential of biosynthesized silver nanoparticles by some plant extracts. *Nanomaterials*, 8(6), 382.
- [205]. Prabu, K., & Natarajan, E. J. A. A. S. (2012). Isolation and FTIR spectroscopy characterization of chitin from local sources. *Advances in Applied Science Research*, 3(2), 1870-1875.
- [206]. Saha, N., & Gupta, S. D. (2016). Biogenic synthesis and structural characterization of polyshaped gold nanoparticles using leaf extract of *Swertia chirata* along with process optimization by response surface methodology (RSM). *Journal of Cluster Science*, 27(4), 1419-1437.
- [207]. Batool, S., Hussain, Z., Niazi, M. B. K., Liaqat, U., & Afzal, M. (2019). Biogenic synthesis of silver nanoparticles and evaluation of physical and antimicrobial properties of Ag/PVA/starch nanocomposites hydrogel membranes for wound dressing application. *Journal of Drug Delivery Science and Technology*, 52, 403-414.

- [208]. Kumar, M., & SINHA, M. P. (2017). Green nanotechnology: synthesis of silver nanoparticles using aqueous leaf extract of *Swertia chirayita*. *Notulae Scientia Biologicae*, 9(3), 443-448.
- [209]. Sanni, O., Popoola, A. P. I., & Fayomi, O. S. I. (2019). Temperature effect, activation energies and adsorption studies of waste material as stainless steel corrosion inhibitor in sulphuric acid 0.5 M. *Journal of Bio-and Tribo-Corrosion*, 5(4), 1-8.
- [210]. Al-Moghrabi, R. S., Abdel-Gaber, A. M., & Rahal, H. T. (2019). Corrosion inhibition of mild steel in hydrochloric and nitric acid solutions using willow leaf extract. *Protection of Metals and Physical Chemistry of Surfaces*, 55(3), 603-607.
- [211]. Guo, L., Tan, J., Kaya, S., Leng, S., Li, Q., & Zhang, F. (2020). Multidimensional insights into the corrosion inhibition of 3, 3-dithiodipropionic acid on Q235 steel in H<sub>2</sub>SO<sub>4</sub> medium: A combined experimental and in silico investigation. *Journal of Colloid and Interface Science*, 570, 116-124.
- [212]. Othman, N. K., Yahya, S., & Ismail, M. C. (2019). Corrosion inhibition of steel in 3.5% NaCl by rice straw extract. *Journal of Industrial and Engineering Chemistry*, 70, 299-310.
- [213]. Hashim, N. Z. N., Kahar, M. A. M., Kassim, K., & Embong, Z. (2020). Experimental and theoretical studies of azomethines derived from benzylamine as corrosion inhibitors of mild steel in 1 M HCl. *Journal of Molecular Structure*, 1222, 128899.
- [214]. Basilio, E., Marcellin, S., Mingant, R., Kittel, J., Fregonese, M., & Ropital, F. (2021). The effect of chemical species on the electrochemical reactions and corrosion product layer of carbon steel in CO<sub>2</sub> aqueous environment: A review. *Materials and Corrosion*, 72(7), 1152- 1167
- [215]. Loto, R. T., Okorie, E., & Olukeye, T. (2019). Synergistic combination effect of clove essential oil extract with basil and atlas cedar oil on the corrosion inhibition of low carbon steel. *South African Journal of Chemical Engineering*, 30(1), 28-41.
- [216]. Mahdavian, M., & Attar, M. M. (2009). Electrochemical behaviour of some transition metal acetylacetonate complexes as corrosion inhibitors for mild steel. *Corrosion Science*, 51(2), 409–414.

- [217]. Parthipan, P., Cheng, L., & Rajasekar, A. (2021). *Glycyrrhiza glabra* extract as an eco-friendly inhibitor for microbiologically influenced corrosion of API 5LX carbon steel in oil well produced water environments. *Journal of Molecular Liquids*, 333, 115952.
- [218]. Yüce, A. O. (2020). Corrosion inhibition behavior of *Robinia pseudoacacia* leaves extract as an eco-friendly inhibitor on mild steel in acidic media. *Metals and Materials International*, 26(4), 456-466.
- [219]. Wu, L. Y., Kuo, Y. L., Chang, K. H., Chen, T. H., Cheng, C. Y., Liu, Y. S., & Huang, C. (2019). Effects of cyclonic plasma deposited organosilicon nano-coating on 316 stainless steel and its surface characterization. *Surface and Interface Analysis*, 51(10), 993-1000.
- [220]. Pragathiswaran, C., Thulasi, G., Al-Ansari, M. M., Al-Humaid, L. A., & Saravanan, M. (2021). Experimental investigation and electrochemical characterization of titanium coated nanocomposite materials for biomedical applications. *Journal of Molecular Structure*, 1231, 129932.
- [221]. Gonzalez, J. L., & Veleva, L. (2021). The Electrochemical Activity of Mg and Mg-Ca0. 3 in Hank's Physiological Solution. *ECS Transactions*, 101(1), 69.
- [222]. Gawad, S. A., Nasr, A., Fekry, A. M., & Filippov, L. O. (2021). Electrochemical and hydrogen evolution behaviour of a novel nano-cobalt/nano-chitosan composite coating on a surgical 316L stainless steel alloy as an implant. *International Journal of Hydrogen Energy*, 46(35), 18233-18241.
- [223]. Manonmani, R. (2021). Deposition of biocompatible nano biocomposite layers on 316L SS surface for bone implant applications. *Journal of the Iranian Chemical Society*, 18(5), 1127-1136.
- [224]. Manonmani, R., & Sridhar, T. M. (2020). Sintering temperature effects on nano triphasic bioceramic composite coated 316L SS for corrosion resistance, adhesion strength, and cell proliferation on implants. *Journal of Materials Research*, 35(6), 580-590.
- [225]. Manonmani, R. (2021). Novel nano triphasic bioceramic composite coating on 316L SS by electrophoretic deposition process for enhanced corrosion resistance and cell proliferation. *Journal of the Australian Ceramic Society*, 57(1), 205-213.

- [226]. Nik Masdek, N. R., Wahab, N. A., Ahmad Nawawi, N., & Tajudin, A. (2021). The effect of pH on the corrosion rate of 316L Stainless Steel, Nitinol, and Titanium-6% Aluminum-4% Vanadium in Hank's Solution. *Scientific Research Journal*, 18(1), 1-13.
- [227]. Prince, R. M. R., Selvakumar, N., Arulkirubakaran, D., Singh, S. C. E., Das, M. C., Bannaravuri, P. K., ... & Robert, R. J. (2021). ZrC-Impregnated Titanium-Based Coating as an Effective Lubricating Barrier for Artificial Hip Prosthesis. *Materials Performance and Characterization*, 10(1), 189-205.
- [228]. Choudhary, G., & Singh, G. (2020). Comparative Analysis of Corrosion Behaviour of Stainless Steel Grades 304 and 316L for Different Applications. *i-Manager's Journal on Material Science*, 7(4), 8.
- [229]. Mali, S. A., Zhu, D., Liu, Y., & Gilbert, J. L. (2021). Fretting Crevice Corrosion of 316 L Stainless Steel in Physiological Phosphate Buffered Saline: Load, Potential and Alloy Counterface Effects. *Tribology International*, 107198.
- [230]. Vafa, E., Bazargan-Lari, R., & Bahrololoom, M. E. (2021). Electrophoretic deposition of polyvinyl alcohol/natural chitosan/bioactive glass composite coatings on 316L stainless steel for biomedical application. *Progress in Organic Coatings*, 151, 106059.
- [231]. Ebrahimi, A., Esfahani, H., Imantalab, O., & Fattah-Alhosseini, A. (2020). Biological, antibacterial activities and electrochemical behavior of borided commercially pure titanium in BSA-containing PBS. *Transactions of Nonferrous Metals Society of China*, 30(4), 944-957.
- [232]. Yue, X., Zhang, L., Hua, Y., Wang, J., Dong, N., Li, X., ... & Neville, A. (2020). Revealing the superior corrosion protection of the passive film on selective laser melted 316L SS in a phosphate-buffered saline solution. *Applied Surface Science*, 529, 147170.
- [233]. Al-Mamun, N. S., Deen, K. M., Haider, W., Asselin, E., & Shabib, I. (2020). Corrosion behavior and biocompatibility of additively manufactured 316L stainless steel in a physiological environment: the effect of citrate ions. *Additive Manufacturing*, 34, 101237.
- [234]. Atapour, M., Wang, X., Färnlund, K., Wallinder, I. O., & Hedberg, Y. (2020). Corrosion and metal release investigations of selective laser melted 316L

stainless steel in a synthetic physiological fluid containing proteins and in diluted hydrochloric acid. *Electrochimica Acta*, 354, 136748.

- [235]. Mahajan, A., Devgan, S., & Sidhu, S. S. (2021). Surface alteration of biomedical alloys by electrical discharge treatment for enhancing the electrochemical corrosion, tribological and biological performances. *Surface and Coatings Technology*, 405, 126583.
- [236]. Kedia, S., Bonagani, S. K., Majumdar, A. G., Kain, V., Subramanian, M., Maiti, N., & Nilaya, J. P. (2021). Nanosecond laser surface texturing of type 316L stainless steel for contact guidance of bone cells and superior corrosion resistance. *Colloid and Interface Science Communications*, 42, 100419.
- [237]. Talha, M., Ma, Y., Lin, Y., Mandal, A. K., Sinha, O. P., & Kong, X. (2021). Corrosion performance of various deformed surfaces of implant steel for coronary stent applications: Effect of protein concentration. *Colloids and Surfaces B: Biointerfaces*, 197, 111407.
- [238]. Kityk, A. A., Pavlik, V., Boča, M., Pangallo, D., Kapustova, M., & Halahovets, Y. (2020). Electrochemical Surface Treatment to Enhance Corrosion Resistance and Bioresistance of Medical-Grade Stainless Steels. *Journal of Materials Engineering and Performance*, 29(9), 5985-5994.
- [239]. Kongsat, P., Kudkaew, K., Tangjai, J., Edgar, A. O., & Pongprayoon, T. (2021). Synthesis of structure-controlled hematite nanoparticles by a surfactant-assisted hydrothermal method and property analysis. *Journal of Physics and Chemistry of Solids*, 148, 109685.
- [240]. Archana, V., Joseph Prince, J., & Kalainathan, S. (2021). Simple One-Step Leaf Extract-Assisted Preparation of  $\alpha$ -Fe<sub>2</sub>O<sub>3</sub> Nanoparticles, Physicochemical Properties, and Its Sunlight-Driven Photocatalytic Activity on Methylene Blue Dye Degradation. *Journal of Nanomaterials*, 2021.
- [241]. Roknian, M., Fattah-alhosseini, A., Gashti, S. O., & Keshavarz, M. K. (2018). Study of the effect of ZnO nanoparticles addition to PEO coatings on pure titanium substrate: microstructural analysis, antibacterial effect and corrosion behavior of coatings in Ringer's physiological solution. *Journal of Alloys and Compounds*, 740, 330-345.

- [242]. Seyfi, M., Fattah-alhosseini, A., Pajohi-Alamoti, M., & Nikoomanzari, E. (2021). Effect of ZnO nanoparticles addition to PEO coatings on AZ31B Mg alloy: antibacterial effect and corrosion behavior of coatings in Ringer's physiological solution. *Journal of Asian Ceramic Societies*, 9(3), 1114-1127.
- [243]. Singh, S., Singh, G., Bala, N., & Aggarwal, K. (2020). Characterization and preparation of Fe<sub>3</sub>O<sub>4</sub> nanoparticles loaded bioglass-chitosan nanocomposite coating on Mg alloy and in vitro bioactivity assessment. *International Journal of Biological Macromolecules*, 151, 519-528.
- [244]. Nikoomanzari, E., Fattah-alhosseini, A., Alamoti, M. R. P., & Keshavarz, M. K. (2020). Effect of ZrO<sub>2</sub> nanoparticles addition to PEO coatings on Ti-6Al-4V substrate: Microstructural analysis, corrosion behavior and antibacterial effect of coatings in Hank's physiological solution. *Ceramics International*, 46(9), 13114-13124.
- [245]. Keyvani, A., Zamani, M., Bahamirian, M., Nikoomanzari, E., Fattah-Alhosseini, A., & Sina, H. (2021). Role of incorporation of ZnO nanoparticles on corrosion behavior of ceramic coatings developed on AZ31 magnesium alloy by plasma electrolytic oxidation technique. *Surfaces and Interfaces*, 22, 100728.
- [246]. Farghali, R. A., Fekry, A. M., Ahmed, R. A., & Elhakim, H. K. A. (2015). Corrosion resistance of Ti modified by chitosan-gold nanoparticles for orthopedic implantation. *International journal of biological macromolecules*, 79, 787-799.
- [247]. Fekry, A. M. (2016). Electrochemical behavior of a novel nano-composite coat on Ti alloy in phosphate buffer solution for biomedical applications. *RSC advances*, 6(24), 20276-20285.
- [248]. Qu, J. E., Ascencio, M., Jiang, L. M., Omanovic, S., & Yang, L. X. (2019). Improvement in corrosion resistance of WE43 magnesium alloy by the electrophoretic formation of a ZnO surface coating. *Journal of Coatings Technology and Research*, 16(6), 1559-1570.
- [249]. Bordbar-Khiabani, A., Bahrapour, S., Mozafari, M., & Gasik, M. (2022). Surface functionalization of anodized tantalum with Mn<sub>3</sub>O<sub>4</sub> nanoparticles for effective corrosion protection in simulated inflammatory condition. *Ceramics International*, 48(3), 3148-3156.



### List of publications

- **Sharma, P.** Bhardwaj, N., & Kumar, V., (2021). Swertia chirata extract mediated synthesis of iron oxide nanoparticles and its use as corrosion inhibitor for stainless steel 316 L in Ringer's solution" Advances in Natural Sciences: Nano science and Nanotechnology, 12(3), 035012.
- **Sharma, P.** Bhardwaj, N., & Kumar, V., (2021). "Greener iron oxide nanomaterials inhibits corrosion of stainless steel 316L in Ringer's solution'', Journal of Bio-Tribo Corrosion, 8(2), 1-11.
- **Sharma, P.** Bhardwaj, N., & Kumar, V., (2021). *Swertia chirata* Extract Synthesized Iron Oxide Nanoparticles as Corrosion Inhibitor for SS-316 L in Hank's Solution. Asian Journal of chemistry, 33(8), 1824-1830.
- Bhardwaj, N., **Sharma, P.**, Analysis, L. G., Dagdag, O., & Kumar, V. (2021). Molecular dynamic simulation, Quantum chemical calculation and electrochemical behaviour of *Punica granatum* peel extract as eco-friendly corrosion inhibitor for stainless steel (SS-410) in acidic medium. *Journal of Molecular Liquids*, 118237.
- Bhardwaj, N., **Sharma, P.**, Singh, K., Rana, D., & Kumar, V. (2021). *Phyllanthus emblica* seed extract as corrosion inhibitor for stainless steel used in petroleum industry (SS-410) in acidic medium. *Chemical Physics Impact*.3, 100038.
- Bhardwaj, N., **Sharma, P.**, & Kumar, V. (2021). Anti-corrosive behaviour of *S. officinarum* plant extract in 15 % hydrochloric acid for stainless steel-410 surface. *Asian Journal of chemistry*, 33(5), 1389-1395.
- Bhardwaj, N., **Sharma, P.**, & Kumar, V. (2021). Corrosion inhibition property and adsorption behaviour of *P. tremula* leaf extract in acidic media for steel used in petroleum industry (S.S- 410). *Protection of Metals and Physical Chemistry of Surfaces*.
- **Sharma, P.** Bhardwaj, N., & Kumar, V., (2020). Defence applications of Nanotechnology: Development and Strategies. *European Journal of Molecular & Clinical Medicine*, 7(7), 4310-4316.
- Bhardwaj, N., **Sharma, P.**, & Kumar, V. (2021). Phytochemicals as steel

corrosion inhibitor: an insight into mechanism. *Corrosion Reviews*, 39(1), 27-41.

- **Sharma, P**, Bhardwaj, N & Kumar, V. (2018) Nanotechnology in corrosion control of biomaterials. *Journal of Emerging Technologies and Innovative Research (JETIR)*, vol. 5 (12), 503- 508.
- **Sharma, P** & Kumar, V. Nanotechnology and Prions. *International Journal of Research and Analytical Reviews (IJRAR)*, vol. 5 (4), (2018) 782- 793.
- Bhardwaj, N., **Sharma, P** & Kumar, V. (2018) Types of corrosion due to rusting of steel used in petroleum industries: A Review. *Journal of Emerging Technologies and Innovative Research (JETIR)*, vol. 5 (12), 509- 513.
- Bhardwaj, N., **Sharma, P.**, Guo, L., Dagdag, O., & Kumar, V. (2021). Molecular dynamic simulation and quantum chemical calculation of phytochemicals present in *Beta vulgaris* and electrochemical behaviour of *Beta vulgaris* peel extract as green corrosion inhibitor for stainless steel (SS-410) in acidic medium. *Colloids and Surfaces A: Physicochemical and Engineering Aspects*, 632, 127707.
- Bhardwaj, N., **Sharma, P.**, & Kumar, V. (2021). *Triticum aestivum* Extract as Corrosion Inhibitor for Stainless Steel (SS-410) In Acidic Media: Experimental and Theoretical Study. *Current Research in Green and Sustainable Chemistry*.
- Bhardwaj, N., **Sharma, P.**, & Kumar, V. (2021). *O. sativa* plant extract as green Corrosion Inhibitor in 15 % hydrochloric acid for stainless steel-410 surface. *Tenside Surfactants Detergents*, 59, 81-94.

#### **Conferences and workshops**

- Oral presentation on “*Terminalia arjuna* synthesized iron oxide nanoparticles as corrosion inhibitor for biomedical steel- SS 316 in phosphate buffer solution” in International Conference on Recent Advances in Applied Sciences, Technology & Health held on March 3rd & 4th, 2021

- Oral presentation on “Effect of temperature on the size and characteristics of green synthesized iron oxide nanoparticles for biomedical applications” in the International Conference on Modern Emerging Trends: Future of Chemical Sciences held on April 23 to 24, 2021.
- Oral presentation on “*Ficus benghalensis* Synthesized Iron Oxide Nanoparticles as Corrosion Inhibitor for Biomedical Steel- SS 316 In Phosphate Buffer Solution” in International Conference ON Environment, Agriculture, Human and Animal Health held on June 05- 06, 2021.
- Participated in the 106th Indian Science Conference held on January 3 to 7, 2019.
- Attended National Workshop on Advanced Instrumentation at Lovely Professional University on April, 20, 2019